SMART, BIOCOMPATIBLE POLYMERSOMES FOR TARGETED DELIVERY OF THERAPEUTIC AGENTS TO CANCEROUS TUMORS

A Dissertation
Submitted to the Graduate Faculty
of the
North Dakota State University
of Agriculture and Applied Science

By

Tayebeh Anajafi Marzijarani

In Partial Fulfillment of the Requirements
for the Degree of
DOCTOR OF PHILOSOPHY

Major Department:
Pharmaceutical Sciences

May 2017

Fargo, North Dakota

North Dakota State University
Graduate School

Title

SMART, BIOCOMPATIBLE POLYMERSOMES FOR TARGETED DELIVERY OF THERAPEUTIC AGENTS TO CANCEROUS TUMORS

By

Tayebeh Anajafi Marzijarani

The Supervisory Committee certifies that this ***disquisition*** complies with North Dakota State University's regulations and meets the accepted standards for the degree of

DOCTOR OF PHILOSOPHY

SUPERVISORY COMMITTEE:

Dr. Sanku Mallik
Chair

Dr. Jagdish Singh

Dr. Chengwen Sun

Dr. Dean Webster

Approved:

05/08/2017
Date

Dr. Jagdish Singh
Department Chair

ABSTRACT

Chemotherapeutics are the major treatment options for cancer. Although we cannot underestimate the importance of the chemotherapeutic drugs, their systemic toxicity is an important limiting factor for their use. Therefore, altering the biodistribution of the therapeutics can be an important step in treating the cancer patients. Thus, there is a growing interest in developing smart, targeted, stimuli responsive, drug delivery vehicles employing nanotechnalogy. The vehicles are often engineered to deliver the theranostics to the tumor microenvironment (extracellular matrix) or intracellular environment (e.g. cytosol, nucleus, mitochondria). The physiochemical changes in the cancerous tissues (e.g. leaky vasculature, proteins overexpression on the cell surface, overexpression of proteolytic enzymes, increased reducing agents concentration, decreased pH, and hypoxia) offer tremendous opportunities for selectively targeting the malignancies. Polymersomes are robust polymeric vesicles which have shown promising drug delivery capabilities. Both hydrophilic and hydrophobic compounds can be loaded to the vesicles. The polymersome's building blocks can be chemically manipulated to provide them with the optimum release profile. Furthermore, the surface of the polymersomes can be decorated with targeting moieties such as peptides, antibodies, or small molecules. We have developed smart, targeted, stimuli responsive polymersomes to combat pancreatic and prostate cancers.

ACKNOWLEDGEMENTS

I would like to convey my sincere gratitude to my advisor, Dr. Sanku Mallik, for his continuous guidance throughout my Ph.D. studies; my graduate advisory committee members Dr. Jagdish Singh (chair of the department), Dr. Chengwen Sun and Dr. Dean Webster for providing me with their insightful suggestions and comments; Dean of the college Dr. Charles Peterson for providing the support to the college.

I also would like to express my thanks to Dr. D.K. Srivastava for being a great mentor; Dr. Bin Guo, Dr. Yongki Choi, Dr. W. Muhonen Wallace, Dr. John B. Shabb, Dr. John Wilkinson, Dr. Seungyong You, and Dr. Kalpana Katti for being excellent collaborators.

I acknowledge National Institute of Health (NIH) and NSF for providing financial support for these projects.

Thanks to the department of pharmaceutical sciences, the college of health professions, the graduate school, and North Dakota State University for providing the support for my studies.

Thanks to my labmates past and present Dr. Michael D. Scott, Dr. Rahul Nahire, Dr. Manas K. Haldar, Dr. Li Feng, Matt Confeld, all my friends and fellow graduate students, faculties and staff for their support. Also, I acknowledge the undergraduate and PharmD students Seth, Heather, and Akilah.

Last but not least, I would like to thank my parents, my husband, my sister, and my brother for their continuous patience, love and support.

DEDICATION

To My Dear Parents and Supportive Husband

TABLE OF CONTENTS

LIST OF TABLES

LIST OF FIGURES

LIST OF SCHEMES

LIST OF ABBREVIATIONS

AFM..... Atomic Force Microscopy

ATCC..... American Type Culture Collection

C..... Centigrade

$CaCl_2$..... Calcium chloride

CD..... Circular Dichroism

$CoCl_2$..... Cobalt chloride

CRAC ..... Ca^{2+} release activated Ca^{2+}

DLS..... Dynamic Light Scattering

DSPE..... 1,2-distearoyl-sn-glycero-3-phosphoethanolamine

EPR..... Enhanced Permeability and Retention

Em..... Emission

ER ..... Endoplasmic reticulum

Ex..... Excitation

GSH ..... Glutathione

HBSS ..... Hank's balanced salt solution

HEPES ..... 4-(2-hydroxyethyl)-1-piperazineethanesulfonic acid

HPLC ..... High Performance Liquid Chromatography

HPMA..... N-(2-hydroxypropyl) methacrylamide

M..... Molar

MW..... Molecular weight

LR ..... Lissamine rhodamine B sulfonyl, ammonium salt

mM..... Millimolar

IP3R..... Inositol-1,4,5- trisphosphate receptors

MALDI-TOF ..... Matrix-assisted laser desorption/ionization- Time of Flight

mg ..... Milligram

mL ..... Milliliter

MMP ..... Matrix Metalloproteinase

nm ..... Nanometer

nM ..... Nanomolar

NMR ..... Nuclear Magnetic Resonance

PBS ..... Phosphate Buffered Saline

PDI ..... Polydispersity Index

PEG ..... Poly (ethylene glycol)

PLA ..... Poly (lactic acid)

PMCA ..... Plasma membrane calcium ATPase

PMDETA ..... N,N,N′,N′,N″-pentamethyldiethylenetriamine

PSMA ..... Prostate-specific membrane antigen

RES ..... Reticuloendothelial system

RG ..... Receptor-gated

RPMI ..... Roswell Park Memorial Institute medium

SERCA ..... sarcoendoplasmic reticulum Ca^{2+} ATPase

TEM ..... Transmission Electron Microscopy

THF ..... Tetrahydrofuran

TMRM ..... Tetramethylrhodamine, methyl ester

µl ..... Microliter

µmol ..... Micromole

UV ..... Ultravoilet

VG..... Voltage-gated

3D ..... Three dimensional

W..... Molecular Weight

LIST OF APPENDIX FIGURES

1. INTRODUCTION[1] AND DISSERTATION ORGANIZATION

1.1. Drug Delivery Using Nanoparticles

Nanotechnology has revolutionized the science and especially medicine. The special physiochemical properties of nanoparticles, e.g., high surface area to mass ratio, small size, and ability to carry materials are attractive to scientists around the world.[1] It was believed in early 1970s that suspensions couldn't be administered via intravenous route because of the possible problems like embolism.[2] However, the nanotechnology and ability to prepare tens to hundreds of nanometer diameter particles has changed this belief.

In medicine, the nanoparticles have been used as "theranostic" agents. In drug delivery, an appropriate nanoparticle has high loading capacity, stability, appropriate release profile, targetability, biocompatibility, and biodegradability.[3] To confer biocompatibility and biodegradability to the nanoparticles, various materials from natural origin (e.g., chitosan,[4] dextran[5], phospholipids[6]) or synthetic (e.g., poly lactic acid[7], polyethylene glycol[7], poly caprolactone[8]) have been used. Different loading strategies are reported for increasing the nanoparticles loading capacity (e.g., passive or active loading[3]). Increasing the loading capacity improves the efficacy of the formulations by decreasing the amount of carrier materials to the patient body. This limits the undesired side effects arising from the carrier itself. Targeted drug delivery is an accepted strategy to increase the therapeutic index of the nanotherapeutic formulations. Targeting the nanoparticles to a special tissue or organ can assist in decreasing the adverse effects on healthy cells or tissues. Chemical conjugations (e.g., Click chemistry) has

[1] This section is coauthored by Tayebeh Anajafi and Sanku Mallik. Tayebeh had primary responsibility to write the review paper. Dr. Mallik advised and verified the manuscript.

provided a spectacular opportunity to conjugate targeting moieties (e.g., small molecules, peptides, antibodies) to the surface of nanoparticles.[7]

Several nanoparticles have been used for drug delivery. Liposomes,[9] polymersomes,[7] micelles,[10] silica nanoparticles[11] are a few promising nanocarriers. In this paper-based thesis, we have focused on polymersomal formulations because of their stability, high loading capacity, and the ability for functionalization with different moieties. I have used my review paper on polymersomes for the following paragraphs of the introduction.

1.2. Polymeric Nanovesicles

The idea of polymeric vesicles (polymersomes) germinated during a discussion about the phase behavior of di-block co-polymers in 1994.[12] This discussion was followed by preparing nano-sized polymer vesicles using a specific di-block co-polymer (polyethyleneoxide-polyethylethylene; *f* EO = 0.39, *M*w = 3,600).[13] These vesicles were proven to be more robust and less water permeable compared to phospholipid vesicles or liposomes.[13] Since then, several research laboratories have been studying polymersomes for different purposes, including drug/gene delivery, diagnosis, bioreactors, and cell/viral capsid mimicking.[14, 15]

These hollow vesicles (Figure 1.1 A) consist of a watery interior that is separated from the aqueous surrounding media by an amphiphilic polymer bilayer. The thickness of the bilayer (5-30 nm) usually causes a more robust and impermeable wall compared to the liposomal structures (3-5 nm).[14] This feature depends on the molecular weights of the co-polymers used in the polymersomes. It has been observed that the membrane thickness (d) is proportional to $MW^{0.55}$.

Among the biomedical applications for polymersomes, drug/gene delivery holds the most promise due to the tunable chemistry of the block co-polymers (including the versatility of monomers and the possibility to change block polymers' molar mass and percentage), their low

critical aggregation concentration, and the robustness of the polymersomes' bilayer. The latter characteristic can increase the stability of encapsulated compounds for a long time.[16] The polymersomes' hollow core can be used to encapsulate hydrophilic compounds, and the bilayer can be dedicated for loading the hydrophobic compounds. In such a scenario, the combination therapy (Figure 1.1 B) and diagnostic purposes can be achieved using polymersomes.

Designing clinically applicable polymersomes has been a challenging area in the last several decades. Herein, we elaborate on the recent developments of biocompatible polymersomes as targeted delivery vehicles for cancer therapy.

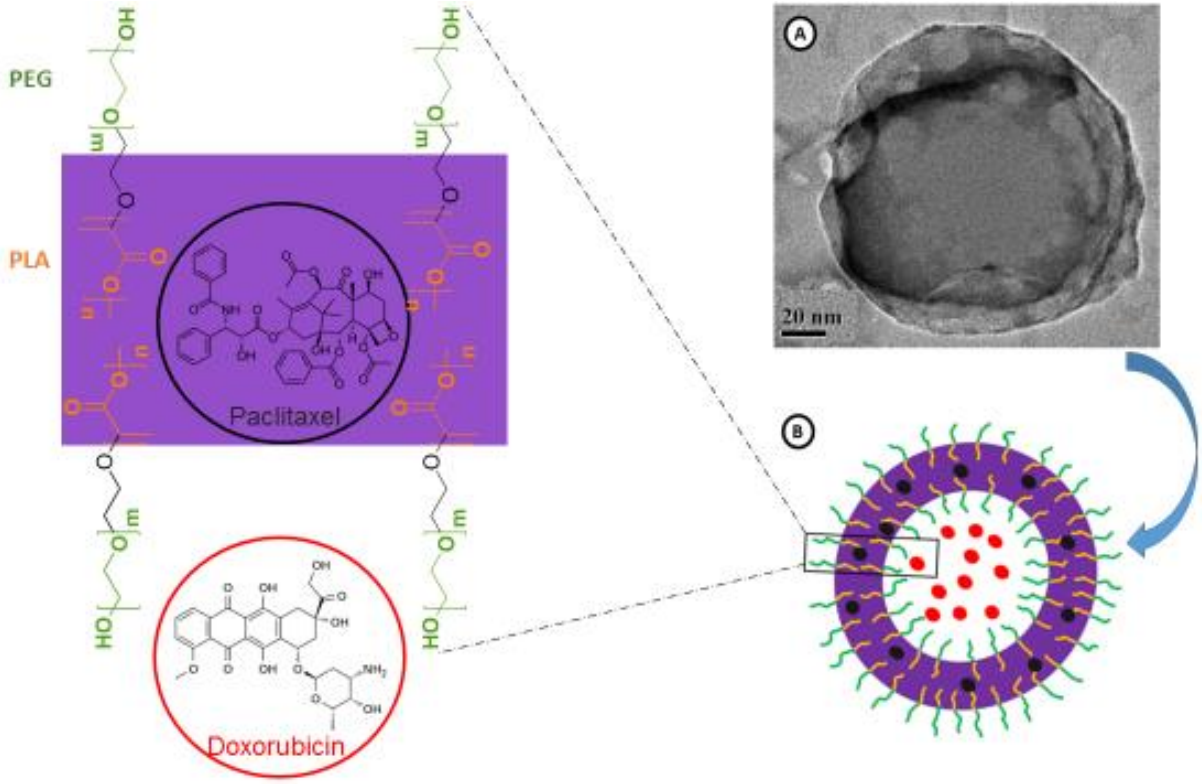

Figure 1.1. Polymersomes. (A) Transmission electron microscopic image of a polymersome constructed using poly (ethylene glycol)-b-poly (lactic acid) copolymer (The scale bar shows 20 nm). (B) Schematic illustration of combination cancer therapy using a polymersome. The hydrophilic core of the polymersome is loaded by a conventional, hydrophilic, anti-cancer drug (Doxorubicin), and a hydrophobic chemotherapy drug (Paclitaxel) is incorporated in the hydrophobic bilayer of the polymersome.

1.2.1. Polymersomes Preparation

Typically, polymersomes are prepared from amphiphilic, linear block co-polymers.[17] The ratio of the hydrophilic part to the total mass of the co-polymers (*f* value) is a determinant factor in the formation of different nano-structures.[17, 18, 19] If the *f* value is higher than 50%, the formation of micelles is possible, and if the value is 40-50%, worm-like structures are more likely. However, if the *f* value is between 25% and 40%, which is similar to natural phospholipids, the formation of vesicles is more favorable[17, 19] (Figure 1.2). In addition to linear block co-polymers, mictoarm polymers have been used as alternative building blocks for polymersomes.[20, 21] These Y-shaped, complex polymers not only have a greater ability to form polymersomes, but are also able to mimic the phospholipid structures.[20, 21]

Several methods have been used to prepare polymersomes, including the solvent-exchange method, film rehydration, electroformation,[13] and the double-emulsion strategy.[22] Electroformation has been used to construct giant polymersomes. Double emulsion (which have been prepared using capillary microfluidics) is a reliable method for preparing polymersomes with acceptable monodispersity in size and uniformity in the bilayer membrane. Among these methods, the solvent-exchange method is widely used for its ease, reproducibility, and control over the size of nano-particles. Although filter extrusion has been used to decrease the polydipersity index of liposomes, this method seems to be a very time-consuming and difficult approach for polymersomes, even at elevated temperatures due to the polymersome membrane's robustness.

1.2.2. Drug Encapsulation in Polymersomes

Drug loading capacity is one of the important factors to be considered in any nano-delivery systems' preparation. If the encapsulation efficiency is not high enough, higher amounts of the nano-particles need to be injected (to reach the therapeutic window), leading to the introduction of

a higher fraction of polymer (in case of polymersomes) in the patient's body. Both passive and active (remote) loading strategies have been utilized for encapsulating hydrophobic or hydrophilic compounds in the polymersomes. For passive loading, hydrophobic compound of interest is solubilized/dispersed in an organic solvent along with the polymers used for the polymersomes. Hydrophilic drugs or imaging agents are usually added to the aqueous buffer during polymersome preparation. However, due to the low water solubility of some compounds, and the pivotal need for high drug loading capacity, active liposomal loading procedures (e.g. salt and pH gradient) have been adapted for polymersomes. Preparation of paclitaxel encapsulated polymersomes (from pre-formed vesicles) revealed that drug loading efficiency is about 10-fold higher than that of liposomes. The higher efficiency is attributed to the presence of thicker hydrophobic membrane in polymersomes' structure compared to the liposomal lipid bilayer.[23] The hydrophilic, cytotoxic drug, doxorubicin, is encapsulated inside the polymersomes' hollow core using either a pH gradient[23, 24, 25] or an ammonium sulfate gradient.[26] The encapsulation efficiency for polymersomes was similar to the corresponding liposomal formulations. Due to the stability and reduced leakage of incorporated compounds, polymersomes have the potential to be more acceptable drug carriers compared to liposomes.

1.2.3. Biomedically Translatable Polymersomes

Ideal polymersomes with biomedically applicable properties need to have enough loading capacity for the active ingredients. Also, these polymersomes should be robust enough to protect the payload from unexpected release. These nano-structures should have a long circulation time and low renal clearance rate while the cargo release needs to be controllable. In addition, specificity toward the desired target site as well as presenting no or minimum immunogenicity are important criteria. Any premature release of the encapsulated drug can increase the risk of side

effects, especially in the case of cytotoxic anti-cancer drugs. However, reduced therapeutic efficacy and drug resistance could be expected as a consequence of slow drug release. Considering these facts, many studies focus on designing polymersomes with improved biodegradability and biocompatibility.

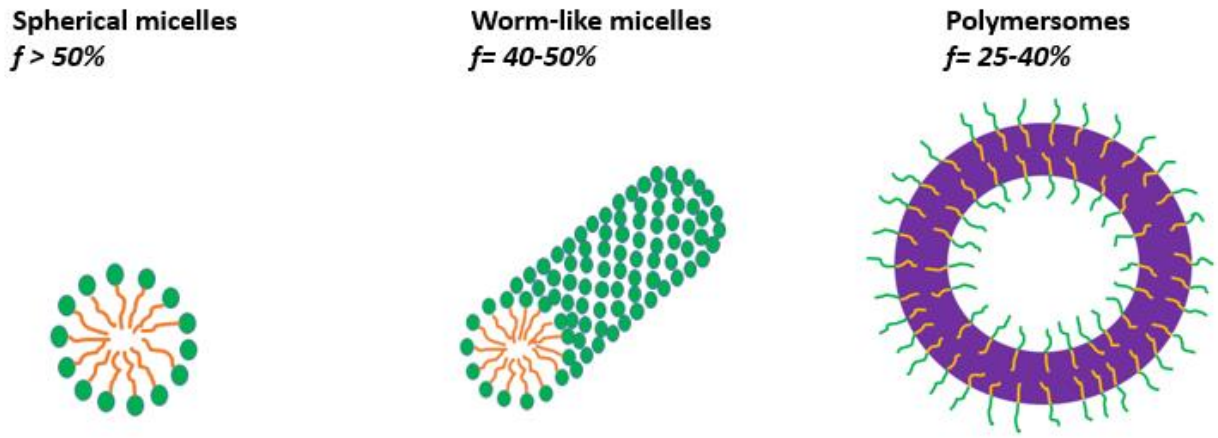

Figure 1.2. Schematic representation of spherical/worm-like micelles and polymersomes. Changing the *f* value of the block co-polymers determines the formation of different structures.

1.2.3.1. Biocompatibility

To increase the polymersomes' biocompatibility, interactions with blood components should be adjusted to be at minimum, and the vesicles should be guided toward the target sites. There are several approaches, including PEGylation and using targeting moieties, to improve the pharmacodynamic and pharmacokinetic properties of theranostic delivery systems.

1.2.3.1.1. PEGylation

The Enhanced Permeability and Retention (EPR) effect is one of the mechanisms (passive targeting) used for delivering drugs to various cancer tumors. With most tumors, the presence of a non-organized, leaky vasculature along with gaps of 100 nm – 2 μm have been established. Therefore, nano-particles with a mean size less than 200 nm are able to extravasate through these

leaky, imperfect vasculatures with most cancers. A poorly developed lymphatic system in the tumor tissues helps retain nano-particles in tumor area. However, it should be noted that blood flow to the tumor site is also restricted in comparison with normal organs. Hence, having a good amount of nano-particle accumulation requires a long circulation time which, itself, is confined by the body's immune system.

The innate immune system is constantly monitoring the body's environment, searching for foreign materials, including pathogens and other exogenous particles such as drug-delivery systems. Therefore, one of the important challenges with drug-delivery approaches is the fate of the carrier and its ability to escape from the reticuloendothelial system's uptake. If the nano-carrier's surface is not covered to evade the innate immune system, blood proteins (e.g., antibodies and complement system) can surround the carrier (opsonization) and make it engulfable by phagocytes in the reticuloendothelial system's (RES) organs. For example, Kupffer cells (resident liver macrophages) are able to distinguish and process the opsonized foreign particles using scavenger receptors. As a result, the half-life of the drug-delivery systems decreases drastically, and more than 50% of the injected dose is usually cleared shortly after administration.[27] Furthermore, accumulation of the drug-delivery systems by phagocytes in secondary immune organs such as the spleen and liver increases the chance of organ toxicity, decreasing the drug's therapeutic index (Figure 1.3). Hence, different hydrophilic polymers [e.g., poly (ethyleneglycol) (PEG) and N-(2-hydroxypropyl) methacrylamide (HPMA)][28] and polysaccharides (e.g., heparin)[29] have been used to sterically hinder the opsonization process by the white blood cells. PEG with no charge and a non-biodegradable[30] characteristic is the most-studied polymer that contributes to the stealth properties of drug-delivery systems.

The PEG surface concentration is also important for imparting stealth properties to the nano- carriers. It has been shown that increasing the PEG surface concentration weakens the protein adsorption on the nano-particles' surface.[31] Another determinant factor which affects the vectors' camouflage is the size of the PEG polymer. For example, a PEG brush with a molecular weight of more than 3,400 Da has the highest effect to decrease human plasma protein adsorption on the surface of polystyrene particles.[31] Electrostatic properties of the vehicle surface area are another determinant factor that should be considered. A slightly positive or negative charge may increase the half-life of drug-delivery systems. However, a highly charged surface should be avoided on the carriers because it not only confers toxicity,[32] but also decreases the nano-particle circulation time by increasing the amount of hepatic uptake.[33]

It should be noted that the stealth properties rendered by the hydrophilic polymers are only effective for a limited time. Eventually, proteins adsorb on the nano-carriers' surface, and clearance of polymersomes is unavoidable.[17] In addition, a long circulation time increases the drug's side effects in healthy tissues[27] and may even initiate immune reactions toward the nano-particles.[34] To further complicate the situation, PEGylation not only decreases the protein adsorption, but also impairs the nano-carriers' interaction with the cells. An interesting solution for this problem is to use sheddable PEG groups.[27, 35] With this strategy, PEG helps to achieve a long circulation time; however, the layer sheds after extravasation and increases the chance of the cellular uptake. The other strategy to circumvent the low cellular uptake of PEG-conjugated nano-particles is to conjugate cell-targeting moieties to the PEG's terminal hydroxyl group.

1.2.3.1.2. Targeted Drug Delivery

Another strategy to alter the biodistribution is active targeting via the incorporation of suitable moieties on the polymersomes' surface. Active targeting can increase the vesicles

'selective cellular uptake and decrease the unwanted toxicity to nearby cells/tissues. Polymersome functionalization has been carried out using proteins (including monoclonal antibodies and antibody fragments), peptides, small organic molecules, carbohydrates, and aptamers. Functionalized polymersomes have been used for theranostic purposes with different diseases such as cancers, inflammations, and brain-related disorders (Table 1.1).

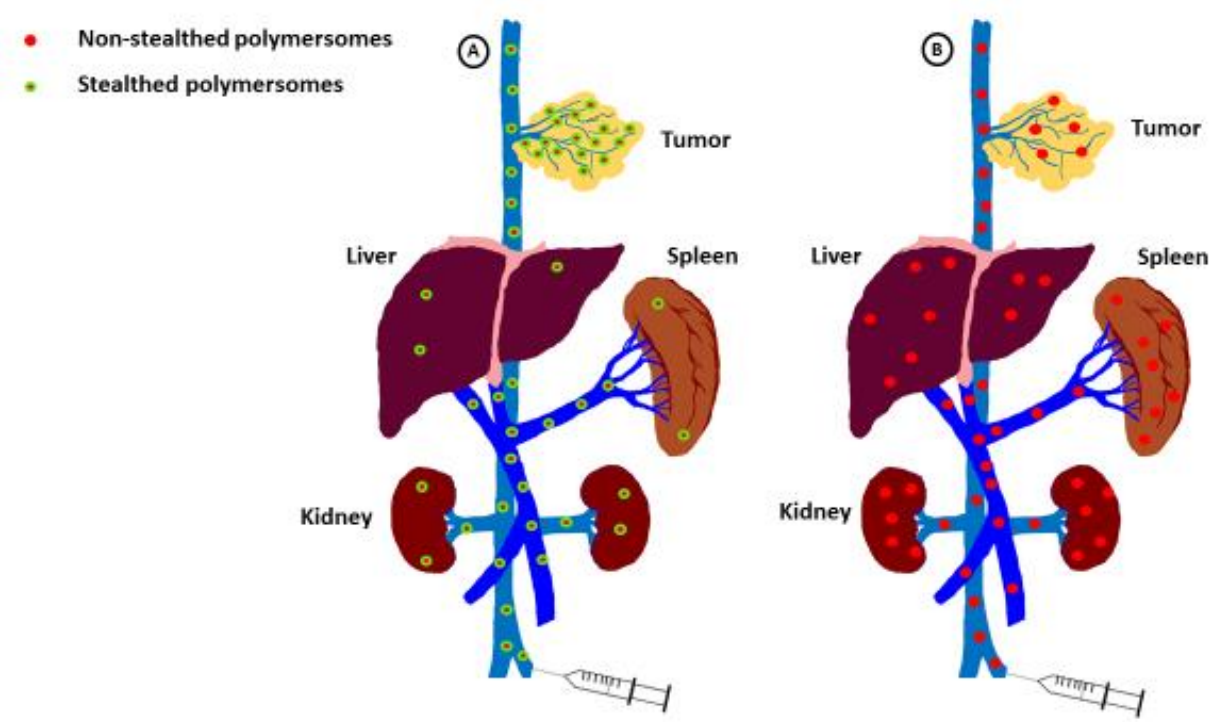

Figure 1.3. Schematic distribution of polymersomes after injection. (A) Stealth polymersomes can evade the RES and accumulate in the tumor tissue as a result of the EPR effect. In this case, systemic toxicity decreases, and the drug's therapeutic index increases. (B) Non-stealth polymersomes can be recognized by the RES and cleared from the blood rapidly. Tumor accumulation is not lower than that for RES organs such as the liver and spleen. In this case, systemic toxicity is an important concern.

Table 1.1. Polymersomes for targeted theranostic delivery.

Targeting moiety	**Target site**	**Polymersomes' building block**	**Drug/Imaging agent loaded**	**Application**	**Ref.**
Trastuzumab	Human Epidermal Growth Factor Receptor-2 (HER2)	Poly (trimethylene carbonate)- *b*-poly(glutamic acid)	Superparamagnetic iron oxide nanoparticles (USPIOs; γFe_2O_3)	Targeting and imaging of breast-cancer bone metastasis	[36]
Anti-EGFR antibody	Epidermal Growth Factor Receptor (EGFR)	Methoxy poly(ethylene glycol) (mPEG)-Gly-Phe-Leu-Gly-Phe-poly(D,L-lactide)	Acridine orange	Targeted drug delivery to the breast-cancer cells	[37]
Anti-ICAM-1 antibody	Intercellular Adhesion Molecule-1 (ICAM-1)	Poly(ethylene oxide) (PEO)-*b*-polybutadiene	–	Targeting the inflammatory tissues	[38]
Anti-HIgG antibody/ Anti-HSA antibody	Human IgG (HIgG)/ Human Serum Albumin (HSA)	poly(ethylene glycol) (PEG)- *b*-poly(D,L-1actic acid)	Carboxyfluorescein	Theranostic targeting	[39]
Trastuzumab	HER2	poly(dimethylsiloxane)-*b*-poly(2-methyloxazoline)	–	Theranostic delivery to the SKBR3 human breast-cancer cells	[40]
Anti-tansferrin receptor antibody (OX26)	Transferrin receptor	PEG-*b*-poly(ε-caprolactone)	NC-1900 / Coumarin-6	Brain drug delivery	[41]
Tet1 peptide	Trisialoganglioside clostridial toxin receptor on neurons	poly(ε-caprolactone)-*b*-PEG	Carboxy cyanine dye DiI	Drug delivery to the cochlear nerve	[42]
PR_b peptide	α5β1 integrins	PEO-*b*-poly(butadiene)	TNFα	Drug delivery to prostate cancer cells	[43]
RGD-containing peptide	Integrin adhesion receptors	PEO-*b*-poly(g-methyl-3-caprolactone)	–	Cell penetration of theranostics	[44]
RGD-containing peptide	Integrin adhesion receptors	PEG-*b*-poly(2-hydroxyethyl aspartamide) substituted with octadecyl chains	FITC-dextran	Cell penetration of theranostics	[45]

Table 1.1. Polymersomes for targeted theranostic delivery (continued).

Targeting moiety	**Target site**	**Polymersomes' building block**	**Drug/Imaging agent loaded**	**Application**	**Ref.**
Des-octanoyl ghrelin	Des-octanoyl ghrelin binding sites on blood-brain barriers	poly(carboxyl ethylene glycol-g-glutamate)-*co*-poly(distearin-g-glutamate)	Doxorubicin / Cy5.5	Blood-brain barrier (BBB) theranostic delivery	[46]
Folate & des-octanoyl ghrelin	Folate receptor & Des-octanoyl ghrelin binding sites on blood-brain barriers	poly(ethylene glycol)-*g*-glutamate)-*co*-poly (distearin-g-glutamate)	Met-enkephalin / Coumarin-6 / Cy5.5	Penetrating and targeting brain-cancer therapeutics	[47]
sLex & anti-ICAM-1 antibody	P/E selectin & ICAM-1	poly(1,2 butadiene)-*b*-poly(ethylene oxide)	Porphyrin, PZn2	Monitoring inflammatory diseases	[12, 48]
Lactoferrin/ Transferrin	Lipoprotein receptor-related protein (LRP)/ transferrin receptor	Poly (butadiene-*b*-ethylene oxide)+ PEG-*b*-lactic acid) (PEG-PLA)+ maleimide-PEG-PLA	Coumarin-6	Brain delivery	[49]
Lactoferrin	LRP	mPEG-poly(ε-caprolactone) + α-carboxyl poly(ethylene glycol)-poly(3-caprolactone)/ PEG-poly (lactide)	Doxorubicin / Tetrandrine / DiR / Coumarin-6	BBB and glioma targeting	[50, 51]

Overexpression of various cell surface receptors in malignancies and other disorders (such as inflammations) has been used for designing theranostic delivery systems. For instance, the expression of epidermal growth factor receptor increases on the cell surface for breast, colorectal, and lung cancers.[52] Hence, the anti-HER2 receptor antibody (trastuzumab) has been used to specifically target cancer cells (breast cancer cells metastasized to the bone) and to deliver contrast agents for magnetic resonance imaging that employs polymersomes.[36] Immobilizing different

antibodies is an interesting strategy, and several researchers have used this approach to target the proper cells/tissues. In this scenario, the antibody is usually immobilized via a covalent bond on the distal end of PEG block to avoid steric hindrance and to promote specific binding. Using antibodies as targeting agents has some disadvantages. These rather-large proteins are mostly immunogenic, and multi-functionalization of one carrier using antibodies is not favorable because of the antibodies' large size. In addition, developing monoclonal antibodies is fairly expensive and time consuming.

The other widely used targeting agents are peptides. Peptides are smaller and less immunogenic than antibodies, and attaching several peptides on the surface of a single polymersome is possible. Like antibodies, some peptides (e.g., Tet-1[42] and PR_b[43]) can be used to target a specific cell's surface receptors or molecules. Moreover, some peptides, such as the transactivator of transcription (TAT, derived from the human immunodeficiency virus), and many other chimeric peptides, such as transportan,[53] are known as cell-penetrating peptides. Some peptides guide the carriers toward subcellular compartments such as the nucleus and mitochondria. For instance, a heptapeptide derived from the Simian virus SV40 T-antigen has been used to construct nuclear-targeted delivery systems. These rather-new, nuclear-targeted drug-delivery systems are promising approaches that can increase drug efficacy, especially in terms of cancer therapy,[54] because they are targeted toward the cell nucleus which contains genetic material. However, there are many barriers that the carrier should overcome to reach the nucleus.

Carbohydrates play important roles with several biological processes, such as fertilization, cell-cell interactions, immune response, and signal transduction.[55] Hence, polymersomes that are conjugated to carbohydrates can be used for the targeted delivery of drugs/imaging agents. For

example, sialyl Lewisx (sLex), a carbohydrate which binds to selectins, has been conjugated to polymersomes as a way of targeting the inflammatory tissues.[12, 48]

Small molecules are sometimes are preferred as targeting groups because of their diversity, low molecular weight, small size, low immunogenicity, and inexpensiveness.[56] For example, folate (Vitamin B_6) is a small, organic molecule that has been widely used for targeted delivery systems because of the folate receptor's overexpression on the cells' surface with cancers of the ovary,[57, 58] urinary bladder,[59] lung,[60] breast,[61] and colon.[62]

1.2.3.2. Biodegradability

One drawback of polymersomes is the slow content release due to the robust and stable bilayer membrane.[25, 63] To control the drug release and increase the drug's bioavailability at the target site, stimuli-responsive polymersomes have been used extensively. These smart nano-structures can receive, transfer, and respond to stimuli effectively. Both external and internal stimuli have been tested for triggering the cargo release. External stimuli can be light[64] or a magnetic field,[65] whereas pH,[20, 66, 67] temperature,[68] and redox potential[19] are examples of internal stimuli. Using internal stimuli appears to be easier, cheaper, and more applicable.[16] Table 1.2 illustrates recently studied biodegradable polymersomes and their stimuli.

1.2.3.2.1. Redox-Responsive Polymersomes

Redox potentials are different for the intra/extracellular environments, and this difference tends to be augmented with the solid tumors of ovary, breast, lung, and head-and-neck cancers.[69] The redox potential is controlled by the concentration of glutathione (GSH, L-γ-glutamyl-L-cysteinylglycine, a tripeptide), free cysteine, and free homocysteine. Although free cysteine and homocysteine have roles in redox equilibria, GSH has been used more frequently as a stimulus for triggered content releases from polymersomes. GSH is the most prevalent reduced thiol source,

and there is a large inherent heterogeneity for intracellular (0.5-10 mM) and extracellular (10-40 μM) GSH concentrations. Hence, extracellular fluid is, naturally, an oxidizing environment. Both the extracellular oxidative environments[70] and intracellular reductive environments[71] have been utilized for polymersomes' drug release.

Table 1.2. Biodegradable polymersomes.

Block co-polymer	**Description**	**Release stimulus**	**Response**	**Ref.**
PEG-S-S-PLA	–	Redox potential	Bond cleavage	[19]
PEG–PTMBPEC	–	pH	Hydrolysis	[66]
mPEG-b-$(polyHis)_2$ -CL	Cholesterol incorporated	pH	Hydrophobic/ hydrophilic transition (structural transition)	[20]
PEG-PTTMA-PAA	–	pH	Hydrolysis	[67]
PEG-PAA PNIPAM	Cystamine-crosslinked	Temperature & reduction	Formation/deformation	[68]
PTMC-b-PGA	Polymersomes loaded with γ-Fe_2O_3	Magnetic field	Local hyperthermia	[65]
PEG-2NPA-PLA	–	Light	Peptide bond cleavage	[64]
PMCL-ONB-PAA	–	Light	Cleavage of linker	[72, 73]
mPEG-pep-PDLLA	–	Enzyme (Cathepsin B)	Peptide cleavage	[37]

PEG-S-S-PLA: poly (ethylene glycol)-b-poly (lactic acid); PEG–PTMBPEC: poly (ethylene glycol)-b-poly (2,4,6-trimethoxybenzylidenepentaerythritol carbonate); mPEG-b-$(polyHis)_2$-CL: methoxy poly (ethylene glycol)-b-poly (L-histidine)-cholesterol incorporated; PEG-PTTMA-PAA: poly (ethylene glycol)-b-poly (trimethoxybenzylidene tris(hydroxymethyl)ethane methacrylate)-b-poly (acrylic acid); PEG-PAA-PNIPAM: poly (ethylene glycol)-b-poly (acrylic acid)-b-poly (N-isopropylacrylamide); PTMC-b-PGA: Poly (trimethylene carbonate)-block-poly (L-glutamic acid); PEG-2NPA-PLA: poly (ethylene glycol)-2-nitrophenylalanine-poly (lactic acid); PMCL-ONB-PAA: poly (methyl caprolactone)-O-nitrobenzyl-poly (acrylic acid); and mPEG-pep-PDLLA: methoxy poly (ethylene glycol)-Gly-Phe-Leu-Gly-Phe- poly (D,L-lactide)

Different strategies have been used to construct redox-sensitive drug carriers. Bioreducible polymersomes that possess disulfide bonds respond to the redox potential changes by reversible bond breakage. The number and location of the incorporated disulfide bonds allow fine-tuning of the release property from the vesicles. A typical composition that has been used widely for preparing redox-sensitive micelles[74] and liposomes[75] has been successfully implemented with polymersomes.[19] These co-polymers contain a disulfide bond to connect the hydrophobic and

hydrophilic polymers. Reductive conditions destabilize the formulation and trigger the release of the encapsulated payload. Crosslinked polymersomes display increased stability and, at the same time, are responsive to a reducing environment.[76] Although the disulfide bond in the polymersomes' backbone increases the drug release in the reducing environments, premature payload leakage may occur due to prolonged circulation with low concentrations of reducing agents in the blood which may decrease the therapeutic efficacy of the redox-sensitive polymersomes.

1.2.4. Pharmacokinetic Properties of Polymersomes

The fate of the pharmaceutical agents after administration are determined by measuring their pharmacokinetic properties. However, polymersomes are new drug carriers, and not many detailed pharmacokinetic animal studies are reported (the reported results are summarized in Table 1.3). It should be noted that a drug's pharmacokinetic properties are related to the carrier chemistry. A comparison of the pharmacokinetic properties of PolyDoxoSomes (doxorubicin loaded polymersomes) with that of LipoDox (commercially available liposomal doxorubicin)[77] is reported. PolyDoxoSome's lower AUC (568 versus 229 μg h/mL), and shorter $t_{1/2}$ (22 versus 35 h) were advantageous for decreasing the dose related toxicities and side effects. Although the AUC and $t_{1/2}$ values were different, the therapeutic efficacy of the PolyDoxoSome was comparable to that of the LipoDox. Another study compared the pharmacokinetics of AmbiSome (liposomal amphotericin B) and amphotericin-B-loaded polymersomes.[78] A Lower AUC value was observed for the polymersomes (11,354 versus 62, 219 ng h/ mL), due to the direct delivery of the drugs to the target tissues. However, higher $t_{1/2}$ (74 versus 27 h) was reported for the polymersomes, due to the slow release of the encapsulated drugs. The polymersomal formulations were deemed to be

better for treating fungal infections due to the longer circulation of these drug-loaded nano-vesicles.

Paper information: Polymersome-based drug-delivery strategies for cancer therapeutics (Ther. Deliv. (2015) 6(4), 521–534).[3]

https://www.ncbi.nlm.nih.gov/pubmed/25996048

1.3. Organization of the Thesis

In an effort to search for more effective treatments (higher therapeutic index and lower systemic toxicity) for pancreatic cancer, we have prepared two different polymersomal formulations which are targeted toward nucleus of pancreatic cancer cells (Chapters 2 and 3). Nucleus is the largest organelle in the cells and contains the genetic materials[79]. Hence, delivering the drugs directly to the nucleus can increase the drug's efficiency. Both polymersomal formulations are stable in the extracellular environment and in the cytoplasm. However, in the presence of high concentration of reducing agents in the cancer cell's nuclei, their bilayer structure disrupts and their content releases in the nucleus.

In one formulation (Chapter 2), we have used a small molecule (acridine orange) which has intrinsic affinity towards DNA[80]. The molecule is conjugated to the surface of polymersomes using the Copper (II)-catalyzed azide-alkyne cycloaddition ("Click" reaction)[81]. The polymersomes encapsulate the drugs gemcitabine and doxorubicin to utilize their synergistic effects against pancreatic cancer. The two-drug combination is currently in the clinical trials for a variety of advanced and metastatic cancers, including pancreatic ductal adenocarcinoma.

Table 1.3. Pharmacokinetic properties of polymersomal formulations.

Polymersomes building blocks	**Drug**	**Dose**	**AUC**	**Free drug AUC**	**Drug $t_{1/2}$ (h)**	**Free drug $t_{1/2}$ (h)**	**Animal**	**Ref.**
Polybutadiene (PBd)-b- PEG	NA	0.42 mg/kg of polymersomes	NA	NA	24 h	NA	Male Balb/C mice	[82]
PEG-b-poly(3-caprolactone (PCL)	Oxymatrine	30 mg/kg of drug	30,602 ± 3982 ng h/ mL	16,234 ± 1385 ng h /mL	3.12 ± 0.25*	1.41 ± 0.57*	Male Sprague-Dawley rats	[83]
PEG-PLA	Doxorubicin	6 mg/kg of drug	569 μg h/mL	4 μg h/mL	21.9	0.49	Female Sprague Dawley rats	[77]
PBD-PEO:PEG-PLA:MAL-PEG-PLA Lactoferrin conjugated	NA	20 mg/kg of polymersomes	219.5 ± 25.6 mg h /L	NA	6.49	NA	Mice	[49]
PBD-PEO:PEG-PLA:MAL-PEG-PLATransferrin conjugated	NA	20 mg/kg of polymersomes	404 ± 49 mg h /L	NA	13.6	NA	Mice	[49]
PEG-PLA	Amphotericin B	1 mg/kg of drug	11,354 ng h /mL	NA	73.84*	NA	Male SD rats	[78]

*Terminal phase half life

In the second formulation (Chapter 3), we have used a different strategy to target the cancer cell nuclei. We have designed an MMP-7 enzyme responsive, nuclear targeted peptide which only gets activated after cleavage by MMP-7 enzyme. MMP-7 enzyme[84] is overexpressed in the pancreatic cancer tumor microenvironment. Therefore, its overexpression can be used to target the tumor microenvironment. Once the peptide on the surface of the polymersomes is cleaved by MMP-7, the nuclear localizing signal is activated and transports the vehicle to the cancer cell's nuclei. We encapsulated with curcumin or doxorubicin in the polymersomes and tested their simultaneous effect on pancreatic cancer cells.

The third formulation is cell cytoplasm-targeted polymersomes, designed to target the prostate cancer cells. Prostate-specific membrane antigen (PSMA) is overexpressed in prostate cancer cells[85]. Since the PSMA protein has folate hydrolysis activity[86], it can be targeted by the folate molecules. We have incorporated folate conjugated-phospholipid PEG derivative in the polymersomes structure to target the PSMA protein. To induce apoptosis, we intentionally disrupted the calcium homeostasis[87] of the cancer cells by suddenly increasing the calcium ion concentration in the cytoplasm. High concentration of calcium ions in the presence of folic acid salcium phosphate crystal nucleation, which leads to cell death[88]. The calcium ion encapsulated polymersomes are responsive to the reducing environment and release their contents in the prostate cancer cell's cytoplasm.

This thesis is a paper based thesis and we have planned to publish all the chapters in peer-reviewed journals (section 2 and 3 are published, and section 4 is submitted). Following paragraphs of the introduction are the abstracts for these papers.

1.3.1. Acridine Orange Conjugated Polymersomes for Simultaneous Nuclear Delivery of Gemcitabine and Doxorubicin to Pancreatic Cancer Cells

Considering the systemic toxicity of chemotherapeutic agents, there is an urgent need for developing new targeted drug delivery systems. Herein, we have developed a new nuclear targeted, redox sensitive, drug delivery vehicle to simultaneously deliver the anticancer drugs gemcitabine and doxorubicin to the nuclei of pancreatic cancer cells. We prepared polymeric bilayer vesicles (polymersomes), and actively encapsulated the drug combination by the pH gradient method. A redox-sensitive polymer (PEG-S-S-PLA) was incorporated to sensitize the formulation to reducing agent concentration. Acridine orange (AO) was conjugated to the surface of the polymersome imparting nuclear localizing property. The polymersomes' toxicity and efficacy were compared with those of free drug combination using monolayer and three-dimensional spheroid cultures of pancreatic cancer cells. We observed that the redox sensitive, nuclear-targeted polymersome released more than 60% of their encapsulated contents in response to 50 mM glutathione. The nanoparticles are non-toxic; however, the drug encapsulated vesicles have significant toxicity. The prepared formulation can increase the drug's therapeutic index by delivering the drugs directly to the cells' nuclei, one of the key organelles in the cells. This study is likely to initiate research in targeted nuclear delivery using other drug formulations in other types of cancers.

Paper information: Acridine Orange Conjugated Polymersomes for Simultaneous Nuclear Delivery of Gemcitabine and Doxorubicin to Pancreatic Cancer Cells. (DOI:10.1021/acs.bioconjchem.5b00694, Bioconjugate Chem. 2016, 27, 762−771).[7]
https://www.ncbi.nlm.nih.gov/pubmed/26848507

1.3.2. Nuclear Localizing Peptide Conjugated, Redox Sensitive Polymersomes for Delivering Curcumin and Doxorubicin to Pancreatic Cancer Micro-tumors

Improving the therapeutic index of anticancer agents is an enormous challenge. Targeting decreases the side effects of the therapeutic agents by delivering the drugs to the intended destination. Nanocarriers containing the nuclear localizing peptide sequences (NLS) translocate to the cell nuclei. In this study, we designed a "masked" NLS peptide which is activated only in the presence of overexpressed matrix metalloproteinase-7 (MMP-7) enzyme in the pancreatic cancer microenvironment. This peptide is conjugated to the surface of redox responsive polymersomes to deliver doxorubicin and curcumin to the pancreatic cancer cell nucleus. We have tested the formulation in both two and three-dimensional cultures of pancreatic cancer and normal cells. Our studies revealed that the drug encapsulated polymeric vesicles are significantly more toxic towards the cancer cells (shrinking the spheroids up to 49%) compared to the normal cells (shrinking the spheroids up to 24%). This study can lead to the development of other organelle targeted drug delivery systems for various human malignancies.

Paper information: Nuclear Localizing Peptide-Conjugated, Redox-Sensitive Polymersomes for Delivering Curcumin and Doxorubicin to Pancreatic Cancer Microtumors. (DOI: 10.1021/acs.molpharmaceut.7b00014).[89]

http://pubs.acs.org/doi/abs/10.1021/acs.molpharmaceut.7b00014

1.3.3. Targeted Cytoplasmic Calcification: A Drug-Free, Polymersomal Prostate Cancer Therapy

Finding new strategies to treat cancer with lower side effects and increased quality of life are important for therapy. Calcium homeostasis dysregulation leads to cell death via several mechanisms. We are testing a new strategy to kill cancer cells by intentionally increasing the

calcium ion concentration inside the cell cytoplasm. We have targeted prostate cancer cells (LNCaP) overexpressing the prostate-specific membrane antigen (PSMA) receptors by polymersomes presenting folic acid on the surface. The polymersomes encapsulate a high concentration of calcium chloride and release the contents in the cytoplasm in response to the increased reducing agent concentration. We used HEK-293 as control cells lacking the PSMA receptor on the plasma membrane. In vitro studies in monolayer and three-dimensional spheroids revealed the efficient cancer cell killing capabilities (cell viability in monolayer culture: 34% ± 10, cell viability in three-dimensional culture: 38 % ± 4) of the formulation. Results of this study can be a promising starting point for using less toxic compounds in cancer treatment.

2. ACRIDIN ORANGE CONJUGATED POLYMERSOMES FOR SIMULTANEOUS NUCLEAR DELIVERY OF GEMCITABINE AND DOXORUBICIN TO PANCREATIC CANCER CELLS[2]

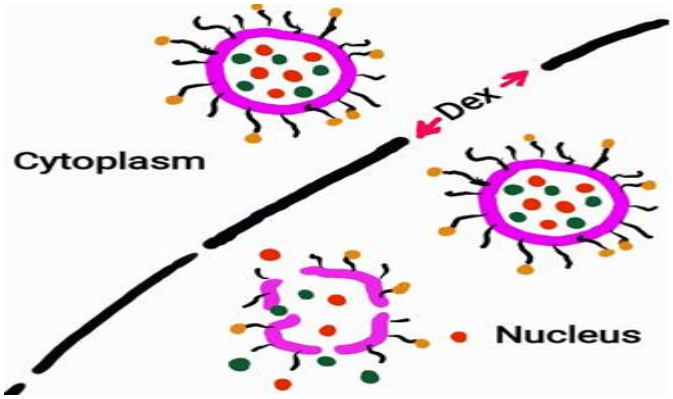

Figure 2.1. Graphical abstract.

2.1. Introduction

Pancreatic cancer is one of the leading causes of cancer-related death in the world.[90] Chemotherapeutics have been used as an adjuvant, neoadjuvant, and palliative treatments for the disease. For both exocrine pancreatic cancers and neuroendocrine pancreatic tumors (NETs), combination chemotherapy is more successful, albeit eliciting severe side effects. While gemcitabine is the first line of therapy for pancreatic cancer, doxorubicin and streptozocin are usually used to treat NETs.[91] The combination of gemcitabine and doxorubicin have shown synergistic benefits in different malignancies.[92, 93, 94] However, chemotherapeutic side effects

[2] This section is coauthored by Tayebeh Anajafi, Michael D. Scott, Seungyong You, Xiaoyu Yang, Yongki Choi, Steven Y. Qian, and Sanku Mallik. Tayebeh had primary responsibility to conduct all the experiments, analyze the data and write the manuscript. Michael had the responsibility to conduct NMR on the polymers. Seungyong imaged the polymersomes using AFM. Xiaoyu recorded mass spectrum for the synthesized polymers. Drs. Choi, Qian and Mallik verified the data and advised on experimental designs.

decrease the patient's quality of life. As a result, increasing the therapeutic efficacy of conventional anti-cancer drugs is one of the important issues in cancer treatment. Targeted drug delivery is an attractive solution with many benefits over conventional chemotherapy.

Mitochondria[95, 96] and nucleus,[97, 98] the two principal subcellular compartments, have been targeted to interrupt cancer cell growth in different malignancies. Mitochondria, known as the powerhouse of cells, control all the primary metabolic processes. Consequently, devitalizing this organelle can be a strong cell toxicant. However, the impermeable inner membrane limits the delivery of therapeutics into this organelle. On the other hand, the nucleus is large compared to the mitochondria and controls several vital cellular processes. Therefore, attacking the nucleus is an attractive strategy for cell cycle arrest and inducing cell death. The nuclear pore complexes[99] in the nucleus membrane connect the nucleoplasm to the cytoplasm and regulate the entry and exit of small molecules. It is estimated that about 500 -1000 transporters (both active and passive) take place through these pores every second.[100, 101, 102]

The diameter of the nuclear pores limits the size of the molecules which can be transported into the nucleus. Therefore, dilating the nuclear pores is a promising strategy for delivering large molecules into the cell nucleus. For example, the glucocorticoid analog dexamethasone dilates the nuclear pores to 110 nm and stimulates the formation of giant pores (~300 nm).[103] As a result, this steroid is recognized as a therapeutic agent not only to counteract the chemotherapeutic side effects, but also to increase the likelihood of nuclear delivery of the drugs (in case of targeted therapy).

Liposomes,[104, 105] silica,[79] and magnetic nanoparticles[106] have been targeted to the cell nucleus to release the contents. However, to the best of our knowledge, there is no report of nuclear drug delivery using polymersomes. Polymersomes are hollow vesicles prepared from amphiphilic

polymers with an aqueous interior (capable of encapsulating hydrophilic compounds), and a bilayer membrane (which can incorporate with hydrophobic drugs).[3] The presence of the long-chain polymers renders these vesicles more stable compared to liposomes [3, 13, 14] The hydrophilic polymer in the outer layer endows the vesicles with long circulating properties. The size can be adjusted (~200 nm) for passive accumulation in tumor site employing the enhanced permeation and retention effect.[107] Incorporation of biocompatible polymers in polymersome's structure decreases the chance of immune response and systemic toxicity.[3, 30]

However, polymersomes' robust membrane hinders drug release at the target site. Consequently, different stimuli have been used to trigger the release of encapsulated contents from these vesicles. These stimuli can be external (light [64] and magnetic field [65]), or internal (redox potential,[19] pH,[20, 66, 67] and temperature[108]). Since the application of internal stimuli is safer, and easier, [16] and eukaryote cell nuclei contain a high concentration of reducing agents,[109, 110] redox-sensitive polymersomes have the potential to release rapidly encapsulated drugs the nucleus.

Herein, we report new redox-sensitive, fluorescent polymersomes, encapsulating the anticancer drugs gemcitabine and doxorubicin. We conjugated acridine orange (AO, which has an intrinsic affinity toward DNA due to intercalation) on the surface of the polymersomes (Figure 2.2) for active targeting to the cell nuclei.[80, 111, 112] AO has been used as imaging agents for *in vivo* models[113] and as a therapeutic agent in human sarcomas.[114] The nuclear localization of the vesicles was confirmed by fluorescent microscopy. We demonstrated the efficacy of the nano-vesicles employing both conventional two-dimensional monolayer culture and three-dimensional spheroids of pancreatic cancer cells. We note that the nuclear localization of AO is not selective for the cancer cells. However, the size of the polymersomes and the presence of the PEG layer will allow

them to accumulate selectively in the tumors due to the Enhanced Permeation and Retention (EPR) effect.[115, 116]

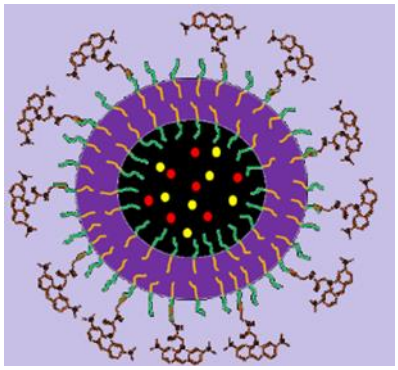

Figure 2.2. Schematic representation of acridine orange conjugated to the surface of polymersomes encapsulating the anticancer drugs doxorubicin and gemcitabine.

2.2. Results and Discussion

2.2.1. Polymer Synthesis, Polymersome Preparation, and Characterization

The ratio of hydrophilic to hydrophobic parts of a copolymer (*f* value) has an important role in polymersome formation.[17, 18] The block co-polymers we have used in this study (Figure 2.1) have *f* values of about 25%. The block copolymers were synthesized using ring-opening polymerization) (Appendix A), and their average molecular weights were measured by ^{1}H NMR spectroscopy. To impart redox-sensitive property, we have prepared the disulfide containing polymer (Figure 2.3 A). In addition, to conjugate the nuclear localizing group (alkyne conjugated acridine orange, Figure 2.4) to the surface of the polymersomes, we used azide-alkyne cycloaddition reaction[81] (Scheme 2.1). Hence, azide-terminated polymers were prepared (Figure 2.3 B) and incorporated into the polymersomes. The ratio of these polymers was optimized based on the release of encapsulated calcein from the vesicles. We have removed any free (un-conjugated) AO from the polymersomes employing a Sephadex gel filtration column (Materials

and Methods). Hence, we do not anticipate any significant amount of free AO in the polymersomes.

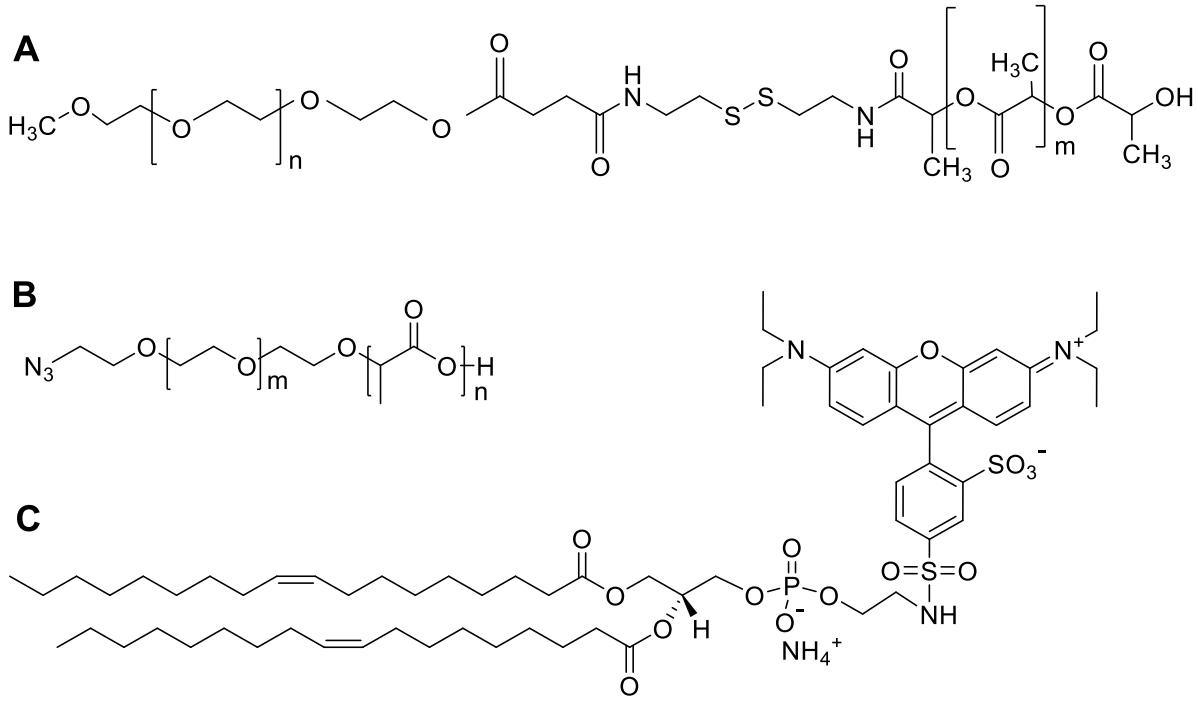

Figure 2.3. The structure of the synthesized polymers used in preparing the polymersomes. **A**: PEG (1900)-S-S-PLA (6100), **B**: N_3-PEG (2000)-PLA (6000). A small amount of the fluorescent lissamine rhodamine lipid (**C**) was incorporated in the polymersomes for ease of visualization.

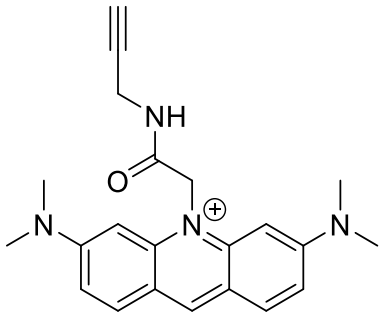

Figure 2.4. Alkyne conjugated acridine orange moiety.

To confirm the presence of the AO on the surface of the polymersomes, we monitored the fluorescence emission spectra (excitation: 450 nm) of polymersomes before and after the "Click" reaction (Figure 2.5 C). We chose the excitation at 450 nm since lissamine rhodamine does not

have significant absorption at this wavelength (Figure 2.5 A). The spectral overlap between the emission from acridine orange (500 nm – 600 nm, Figure 2.5 B) and absorption of lissamine rhodamine (Figure 2.5 A) indicated the possibility of energy transfer between these two dyes when present on the surface of the polymersomes. The clear difference between the emission intensity of the lissamine rhodamine at 575 nm before and after AO conjugation (Figure 2.5 C, blue and green traces) is likely due to the energy transfer from excited state AO to the ground state of lissamine rhodamine. The energy transfer precluded us from determining the concentration of conjugated AO using fluorescence spectroscopy. Before the release experiments, we removed any free AO from the polymersomes by gel filtration (Materials and Methods). From the initial concentrations of the polymersome components and the dilution factor for gel filtration, we estimated that the concentration of the lissamine rhodamine to be nearly the same before and after the AO conjugation reaction. We used 40 mol% of azide containing polymer, and considering about 60% of this polymer will be exposed to the surface, we estimate that 0.03 µmol of the AO moiety has been conjugated to the surface of the polymersomes.

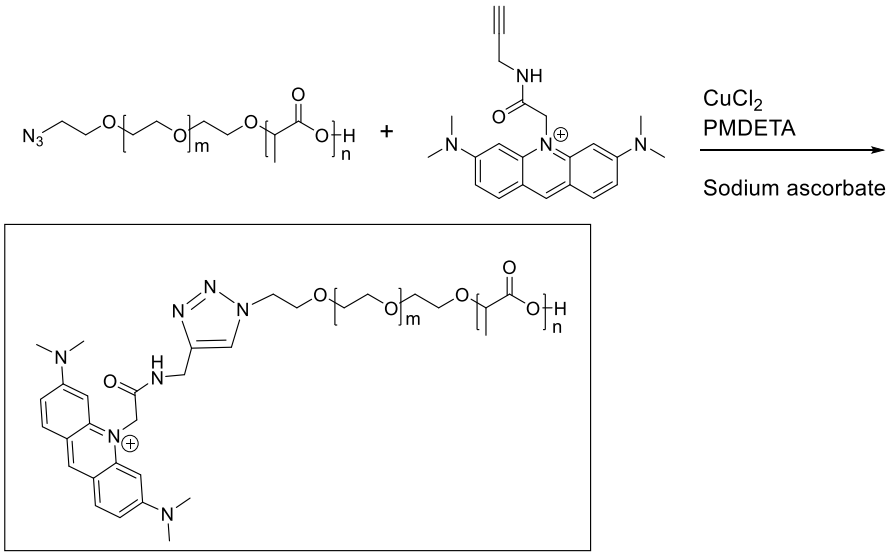

Scheme 2.1. Functionalization of the polymersomes using the Cu2+ catalyzed [2+3]-cycloaddition reaction.

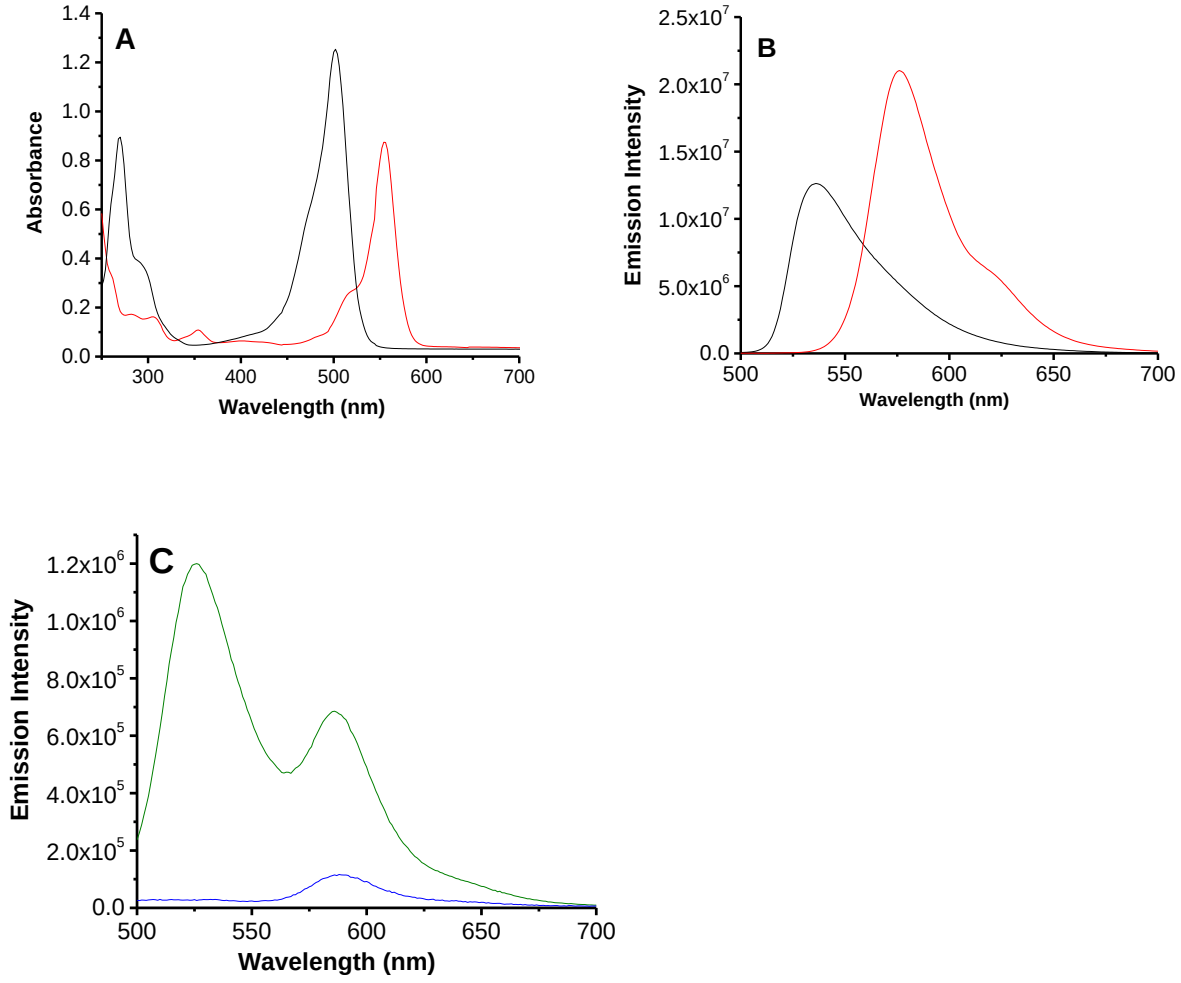

Figure 2.5. Characterization of acridine orange (AO) conjugation to the polymersomes by fluorescence spectroscopy. (A) Absorption spectra of lissamine rhodamine lipid (red trace) and AO (black trace). (B) Emission spectra for lissamine rhodamine lipid in chloroform (red trace), and AO in DMSO (black trace) (excitation: 450 nm). (C) Emission spectra (excitation: 450 nm) of the polymersomes before (blue trace) and after (green trace) the "Click" reaction.

Polymersomes were prepared using the solvent exchange method,[3] and their morphology were confirmed by transmission electron microscopy (TEM, Figure 2.6) and atomic force microscopy (AFM, Figure 2.6). Size distribution and polydispersity index of the polymersomes were determined by light scattering method (Figure 2.9). To improve the tumor accumulation by the enhanced permeation and retention effect,[107] the prepared polymersomes possess a hydrodynamic diameter of 170 $\pm$ 4nm. We observed that the size of the polymersomes increased

slightly after conjugation of acridine orange (Table 2.1). We noted a similar size increase after drug encapsulation, possibly due to drug precipitation[117] inside the polymersomes' aqueous core (Table 2.1).

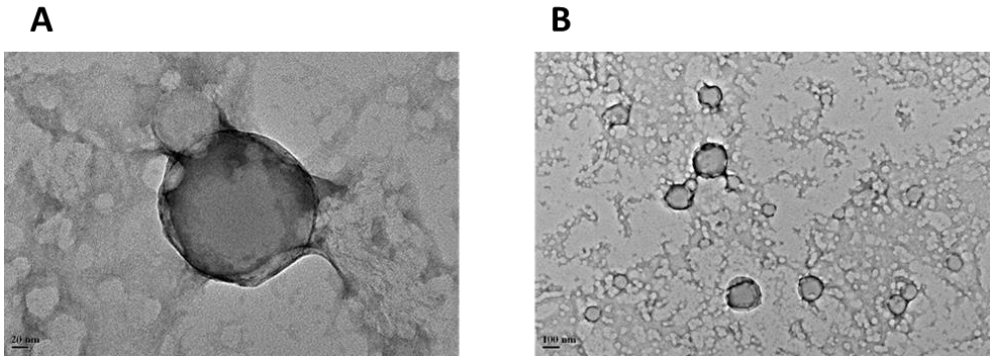

Figure 2.6. Transmission electron microscopic (TEM) images of polymersomes. The scale bar in A is 20 nm, and in B is 100 nm.

2.2.2. Demonstration of Redox-Triggered Contents Release from the Polymersomes

The tripeptide glutathione (γ-glutamyl-cysteinyl-glycine, GSH) is one of the major components for maintaining redox homeostasis in the cytoplasm and organelles such as nucleus and mitochondria.[118] GSH concentration is higher in the cancer cells compared to the healthy counterparts. In addition, the cell nucleus contains higher amounts of this tripeptide compared to the cytosol.[118] We have used these concentration differences to trigger drug release from the polymersomes inside the nuclei of PANC-1 cells. Specifically, we have studied the release of encapsulated calcein in the presence of 10 mM (mimicking cytosol) and 50 mM (mimicking cell nucleus) GSH. We observed that 10 mM GSH released about 15% of the encapsulated calcein from the polymersomes during 40 minutes. However, in the presence of 50 mM GSH, 55% of calcein was rapidly released from the vesicles (Figure 2.9). The lack of complete contents release possibly indicates that the vesicles are undergoing morphological changes in the presence of 50

mM GSH, rather than a complete loss of structure. Our atomic force microscopic studies corroborate this hypothesis (Figure 2.7, Panel I).

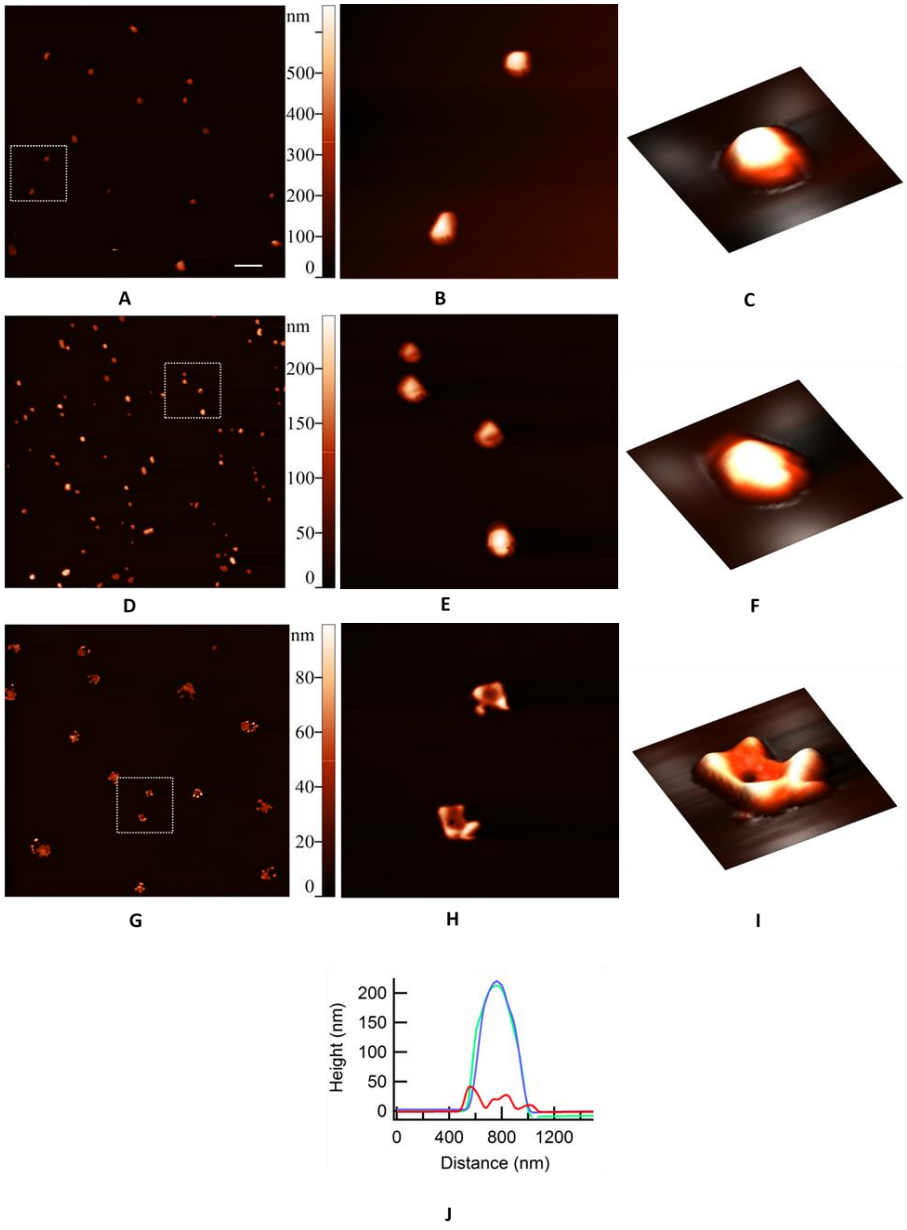

Figure 2.7. Atomic Force Microscopy (AFM) images of polymersomes. (A-C) AO-polymersomes before glutathione treatment. (D-F) AO-polymersomes treated with 10 mM glutathione. (G-I) AO-polymersomes treated with 50 mM glutathione. (J) Height profile overlay of the polymersomes (green trace: no glutathione), blue (10 mM glutathione), and red trace (50 mM glutathione). The scale bar in (A) is 2 µm.

Table 2.1. Hydrodynamic diameters of the polymersomes before and after AO conjugation, and after drug encapsulation.

Polymersomes	Average hydrodynamic diameter (nm)	Polydispersity Index (PDI)
Polymersomes	129.1 ± 6.6	0.2 ± 0.02
AO-polymersomes	170.3 ± 4.1	0.2 ± 0.01
Polymersomes encapsulating doxorubicin and gemcitabine	242.1 ± 6.6	0.3 ± 0.02

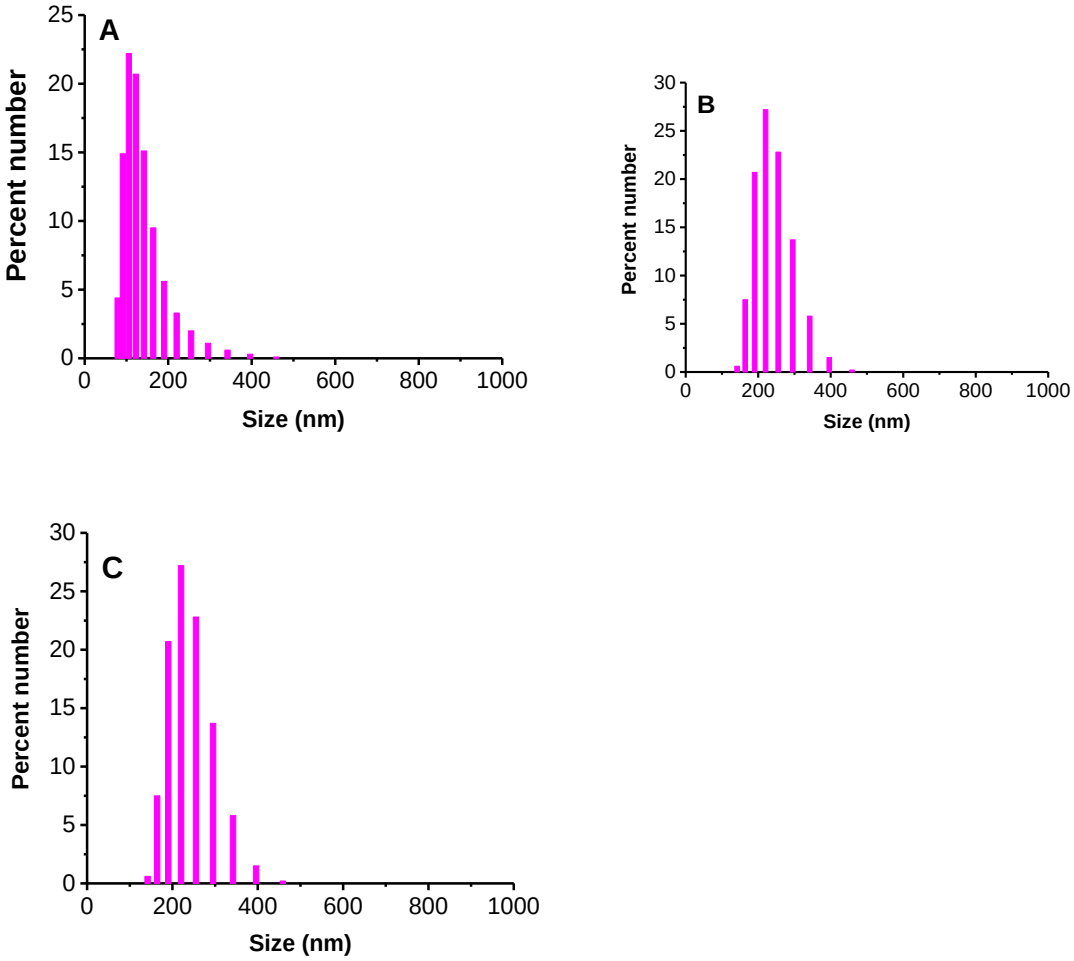

Figure 2.8. Size distribution of the polymersomes as determined by dynamic light scattering. (A) Polymersomes before AO conjugation, (B) AO-conjugated polymersomes, and (C) AO-polymersomes encapsulating gemcitabine and doxorubicin.

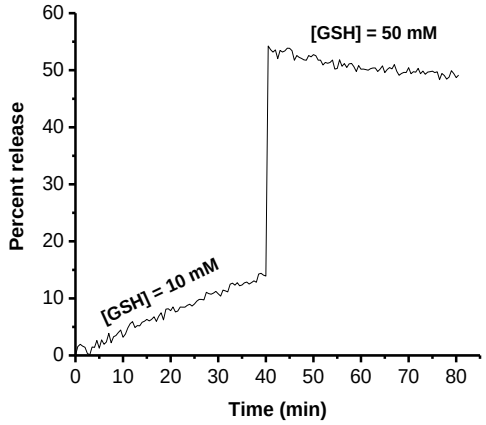

Figure 2.9. Release profile of the polymersomes. Calcein release was monitored for 40 minutes after adding 10 mM GSH to the polymersomes. The concentration of GSH was then increased to 50 mM, and the release was monitored for another 40 minutes. The plot is the average of three release profiles.

2.2.3. Effect of Redox Potential Changes on Polymersome Structure

We decided to study the GSH-mediated changes in the polymersome structure employing atomic force microscopy (AFM). We observed that treating the polymersomes with 10 mM GSH did not have a significant effect on their spherical shape (Figure 6B). However, incubation of the vesicles with 50 mM GSH destroyed the spherical shape (Figure 6C).

2.2.4. Gemcitabine and Doxorubicin Encapsulation in the Polymersomes

For the cellular studies, we encapsulated gemcitabine and doxorubicin in the polymersomes using the active pH gradient method (described in the Material and Methods). The encapsulation efficiency, determined employing a dual-wavelength method developed in our laboratory,[19] was found to be 76% for gemcitabine and 22% for doxorubicin. These two anticancer drugs affect different biochemical pathways to kill cancer cells, and the combination shows synergistic benefits.[119]

2.2.5. Demonstration of Nuclear Localization and Polymersomes' Efficacy Using Monolayer Cell Culture

After optimizing the release from the polymersomes, we proceeded to demonstrate nuclear localization of the vesicles employing the conventional, monolayer culture of the PANC-1 cells. To facilitate nuclear localization, we treated the cells with dexamethasone (80 μM) before adding the polymersomes. Dexamethasone is reported to dilate the nuclear pores.[103] After incubation and washing, we imaged the PANC-1 cells in a confocal fluorescence microscope (Figure 2.10). We observed that the AO-polymersomes accumulated in the cell nuclei more efficiently (Figure 2.10, Column 2, AO-polymersomes loaded with drugs) compared to the control vesicles lacking the AO moiety (Figure 2.10, Column 1, Polymersomes loaded with drugs) or the free drugs (Figure 2.10, Column 3, Free Dox). The efficiency of AO-polymersomes is likely due to the intercalation of the AO group to nuclear DNA[106] in the PANC-1 cells. In a separate experiment, we incubated the PANC-1 cells with AO-polymersomes without dexamethasone pre-treatment. We noticed a decrease in nuclear localization of the polymersomes, indicating the effect of dexamethasone in enhancing nuclear delivery (Figure A1).

To evaluate the efficacy of the drug encapsulated polymersomes, we performed Alamar Blue assay using the monolayer cultures of PANC-1 cells (Figure 2.11). We observed that the AO-polymersomes (without any drugs) were non-toxic to the cells (Figure 2.11, green column). The combination of gemcitabine and doxorubicin was toxic to the cells, with a cell viability of 31% (Figure 2.11, blue column). Also, the AO-polymersomes encapsulating the two drugs decreased the cell viability to 36% (Figure 2.11, red column).

2.2.6. Demonstration of Polymersomes' Efficacy Using Three-dimensional, Spheroid Cultures

The multicellular spheroids are better mimics of tumors due to the cell-cell interactions and the three-dimensional shape. Among the reported approaches to growing cancer cell spheroids,[120, 121, 122] we selected the agar micromolds.[123] In this approach, 96 similar size spheroids are obtained. We monitored the growth of the PANC-1 cell spheroids (Figure 2.12) employing a confocal microscope. After 8 days of culture, we observed a hypoxic core and a surrounding proliferating layer of the cells in the spheroids (Figure 2.12, Panel D). Furthermore, to better understand the spheroids shapes, we have imaged the 8-day old spheroids at multiple focal planes (Appendix A). To determine cell viability, we treated the 5 day old spheroids with the polymersomes. After 72 hours, the spheroids were dislodged, trypsinized to prepare a homogenous single cell suspension, and the cell viability assays were performed (Figure 2.11). We observed that the drug encapsulated AO-polymersomes reduced the cell viability to 30% (Figure 2.11, red column). Comparison of Figures 10 A and 10 B also demonstrates that the polymersomes' effectiveness is not diminished in cancer cell spheroids compared to the monolayer cultures.

To further demonstrate the efficiency of the drug encapsulated AO-polymersomes, we treated the 8 day old spheroids with the polymersomes, washed, and monitored their growth for another 6 days (Figure 2.13). We observed that the untreated spheroids nearly doubled in size in 11 days (Figure 2.13, green circles). The free drug combination decreased the growth to 29% (Figure 2.13, pink inverted triangles). However, the drug encapsulated, AO-polymersomes shrank the PANC-1 spheroids to 3% after 14 days, rendering them nearly same in size as the 3-day old cultures (Figure 2.13, red circles).

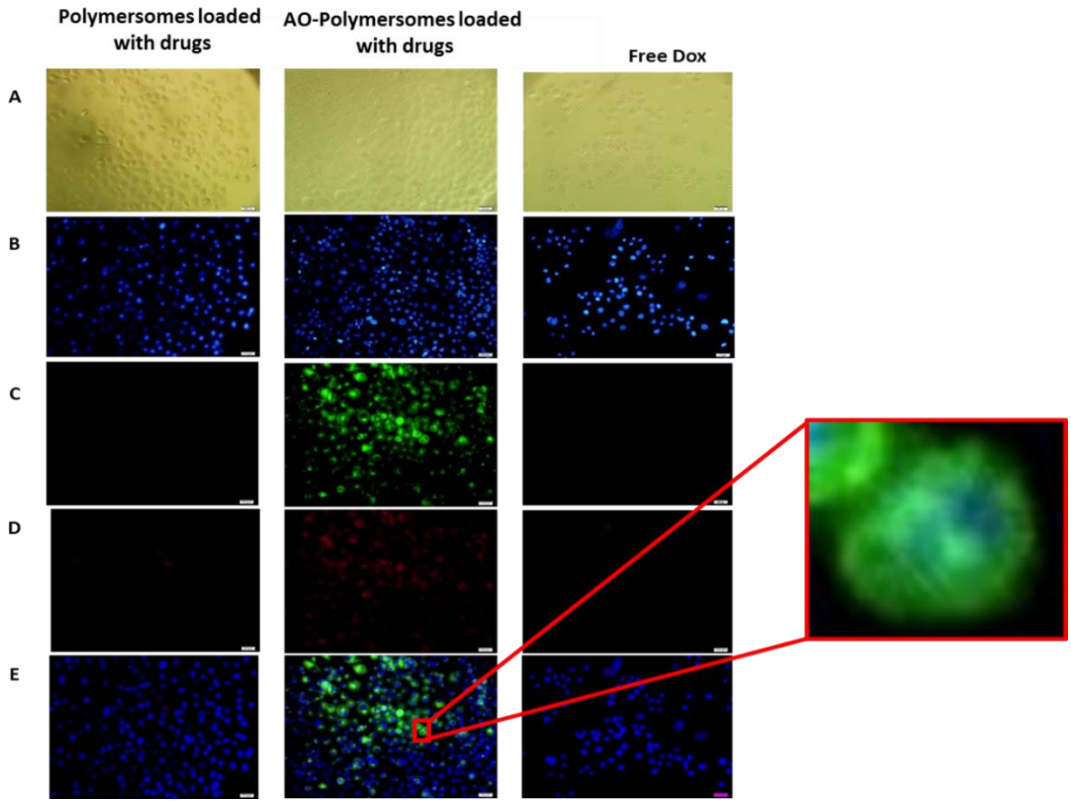

Figure 2.10. Confocal fluorescence microscopic images of nuclear localization of polymersomes in PANC-1 cells. (A) Bright field microscopy image, (B) Hoechst stained nuclei of the cells (DAPI filter), (C) images recorded with FITC filter (the green color is showing the AO location), (D) images recorded using TRITC filter (the red color is showing the presence of doxorubicin or lissamine rhodamine), and (E) overlayed images (scale bars: 200 µm).

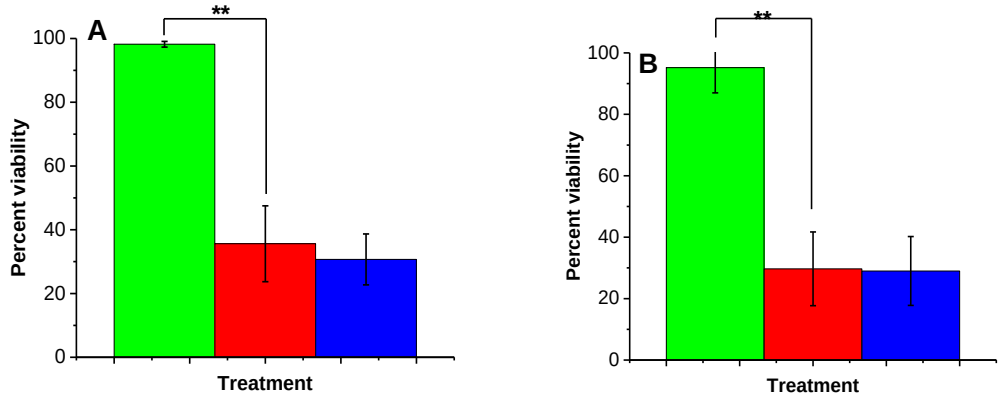

Figure 2.11. Viability analysis of PANC-1 cells. The cells were treated with AO-polymersomes (green column), drug encapsulated AO-polymersomes (red column) or free drug combination doxorubicin-gemcitabine (blue column) in monolayer culture (A), and in 3D spheroids (B). (*P < 0.05, **P < 0.01, N = 4)

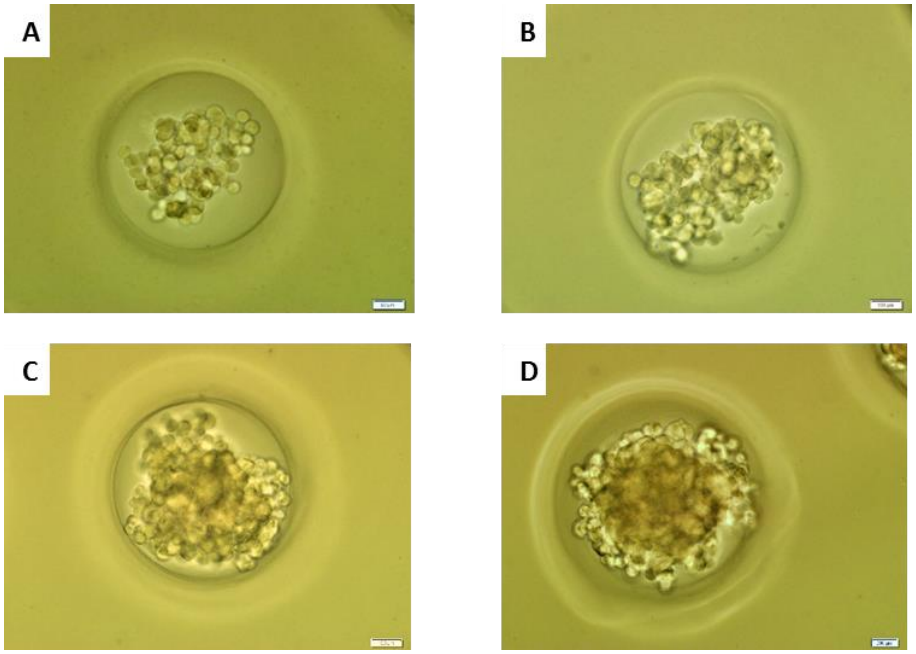

Figure 2.12. Confocal microscopic image of 3D spheroids of PANC-1 cells. (A) Spheroids after 2 days, (B) 4 days, (C) 5 days, and (D) 8 days. The presence of the hypoxic core is apparent in the Panels C and D. The proliferating layer of the cells surround the hypoxic core (Scale bars: 50 µm).

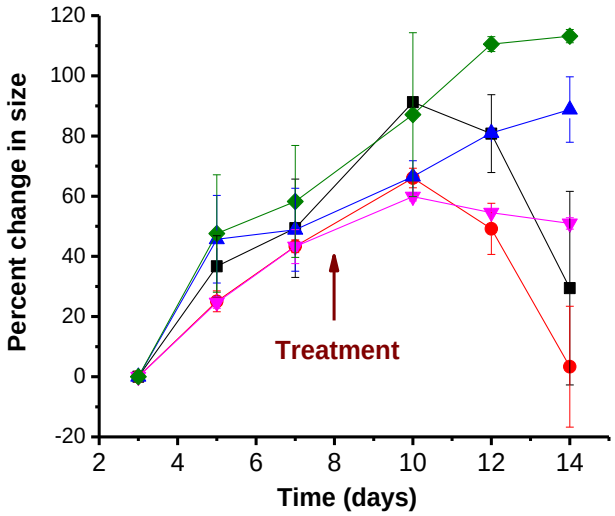

Figure 2.13. Growth curves for the PANC-1 cell spheroids treated with polymersomes. The 8 days old spheroids were treated with drug encapsulated non-targeted polymersomes (black squares), drug encapsulated targeted polymersomes (red circles), targeted polymersomes without any drugs (blue triangles), and the free drug combination (pink inverted triangles). The Control group was treated with HBSS buffer (green circles). The lines connecting the observed data points are depicted in the figure (N = 3).

2.3. Conclusions

We prepared polymersomes incorporating the reduction-sensitive copolymer and another amphiphilic copolymer with the azide group at the hydrophilic terminus. The cell nucleus targeting group acridine orange was conjugated to the polymersomes employing the [2+3]-cycloaddition reaction. We demonstrated that the resultant polymersomes were stable in cytosolic concentration of glutathione. However, the polymeric vesicles are unstable in a higher concentration of the reducing agent, as observed in the cell nucleus. We have successfully encapsulated the anticancer drugs gemcitabine and doxorubicin in the acridine orange-conjugated polymersomes. We have demonstrated that acridine orange facilitates the accumulation of the polymeric vesicles in the nuclei of pancreatic cancer cells. Although the polymeric vesicles are non-toxic, we observed that the drug encapsulated polymersomes significantly reduced the viability of pancreatic cancer cells in monolayer as well as in three-dimensional spheroid cultures, and decreased the volume of the pancreatic cancer cell spheroids.

2.4. Materials and Methods

2.4.1. Synthesis and Characterization of Polymers

Two different polymers have been synthesized in our laboratory to form the polymersomes. PEG (1900)-S-S-PLA (6100) polymer (Figure 2.3A) was synthesized as previously [19]. The other polymer, N_3-PEG (2000)-PLA (6000), Figure 2.3B, with an azide moiety to facilitate the conjugation reaction, was synthesized and characterized by NMR spectroscopy.

2.4.2. Synthesis and Characterization of Alkyne-conjugated Acridine Orange

The alkyne conjugated acridine orange (Figure 2.4) was synthesized and characterized by NMR and ESI mass spectroscopy as described in Figure A2.

2.4.3. Polymersome Preparation

To prepare the polymersomes with controlled size and narrow size distribution, we used the solvent exchange method [3]. We dissolved the polymers in tetrahydrofuran (THF), and added dropwise to an aqueous buffer under stirring. The method is described in the following paragraph.

2.4.4. Preparation of Calcein Encapsulated Polymersomes

The synthesized polymers (PEG-S-S-PLA and N_3-PEG-PLA, Figure 2.3) were solubilized in THF in molar ratio of 60:40 respectively. A calcein solution (10 μM) was prepared in HEPES buffer (10 mM, pH 7.4). The polymer solution was added dropwise to the calcein solution while stirring to prepare a 1 mg/mL polymersome suspension. Subsequently, THF was evaporated by passing air through the solution, and the polymersomes were subjected to bath sonication (Aquasonic, 250D, power level 9) for an hour at room temperature.

2.4.5. Acridine Orange (AO) Conjugation and Characterization

To conjugate the acridine orange moiety to the surface of polymersomes (Figure 2.2), copper catalyzed azide-alkyne cycloaddition ("click" reaction) was used. To 1 mL of polymersome solution (1 mg/mL), the alkyne conjugated acridine orange (1:2 molar ratio of azide: alkyne), Cu^{2+} complex (50 μL of 0.053 M aqueous solution, prepared by mixing aqueous solution of $CuCl_2$, 0.53 mmol, and *N*,*N*,*N*′,*N*′,*N*″-pentamethyldiethylenetriamine, PMDTA, 2.1 mmol), and sodium ascorbate (50 μL of 27 mg/mL aqueous solution, 1.4 μmol) was added [124, 125]. The resultant mixture was kept overnight at room temperature in dark while stirring (Scheme 2.1). The conjugated polymersomes were separated from the reaction mixture by passing the solution through a Sephadex G-100 (GE Healthcare) size exclusion column. To verify the presence of AO on the surface of polymersomes, we compared the fluorescence emission spectra (excitation: 450 nm) of the polymersomes before and after the "Click" reaction (Figure 2.5).

2.4.6. Preparation of Doxorubicin and Gemcitabine Encapsulated Polymersomes

We prepared the polymersomes via solvent exchange and used the pH gradient method [19] for active drug encapsulation. PEG-S-S-PLA and N_3-PEG-PLA polymers along with 1,2-dioleoyl-*sn*-glycero-3-phosphoethanolamine-N-(lissamine rhodamine B sulfonyl, ammonium salt) (60:35:5 molar ratio) were used for preparing the polymersomes. The polymersomes were prepared in citrate buffer (pH 4.0, 20 mM), and before drug encapsulation, the pH of the external solution was increased to 7.0 by the addition of aqueous sodium bicarbonate. Subsequently, a solution containing doxorubicin hydrochloride (Bridge Bioservices) and gemcitabine (Matrix Scientific) with 1:1 ratio (0.2 mg/mL in water each) was added to the prepared polymersomes. The resultant mixture was heated for 10 minutes at 60 °C and then kept at room temperature for 3 hours. The mixture was passed through a Sephadex G-100 (GE Healthcare) size exclusion column to separate the un-encapsulated drugs from the polymersomes. The drug loading efficacy was calculated by comparing absorbance spectra of polymersomes before and after size exclusion chromatography (Figure A3).

2.4.7. Determination of Doxorubicin and Gemcitabine Encapsulation Efficiency

The drug encapsulation efficacy was calculated based on a previously established protocol in our laboratory [19]. Briefly, the concentration of doxorubicin was calculated by monitoring the polymersomes' absorbance at 483 nm. Doxorubicin has equal absorbance at 483 nm and 279 nm, and gemcitabine has the absorbance maximum at 270 nm. We estimated the gemcitabine concentration by subtracting the absorbance of polymersomes at 483 nm from the absorbance at 270 nm, and using a calibration curve for gemcitabine.

2.4.8. Size-distribution Analysis

Size distribution analysis of the polymersomes (1 mg/mL) was performed using a dynamic light scattering instrument (NanoZS 90, Malvern Instruments). Measurements were conducted at a scattering angle of 90° in disposable polystyrene cuvettes. Each sample was equilibrated for 30 seconds, and 10 measurements per sample were recorded (repeated 4 times).

2.4.9. Atomic Force Microscopy (AFM)

An atomic force microscope (AFM) was used to image the polymersomes on a mica surface. AFM measurements were carried out in non-contact mode at a scanning rate of 0.7 Hz and a resonance frequency of 145 kHz using an NT-MDT NTEGRA (NT-MDT America). The scanning areas were 5 × 5 or 20 × 20 μm at the resolution of 512 or 1024 points per line, respectively. The images were flattened by a first order line correction and a first order plane subtraction to compensate a sample tilt. The polymersome solution was dropped on top of a freshly cleaved mica surface. The dropped solution was left at room temperature for 10 minutes for non-specific attachments of the polymersomes on the mica surface. The remaining solution was rinsed away with water and dried extensively with an air blow gun, and then the images were recorded. For imaging the polymersomes after GSH treatment, the same procedure was followed.

2.4.10. Transmission Electron Microscopy (TEM)

Polymersomes prepared in HEPES buffer (1 mg/mL, pH: 7.4), were subjected to negative staining for imaging using a Transmission Electron Microscope (JEOL JEM 2000, accelerating voltage set to 100 kV). The polymersome solution (10 μL) was dropped on a 300-mesh, Formvar-coated copper grid (coated with 0.01% poly-L-lysine). After one minute, the extra sample was wicked using a filter paper and stained using 1% phosphotungstic acid for 1.5 minutes. Subsequently, excess dye was blotted using filter paper, and dried samples were imaged.

2.4.11. Redox-triggered Release from the Polymersomes

We used the calcein-encapsulated polymersomes to demonstrate contents release in the presence of glutathione (GSH). The un-encapsulated calcein was quenched by adding 10 mM $CoCl_2$ solution to the buffer. The release of the encapsulated calcein (10 μM) was monitored by fluorescence spectroscopy in a 96-well plate (Spectramax M5, Molecular Devices; excitation: 495 nm, emission: 515 nm) over 40 minutes after treating the polymersomes (20 μL, 1mg/mL) with 10 mM GSH. Subsequently, 40 mM GSH was added to the solution and release profile was monitored for another 40 minutes (the experiment was repeated 3 times). Subsequently, the percent release of calcein was calculated and plotted.

2.4.12. Cell Culture

PANC-1 cells (pancreatic ductal carcinoma cell line, purchased from ATTC), was cultured in DMEM medium supplemented with 1% (v/v) antibiotic-antimycotic solution (containing penicillin, streptomycin, amphotericin B), and 10% fetal bovine serum in 75 cm^2 tissue culture flasks incubated at 37 °C in humidified atmosphere and 5% CO_2.

2.4.13. Nuclear-targeting Studies

The PANC-1 cells, when 90% confluent, were trypsinized and subcultured in a sterile, 96-well tissue culture plate. Once confluent, the cells were divided into three different treatment groups, including plain polymersomes (without AO on the surface), AO-polymersomes, and a negative control group without any treatment. Polymersome concentration was 0.02 mg/mL, and we repeated each experiment 3 times. After treatment, the cell nuclei were stained using HOESCHT 33342 dye (Enzo Life Sciences) according to the manufacturer's protocol. Subsequently, excess polymersomes and dye were washed out gently from the wells using HBSS

(HyClone, ThermoScientific), and cells were imaged using 20X objective of an Olympus IX81 motorized inverted fluorescent microscope.

2.4.14. Cell Viability Studies (Monolayer Cell Culture)

Alamar Blue cell viability assay was used to determine the cytotoxicity of the formulations. Five thousand cells were seeded in a 96-well, clear bottom plate and incubated until 70% confluent. The confluent wells were pretreated with dexamethasone and then treated with AO-polymersomes encapsulating HEPES buffer (10 mM), AO-polymersomes encapsulating gemcitabine and doxorubicin, and gemcitabine-doxorubicin combination (4 repeats per treatment). The treated cells were incubated for 72 hours at 37 °C. Subsequently, the cells were washed using HBSS solution, fresh media was added to the wells, and Alamar Blue assay was conducted to measure the viability of cells by following the manufacture's (Life Technologies) protocol. The fluorescence intensity of the reduced form of resazurin (resorufin) was monitored (excitation at 560 nm and emission at 590 nm) using a spectrofluorimeter, and cell viability were compared to the control wells (no treatment).

2.4.15. Three Dimensional (3D) Spheroid Cell Culture

To form the PANC-1 cell spheroids, 3D Petri Dish® (Microtissues, natural 3D) were used. The agar molds capable of forming 96 similar spheroids were equilibrated with DMEM media overnight at 37 °C. Subsequently, the PANC-1 cells were seeded in the agar plates following the manufacturer's protocol and were incubated for 3 days to form spheroids. The media surrounding the agar plates were replaced with fresh media as needed. The spheroids were imaged at different time points using a confocal microscope (Olympus Fluoview) and finally imaged at different focal planes.

2.4.16. Cell Viability Studies (3D Spheroid Culture)

The 5 days old spheroids were used for cell viability studies using Alamar Blue. Each plate containing 96 spheroids were pretreated with dexamethasone (8 μM), and then treated using AO-polymersomes (0.02 mg/mL) encapsulating HEPES (10 mM), gemcitabine and doxorubicin loaded polymersomes, and gemcitabine-doxorubicin combination for 72 hours. Then, the media were replaced with fresh media and the spheroids were dislodged from the agar plate by extensively triturating. The Spheroids were trypsinized to make a single cell suspension, and the cells were seeded in a 96 well plate (each 4 repeats). The cells were incubated for one doubling time and treated with fresh media-Alamar Blue mixture. The fluorescence of the reduced form of resazurin was monitored as described previously.

In a separate experiment, to check the ability of the polymersomes to shrink the spheroids, we treated the 7 day old spheroids with different formulations: AO-polymersomes (0.02 mg/mL) encapsulating HEPES (10 mM), gemcitabine and doxorubicin loaded polymersomes targeted with AO, gemcitabine and doxorubicin loaded, non-targeted polymersomes, and gemcitabine-doxorubicin combination for 72 hours. The growth of the spheroids was monitored for 14 days to obtain a growth curve. Spheroid's images were analyzed by an image processing software (cellSens Standard 1.6, Olympus Corporation).

3. NUCLEAR LOCALIZING PEPTIDDE CONJUGATED, REDOX SENSITIVE POLYMERSOMES FOR DELIVERING CURCUMIN AND DOXORUBICIN TO PANCREATIC CANCER MICRO-TUMORS[3]

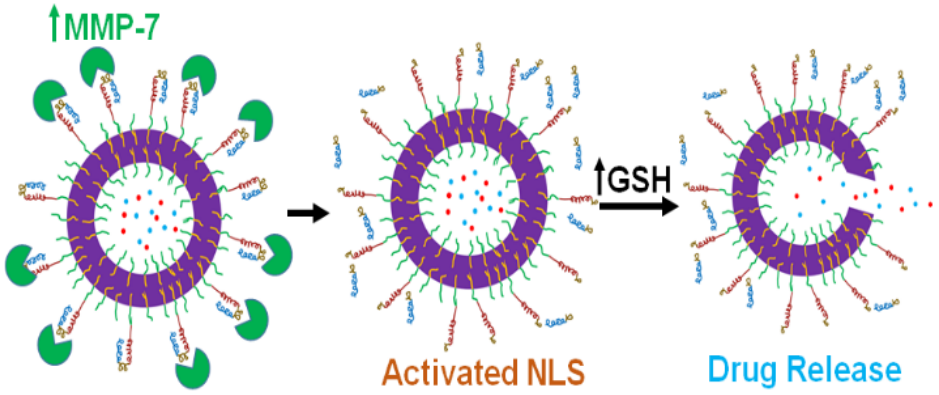

Figure 3.1. Graphical abstract.

3.1. Introduction

Chemotherapeutic agents are commonly used in treating most of the cancers. Due to the non-specific distribution of the drugs, patients suffer from significant side effects of the chemotherapy. The development of chemo-resistance is another limiting factor in treating cancer[126]. Considering the limited number of targeted drug delivery systems in clinical development[127], there is an urgent need for efficient carriers which release the drugs only at the

[3] This section is coauthored by Tayebeh Anajafi, Junru Yu, Abbas Sedigh, Manas K. Haldar, Wallace W. Muhonen, Seth Oberlander, Heather Wasness, Jamie Froberg, MD Shahjahan Molla, Kalpana S. Katti, Yongki Choi, John B. Shabb, D. K. Srivastava, and Sanku Mallik. Tayebeh had primary responsibility to conduct all the experiments, analyze the data in and write the manuscript. Junru and Abbas synthesized recombinant MMPs. Manas had primary synthetized the polymers. Wallace recorded MALDI mass spectrum for synthesized peptide. Seth and Heather assisted in peptide purification. Jamie imaged the polymersomes using AFM. MD Shahjahan recorded the IR spectra. Drs. Katti, Choi,Shabb, Srivastava and Mallik verified the data and advised on experimental designs.

target site. After reaching the intended site, often the drug molecules need to traverse through cellular barriers and reach the particular cell compartment to exert the biochemical effects. As a result, only a small percentage of the active drug reaches the intracellular target organelle[54]. Therefore, delivering the drugs in the cell organelles is a more promising strategy to increase the chemotherapeutic efficacy. The cell nucleus, the largest organelle housing the genetic materials and the transcription machinery, is an attractive target for drug delivery[79].

Several nuclear localizing peptides [e.g., simian virus 40 (SV40) T-antigen derived peptide[54, 128], TAT peptide[129], and transportan[53]] are widely used as targeting agents for drug and gene delivery. For example, the Lima group have used an SV40 T-antigen derived peptide to develop a nonviral delivery system for high molecular weight cargos[130]. The peptide rapidly enters the cell nucleus in a dose-dependent manner[131]. However, the nuclear localization peptides are non-selective and cannot distinguish the malignant cells from the healthy counterparts.

Matrix metalloproteinase (MMPs) enzymes are the largest group of endopeptidases with an important role in extracellular matrix remodeling[132] in physiological (e.g. tissue remodeling[133]) and pathological conditions (e.g. cancer[134] and heart diseases[135]). Among MMPs, the matrix metalloproteinase-7 (MMP-7) isozyme is overexpressed in the tumor site in several malignancies[84, 136] including pancreatic cancer. Hence, designing a nuclear localizing peptide which gets activated at the tumor site, in response to MMP-7 overexpression, is a promising strategy for targeting the tumor microenvironment.

Our overall goal is to prepare smart delivery vehicles to target the tumor cell nuclei and decrease the side effects of chemotherapeutic drugs. Herein, we have designed nanocarriers (polymersomes[3]) that accumulate at the tumor site by the Enhanced Permeation and Retention (EPR) effect[115] and release the drugs (doxorubicin/curcumin) in response to the local biochemical

abnormalities[137]. We have prepared MMP-7 isozyme responsive, nuclear localizing, redox-sensitive polymersomes by conjugating the vesicles to a protected nuclear localization peptide[137]. We have shown that MMP-7 hydrolyzes the masking peptide and exposes the nuclear localization sequence (NLS) on the polymersome surface, facilitating the cellular internalization preferentially in the cancer cells, and subsequent nuclear transport of the vesicles. The high reducing agent concentration in the nucleus destabilizes the vesicles and release the encapsulated content (Figure 3.2). The polymersome formulation is tested *in vitro* using monolayer and three-dimensional spheroid cultures of human pancreatic cancer cells. Results of this study have the potential to contribute to the design of polymersome formulations which are more efficient than the current triggered release vehicles against various malignancies, and especially pancreatic cancer.

3.2. Results and Discussion

3.2.1. Polymer Synthesis and Characterization

To impart redox-sensitive properties to the polymersomes, we have synthesized a copolymer with a disulfide bond (Figure 3.3A) linking the hydrophilic and hydrophobic blocks. To conjugate the "masked" NLS peptide to the surface of polymersomes, we have used the azide-alkyne cycloaddition reaction[138]. Hence, we have also synthesized an azide terminated PEG-PLA copolymer (Figure 3.3B). Polyethylene glycol (PEG) was used as the hydrophilic block for both polymers to increase the circulation times of the resultant polymersomes[139]. The ratio of the hydrophilic part to the total mass of a copolymer (*f* value) is important for polymersome formation, with an *f* value between 25-40% being optimal[140]. Therefore, we have synthesized the polymers such that the *f* values are close to this range (PEG-S-S-PLA, *f:* 24%, N_3-PEG-PLA, *f: 25*%).

3.2.2. Peptide Design, Synthesis, and Purification

We chose the SV40 nuclear localizing signal peptide (PKKKRKV)[141] as the organelle (cell nucleus) targeting moiety. However, the NLS peptide is nonspecific in the electrostatic interactions with the cell membrane[142]. Hence, we have used a negatively-charged masking domain (EEEE) to neutralize the positive charges of the NLS peptide[143]. The matrix metalloproteinase isozyme MMP-7 is overexpressed in the pancreatic cancer microenvironment[84]. We have linked the NLS peptide and the masking domain via a short peptide containing the MMP-7 cleavage site (GPMG-IAGQ)[144] (Figure 3.4). Considering the low MMP-7 enzyme concentration in the blood[145], we anticipate that the resultant vesicles would be stable in the circulation with the negative charges masking the NLS peptide. However, as the polymersomes accumulate at the tumor site by the EPR effect, MMP-7 would cleave the substrate peptide, separating the NLS from the masking domain (illustrated in Figure 3.2). Hence, conjugating the peptide to the surface of the vesicles would confer tumor and cellular organelle (nucleus) targeting properties to the polymersomes. To attach the peptide to the surface of the polymersomes, we conjugated hexynoic acid to the peptide's N-terminus.

We synthesized the peptide using a microwave-assisted, solid phase synthesizer, purified by RP-HPLC, and characterized by mass spectrometry (Figure B1). We anticipated that the electrostatic interactions between the NLS and masking domains of the synthesized peptide would be affected by temperature. Temperature-dependent CD spectroscopy showed an isosbestic point – indicating the lack of any intermediate during the melting process (Figure 3.5).

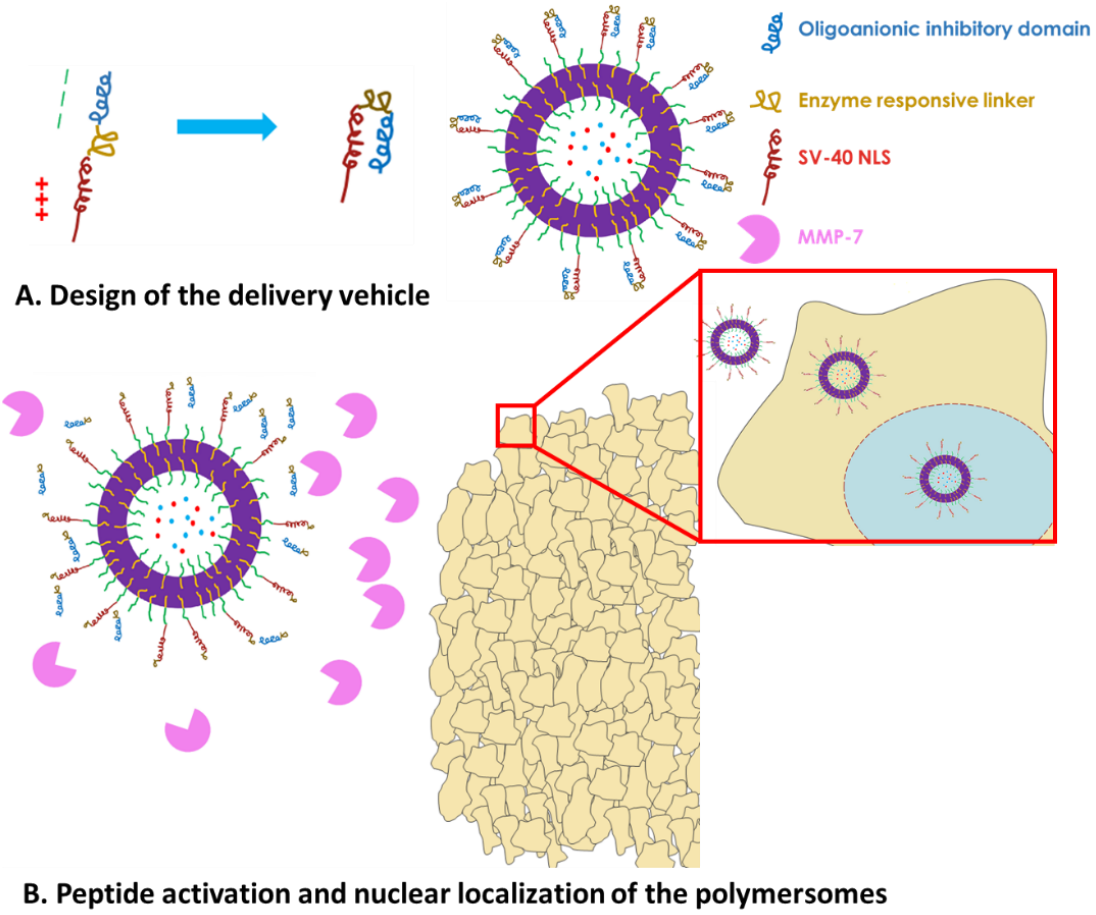

Figure 3.2. Schematic representation of the study design. (A) Peptide design and delivery vehicle representation. (B) Enzymatic cleavage of the peptide by MMP-7 (activation of the NLS) in the proximity of tumor, and nuclear localization of the nanovesicles.

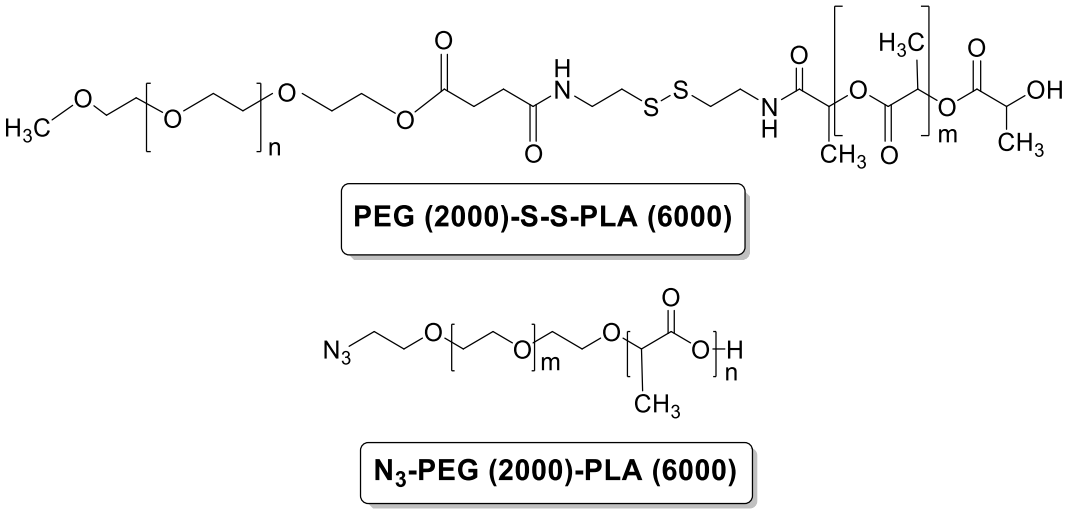

Figure 3.3. The structures of the synthesized amphiphilic block copolymers.

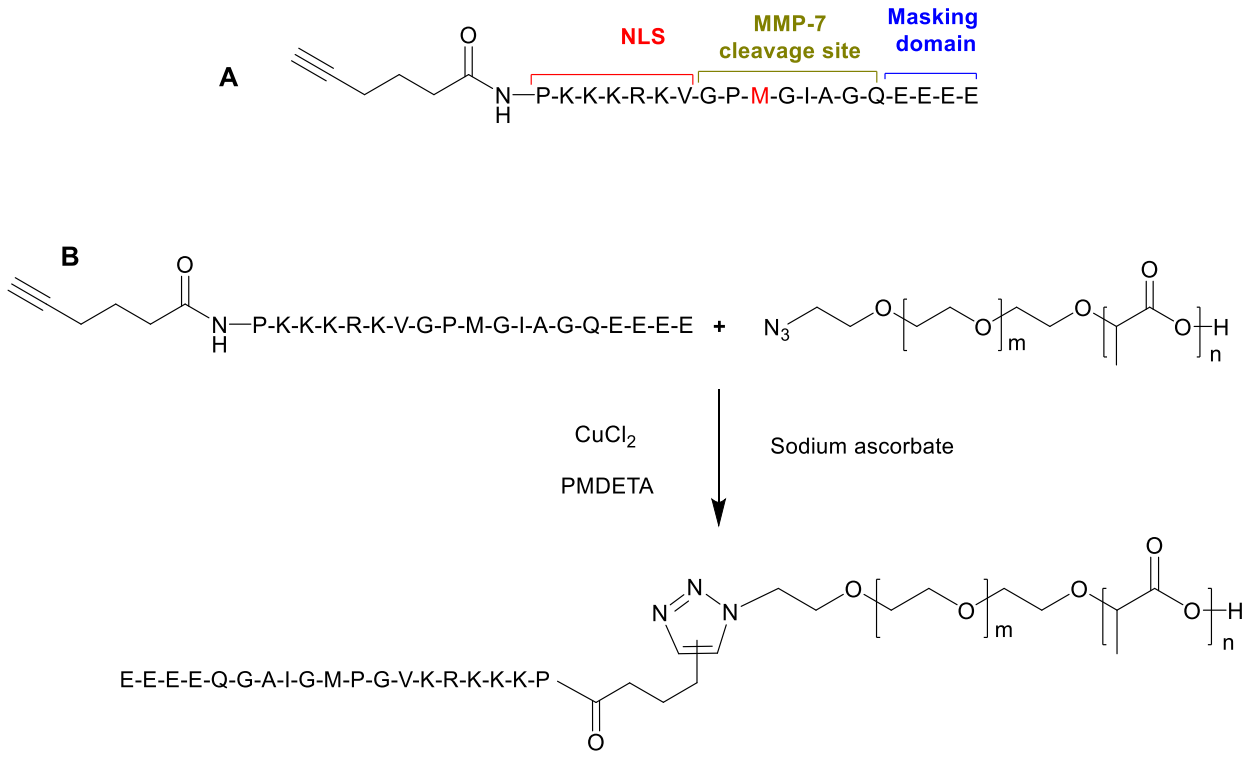

Figure 3.4. Peptide structure and the Click reaction. (A) Synthesized peptide sequence. Methionine in position P2 is labeled by red color. (B) Conjugation of the peptide to the polymersome surface (N_3-PEG-PLA) employing the Cu^{2+} catalyzed [2+3]-cycloaddition reaction (PMDTA: *N*, *N*, *N′*, *N′*, *N″*-pentamethyldiethylenetriamine).

3.2.3. Peptide Cleavage Studies

Previous studies indicated that the substitution of methionine in the P_2 position of the substrate peptide provides selectivity for the MMP-7 isozyme over MMP-9[144]. We tested the selectivity of MMP-1, -7, and -9 to hydrolyze the synthesized peptide (shown in Figure 3.3). In this endeavor, we incubated the pure peptide with recombinant human MMP-1, -7, and -9 separately at room temperature for an hour, and recorded the CD spectra (Figure 3.6). We subtracted the CD spectra of the MMP isozymes as the "blank." We observed that only MMP-7 significantly changed the CD spectrum of the peptide, indicating selective hydrolysis.

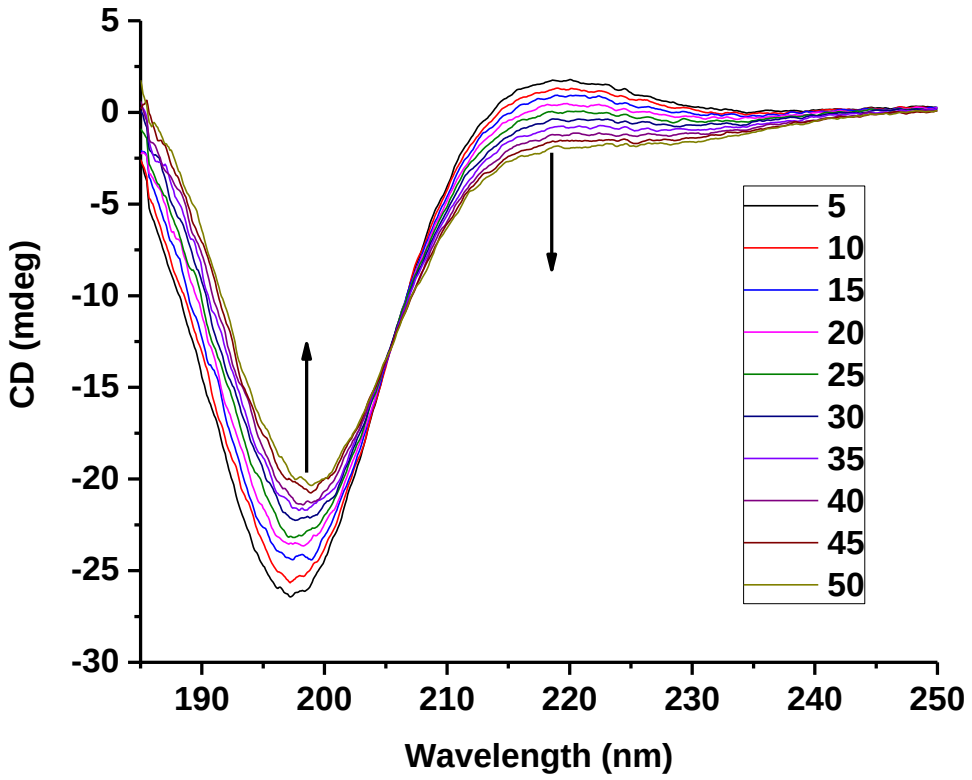

Figure 3.5. Temperature-dependent (5 – 50 oC) CD spectra of the purified peptide. The peaks at 218 nm and 197 nm decreased with increase in temperature (indicated by the arrows). The isosbestic point suggests the lack of any intermediate during the melting process of the peptide.

3.2.4. Polymersome Preparation and Characterization

We prepared the polymersomes by solvent exchange (Materials and Methods) using our previously-optimized ratio of the PEG-S-S-PLA and N_3-PEG-PLA (60:40) for the reduction-triggered release of encapsulated contents[7]. The hydrodynamic diameter and size of the polymersomes were determined using dynamic light scattering (DLS, Figure 3.7A) and transmission electron microscopy (TEM, Figure 3.7B). DLS indicated that the average diameter of the vesicles was 143 $\pm$ 3 nm with a polydispersity index of 0.2 $\pm$ 0.02.

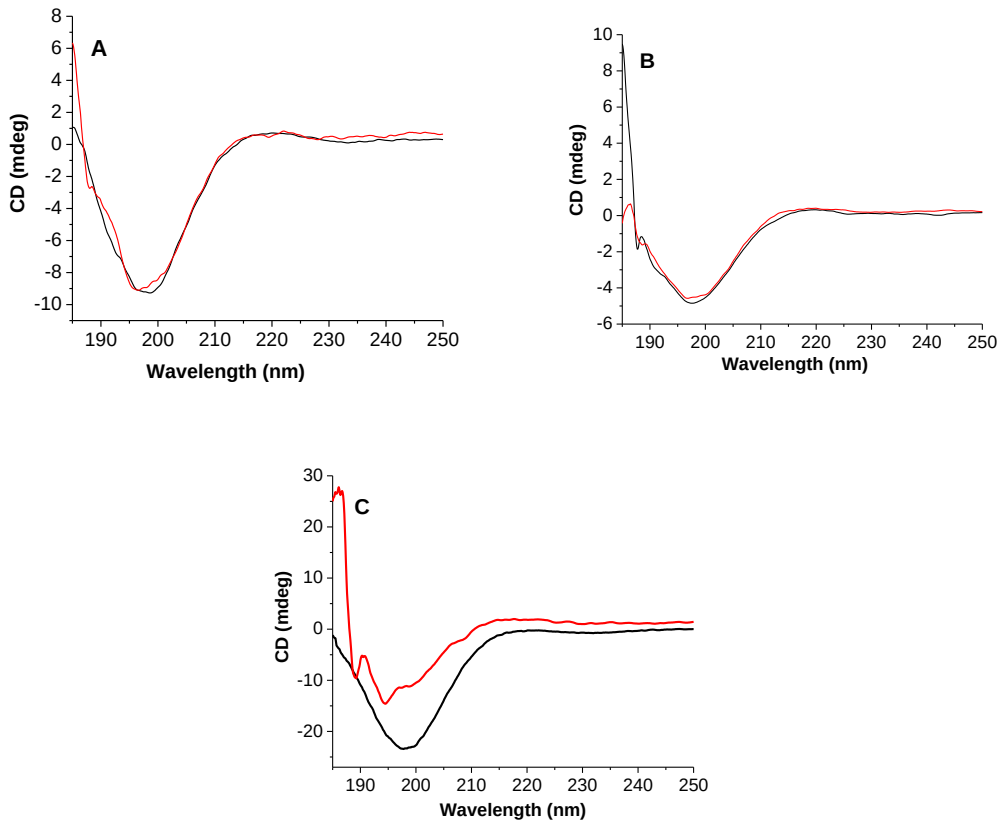

Figure 3.6. Selective hydrolysis of the synthesized peptide by MMP-7. The CD spectrum of the peptide after 1 h incubation with 2 μM of MMP-9 (A), MMP-1 (B), or MMP-7 (C). The CD spectra of the MMP isozymes were used as the "blank." Black trace: pure peptide before cleavage, red trace: peptide after incubation with the enzymes.

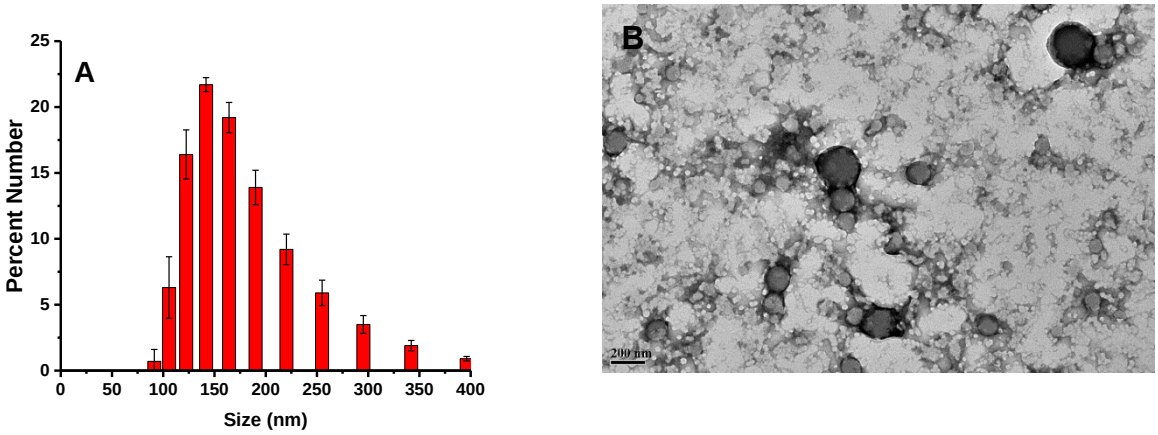

Figure 3.7. Characterization of the polymersomes. (A) Size distribution of the polymersomes by dynamic light scattering (N = 5). (B) TEM images of the polymersomes (scale bar: 200 nm).

3.2.5. Conjugation of the "Masked" NLS Peptide on the Polymersomes ("Click" Reaction)

We conjugated the NLS–MMP-7 substrate–EEEE peptide (shown in Figure 3.4A) to the surface of the polymersomes applying the azide-alkyne cycloaddition reaction (schematically shown in Figure 3.4B). After removing any unconjugated peptide by extensive dialysis, we recorded the FT-IR spectrum of the vesicles (Figure 3.8). The 1, 2, 3-triazole ring has a characteristic absorbance near 1110-1050 cm^{-1} [146]. The band at 1108 cm^{-1} can be assigned to that structure. The band at 1419 cm^{-1} is likely due to the N=N stretching or triazole ring skeletal vibration. The band at 1351 cm^{-1} and 1214 cm^{-1} likely indicate the C-N stretching[147]. Analyzing the spectra, we concluded that the reaction between polymer and peptide has occurred, generating the cyclic 1, 2, 3-triazole. The band at 720 cm^{-1}, present only in the peptide spectra (Figure 3.8A), is possibly due to the C-H deformation from the -C≡CH. A characteristic absorbance is observed in the region 2170-2080 cm^{-1} for organic azides[148, 149]. In the spectra of the polymer N_3-PEG-PLA, the band at 2104 cm^{-1} could be assigned for N=N=N asymmetric stretching vibration (Figure 3.8B). We note that this band is not observed in the IR spectra for the peptide conjugated polymersomes (Figure 3.8B), indicating the success of the reaction.

We also recorded the CD spectrum of the peptide-conjugated vesicles (Figure 3.9). The similarity of the CD spectrum of the pure peptide (Figure 3.9, black trace) and the product from the cycloaddition reaction (Figure 3.9, red trace) indicated the presence of the peptide on the surface of the polymersomes. We measured the zeta potential and electrophoretic mobility of the polymersomes before and after peptide conjugation (Table 3.1). We did not observe any increase in the zeta potential – indicating efficient masking of the positive charges on the NLS peptide by the aspartic acid residues.

Table 3.1. Zeta potential and electrophoretic mobility of polymersomes before and after peptide conjugation.

Formulation	Zeta potential (mV)	Mobility (μm cm/Vs)
Polymersomes devoid of peptide	-13.8 ± 0.7	-1.08 ± 0.05
Peptide-conjugated polymersomes	-16.6 ± 0.9	-1.3 ± 0.07

3.2.6. Drug Encapsulation in the Polymersomes

Curcumin (diferuloylmethane) is an extensively studied anticancer and anti-inflammatory natural compound. However, curcumin has low water solubility and low bioavailability[150]. Hence, increasing the water solubility and bioavailability of this compound using nanoparticles is a promising strategy to enhance the therapeutic potential[151]. We were not successful in encapsulating a significant amount of curcumin in the polymersomes' hydrophobic bilayer by the solvent exchange or thin film rehydration method. Hence, to increase the water solubility, we formed the curcumin complex of sulfobutyl-β-cyclodextrin (Captisol)[152]. To test the complex formation, we used seven different concentrations of Captisol solution in water [40, 20, 10, 5, 2.5, 1.25, 0% (W/V)] to solubilize the same amount of curcumin (25 mg). The increase in the curcumin solubility with the addition of more Captisol indicated the complex formation (Figure B2). We prepared a calibration curve by measuring the curcumin absorbance at 429 nm (Figure B3) and determined the maximum curcumin solubility to be 2.2 mM. Subsequently, we passively encapsulated the hydrophilic Captisol-curcumin complex in the aqueous interior of the polymersomes (Materials and Methods). The unencapsulated curcumin complex was removed by size exclusion chromatography. Comparing the curcumin absorbance (at 429 nm) before and after gel filtration, the encapsulation efficiency was calculated to be 47% (Figure B4A).

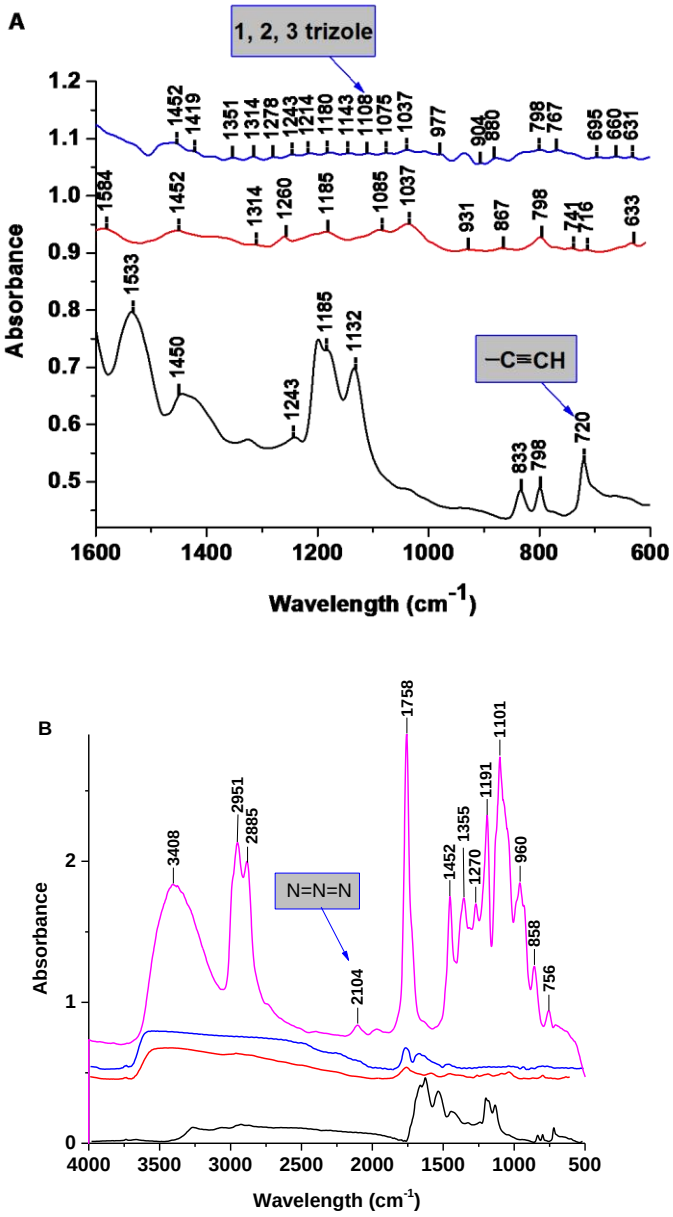

Figure 3.8. Demonstration of the successful cycloaddition reaction between NLS peptide and polymer's azide group. FT-IR analysis of polymersomes clicked to the peptide, polymersomes before the reaction and peptide [analyzing the wavelength range 1600-600 nm (A), and 4000-500 nm (B)]. Stretches attributed to cyclic ring 1, 2, 3 triazole, and –C≡C are marked. Black trace: peptide, red trace: polymersomes, blue trace: polymersomes with the conjugated peptide, pink trace: N_3-PEG-PLA polymer (the stretch attributed to the azide moiety is marked). For clarity, the spectra are plotted with offsets in the y-axis.

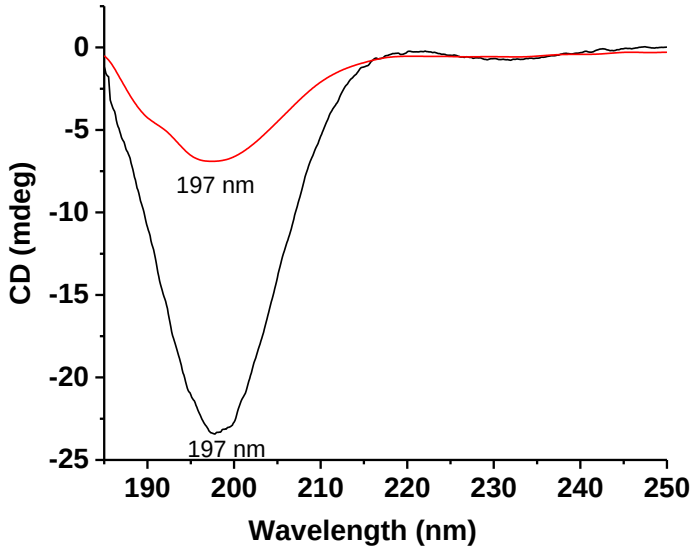

Figure 3.9. Confirmation of the peptide conjugation reaction by CD spectroscopy. The similarity of spectra of the peptide (black trace) and the peptide-conjugated polymersomes (red trace) indicates successful conjugation reaction. The minima for both spectra (197 nm) are marked in the plot.

Doxorubicin is an intercalation agent which induces cell apoptosis in several types of malignancies[153, 154, 155] (e.g., pancreatic cancer[156], human ovarian teratocarcinoma, and human breast adenocarcinoma[157]). To test the simultaneous effect of doxorubicin and curcumin in pancreatic cancer cells, we also prepared doxorubicin-encapsulated, peptide-conjugated polymersomes by the active pH gradient method (Materials and Methods). The unencapsulated doxorubicin was removed from the polymersomes by size exclusion chromatography. We calculated the encapsulation efficiency of doxorubicin to be 56% (Figure B4B).

3.2.7. Demonstration of Contents Release from the Polymersomes and Structural Characterization

We have used the intrinsic difference in reducing agent concentrations in the nucleus and cytoplasm[118] to trigger content release from the polymersomes. To mimic the intracellular environment, we have studied the release profiles of the vesicles in the presence of two different

concentrations of the cellular reducing agent glutathione (GSH): 10 mM (mimicking the cytosolic environment) and 50 mM (mimicking the nuclear environment). We observed about 15% content release of the encapsulated hydrophilic dye calcein in the presence of 10 mM GSH in one hour. Increasing the GSH concentration to 50 mM resulted in 70% release of the encapsulated dye (Figure 3.10, black trace) in one hour. We also observed that addition of 2 μM MMP-7 enzyme to GSH did not affect calcein release from the polymersomes significantly (Figure 3.10, red trace).

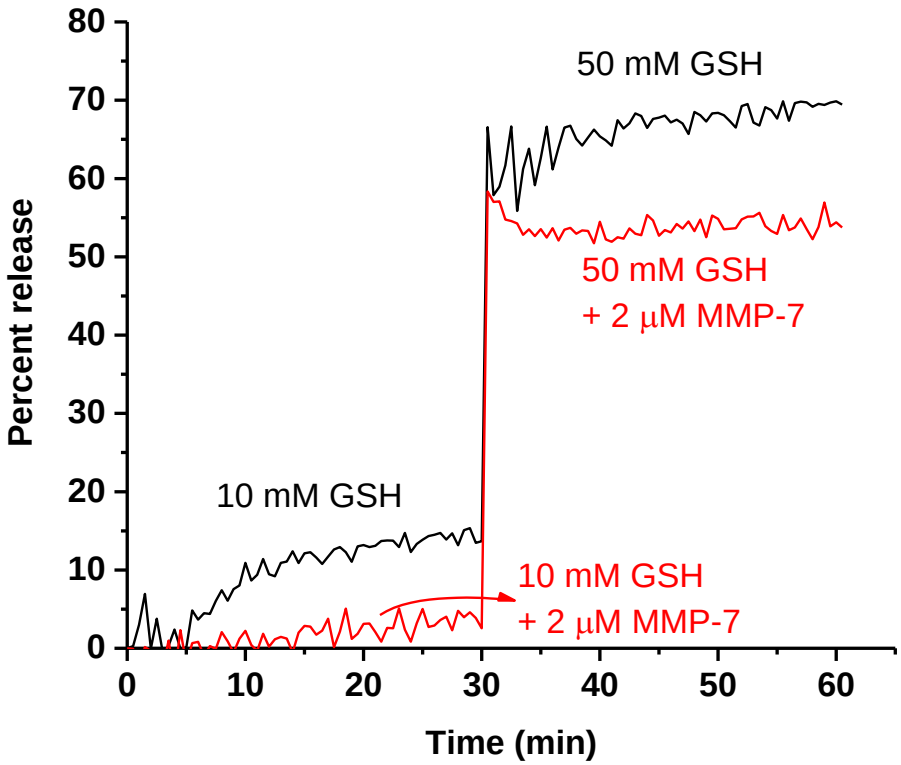

Figure 3.10. The release profiles of encapsulated calcein from the peptide conjugated polymersomes. Calcein release was monitored in the presence of 10 mM and 50 mM GSH (black trace). The release was also tested in the presence of both GSH and MMP-7 enzyme (2 μM, red trace). Each experiment was repeated four times, and the plots are the average of four release profiles.

In separate experiments, we tested the release of doxorubicin and Captisol-curcumin complex from the polymersomes in the presence of the MMP-7 enzyme and GSH (50 μM, 10 or

50 mM). We observed that the curcumin-complex encapsulated polymersomes do not significantly release their content after treatment with 50 μM and 10 mM GSH. However, adding 50 mM GSH triggers 45% release of the curcumin complex from the polymersomes (Figure 3.11 A). Similarly, the doxorubicin-encapsulated polymersomes did not show significant release in the presence of low GSH concentrations. However, the vesicles released up to 94% of their content in the presence of 50 mM GSH (Figure 3.11 B).

We imaged the polymersomes before and after GSH-triggered contents release by atomic force microscopy (AFM, Figure 3.12). We observed that the polymersomes' spherical shape is retained after treatment with 10 mM GSH (Figure 3.12, Panel B). However, treatment with 50 mM GSH deformed the vesicles (Panel C), indicating substantial structural changes.

We also measured the hydrodynamic diameter of the polymersomes before and after reduction triggered release employing dynamic light scattering. We incubated the vesicles (average diameter: 143 $\pm$ 3 nm, Figure 3.7) with 10 and 50 mM GSH for 10 minutes. We observed that treating the polymersomes with 10 mM GSH did not significantly change the size (size: 142 ± 4 nm, PDI: 0.4 ± 0.03, Figure 3.13 A). However, increasing the reducing agent concentration to 50 mM significantly altered the size distribution and polydispersity of the polymersomes (size: 308 ± 143 nm, PDI: 0.9 ± 0.08, Figure 3.13 B). The atomic force microscopic images and the dynamic light scattering data indicate the disruption of the polymersome after in the presence of a high concentration of GSH.

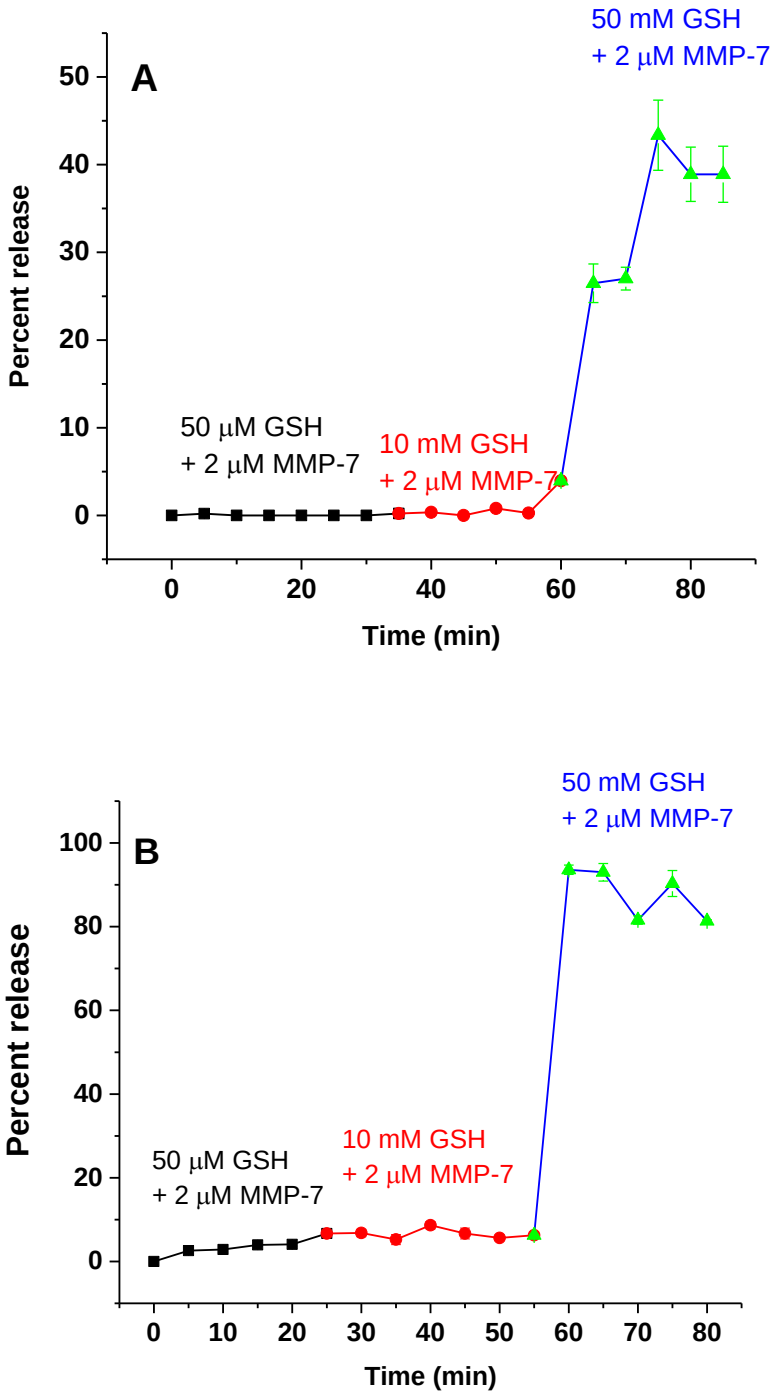

Figure 3.11. Drug release profiles from the peptide conjugated polymersomes. The GSH triggered release of Captisol-curcumin complex (A) and doxorubicin (B) from the peptide conjugated polymersomes (N = 3). Drug encapsulated polymersomes were treated with 50μM GSH + 2 μM MMP-7 (black squares), 10 mM GSH + 2 μM MMP-7 (red circles), and 50 mM GSH + 2 μM MMP-7 (green triangles). The lines connecting the observed data points are shown on the plots.

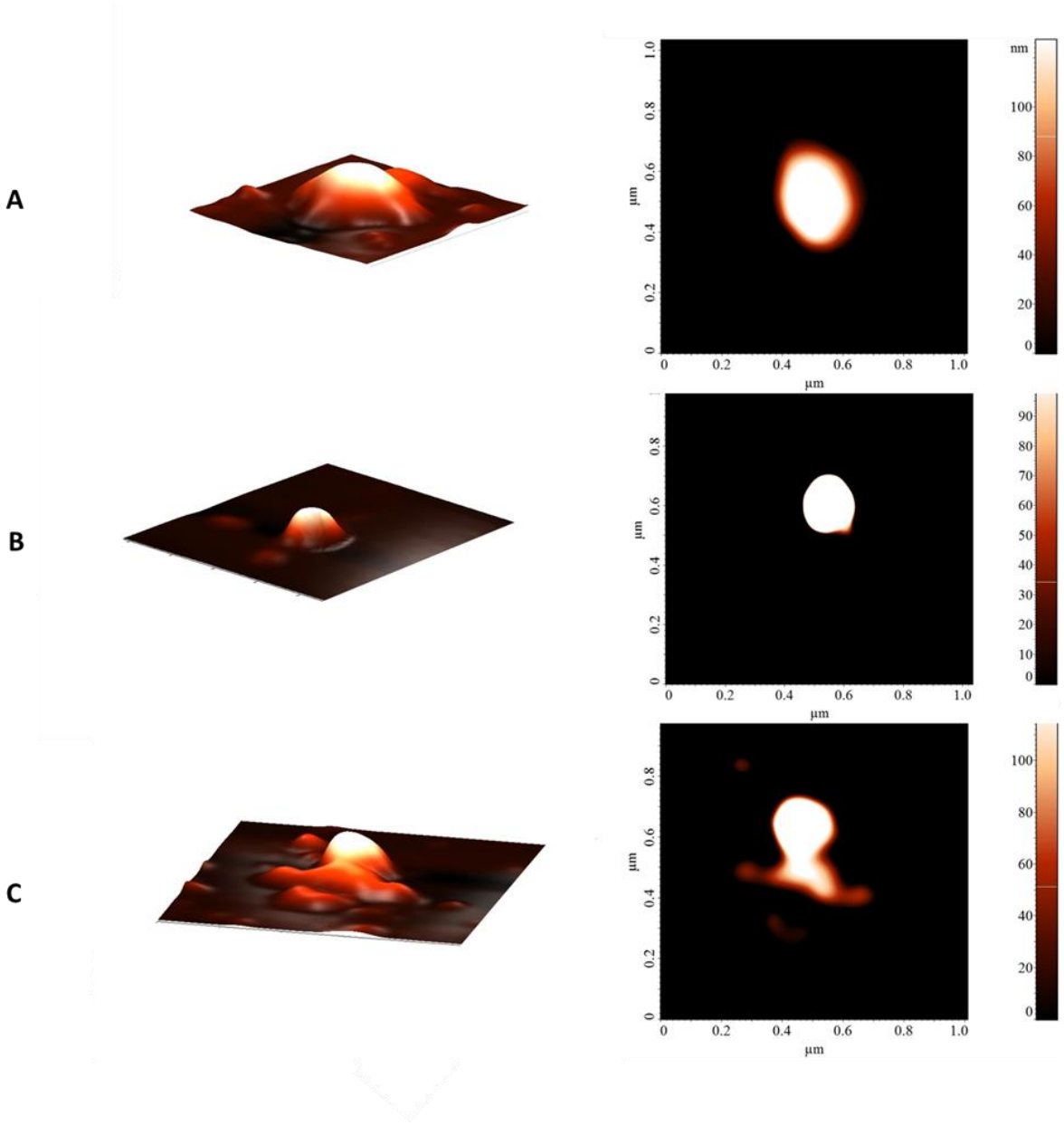

Figure 3.12. Atomic force microscopic images of the polymersomes (A), after a 10-minute incubation with 10 mM GSH (B), and 50 mM GSH (**C**).

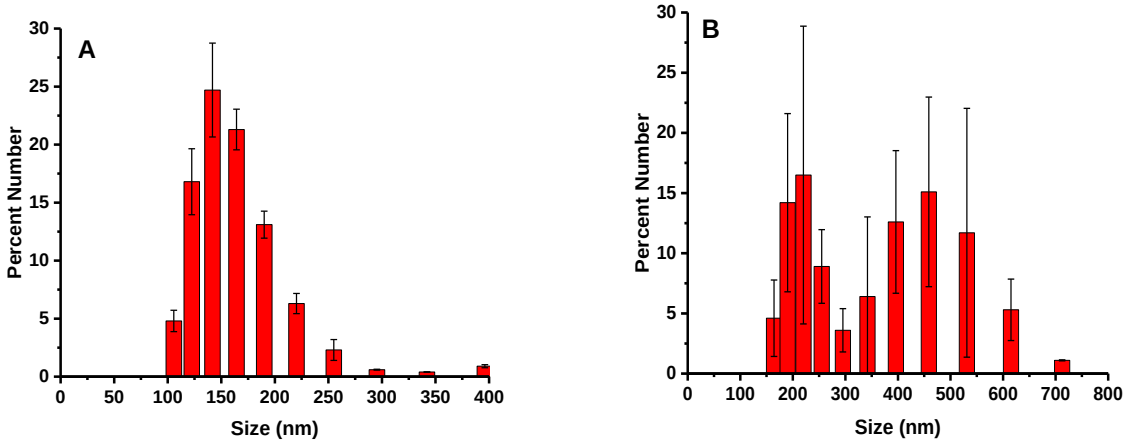

Figure 3.13. Hydrodynamic diameters of the peptide conjugated polymersomes after treatment with 10 mM (A) and 50 mM GSH (B) (N = 5).

3.2.8. Demonstration of Polymersomes' Efficiency in Monolayer Cell Culture

MMP-7 overexpression has been shown in 98% of human pancreatic cancer tissues[158]. To test the selectivity of our polymersomes, we used the BxPC3 pancreatic cancer cells overexpressing the MMP-7 enzyme[159]. We also used a normal cell line (bEnd-3) as a control group. We measured the amount of secreted MMP-7 in the concentrated conditioned media by ELISA and observed a significant difference between the BxPC3 (6.9 ± 2.9 ng/mL) and the bEnd-3 cells (3.7 ± 1.7 ng/mL). Subsequently, we compared the cellular uptake of the drug-encapsulated, peptide-conjugated and the drug-encapsulated polymersomes devoid of the "masked" NLS peptide (Figure 3.14). In this endeavor, we treated the pancreatic cancer cells (BxPC-3) with the combination of the curcumin-encapsulated and the doxorubicin-encapsulated polymersomes with and without the conjugated peptide on the surface. We observed that the polymersomes lacking the peptide are not significantly transported to the BxPC-3 cell nuclei. However, the peptide-conjugated polymersomes entered the cell nucleus efficiently (Figure 3.14A). We also tested the effect of the tumor microenvironment (presence of secreted MMP-7) on the NLS peptide activation

and subsequent cellular internalization of the polymersomes. We observed that the brain endothelial cells (bEnd-3), which do not secrete high amounts of MMP-7, failed to internalize the peptide-conjugated, drug-encapsulated polymersomes (Figure 3.14B). It is likely that the low MMP-7 concentration limits the polymersomes-cell interaction due to the presence of the masking domain in the peptide, which neutralizes the positive charges of the NLS.

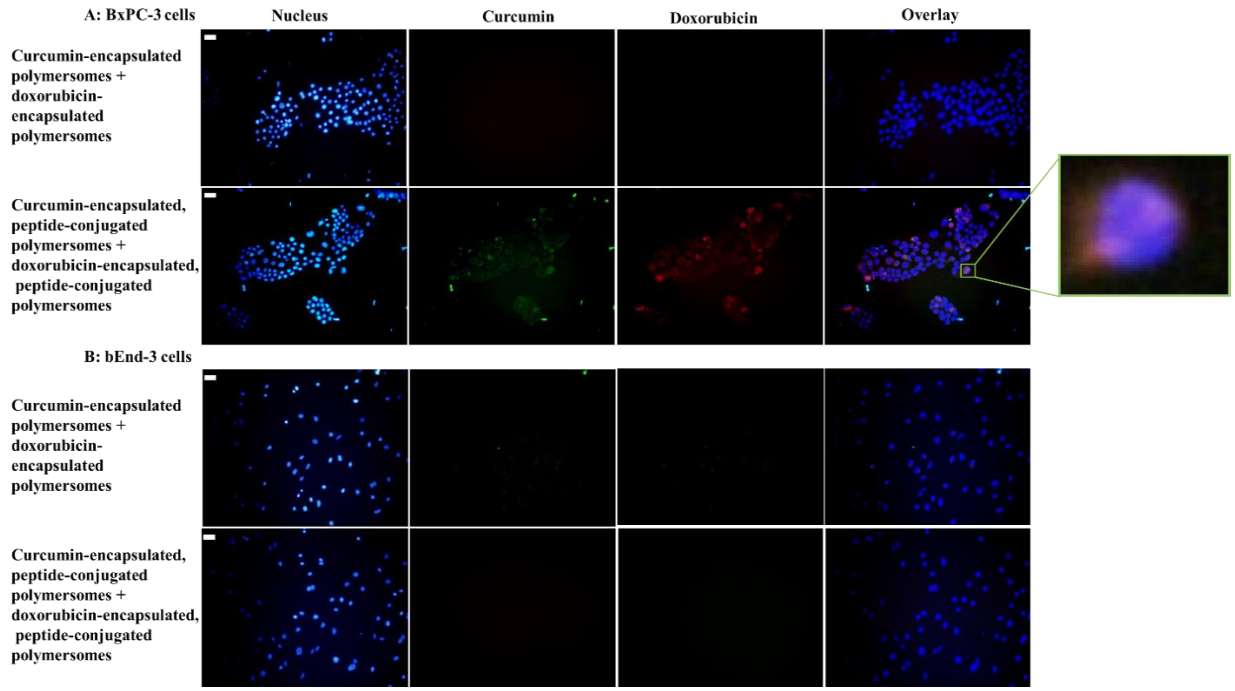

Figure 3.14. Determination of the cellular uptake and nuclear localization of the polymersomes in monolayer cell culture. (A) Uptake was monitored in the BxPC-3 cells and (B) the bEnd-3 cells after treatment with the polymersome formulations. The images were obtained with a confocal fluorescence microscope. The nuclei were imaged using DAPI, curcumin using FITC and doxorubicin using TRITC filter (scale bar: 200 µm, $N = 4$).

The buffer-encapsulated polymersomes were non-toxic to both BxPC-3 and bEnd-3 cells in vitro (Figure 3.15). To determine the viability, we treated the BxPC3 and the bEnd-3 cells with the polymersomes encapsulating Captisol-curcumin complex (27 µM curcumin) and doxorubicin (20 µM drug) for 72 hours. We observed that the combination of the two drug encapsulated polymersomes containing the peptide on the surface significantly decreased the BxPC-3 cells'

viability (65%) compared to the bEnd-3 cells (88%). The drug-encapsulated polymersomes devoid of the peptide was less toxic to the BxPC-3 cells (viability: 87%) and more toxic to the bEnd-3 cells (viability: 67%). This reversal may reflect facile endocytosis of the vesicles in the bEnd-3 cells. In addition, it might be due to faster drug release from the nanoparticles devoid of the peptides compared to the peptide-conjugated polymersomes (Figure 3.15). We also observed that the free drugs were more toxic to both the cells compared to the drug-encapsulated polymersomes, possibly indicating increased diffusion of the drugs across the cell membrane.

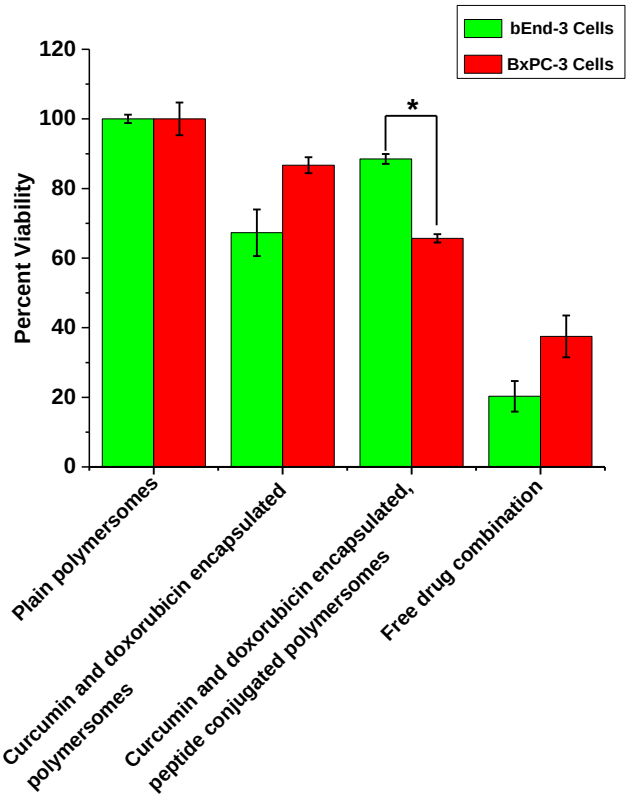

Figure 3.15. The viability of the BxPC-3 (red bars) and bEnd-3 cells (green bars) after treatment with different polymersome formulations in monolayer cultures (* $P < 0.05$, $N = 6$).

3.2.9. Demonstration of Polymersomes' Efficiency in Three-dimensional (3D) Spheroids

Considering the biochemical and genetic differences between the monolayer cell culture and the three-dimensional tumors *in vivo*[160], we cultured the BxPC-3 and bEnd-3 cells as 3D spheroids and tested the efficiency of the polymersomes. We used agar molds capable of supporting the growth of 96 uniform size cell spheroids (Materials and Methods). The growth of the spheroids was monitored using an optical microscope. The 8-day old spheroids (Figure 3.16) were subjected to treatment with four different formulations: a combination of peptide-conjugated polymersomes encapsulating curcumin or doxorubicin (containing 27 μM curcumin complex and 20 μM of the doxorubicin), a combination of polymersomes encapsulating curcumin or doxorubicin (without any peptide conjugation), the free drug combination, and the phosphate buffer encapsulated polymersomes (plain polymersomes). The control group was treated with HBSS, and after 72 hours, the cell viability was determined. We observed that although the drug-encapsulated polymersomes do not show severe cell toxicity in both cell lines, the drug-encapsulated, peptide-conjugated polymersomes are significantly more toxic to the BxPC-3 pancreatic cancer cells (viability: 9%) compared to the normal cells (viability: 36%, Figure 3.16). To demonstrate the generality of our approach, the also tested the efficacy of the polymersomes in another pancreatic cancer cell line, AsPC-1. We observed that the drug-encapsulated, peptide-conjugated polymersomes reduced the viability of the AsPC-1 cells to 22% (Figure B6).

To further test the efficiency of the formulations in 3D spheroid cultures, we treated another set of 8-day old spheroids with the polymersome formulations, encapsulating 27 μM Captisol-curcumin complex and 20 μM of the doxorubicin, for 72 hours and monitored their growth for 10 days (Figure 3.17). We observed that the peptide-conjugated, drug-encapsulated polymersomes are more toxic toward the BxPC-3 cells (shrinkage of the spheroids up to 49%, Figure 3.17 A, blue

triangles) compared to the bEnd-3 cells (shrinkage of spheroids up to 24%, Figure 3.17 B, blue triangles). In addition, the polymersomes devoid of the peptide showed less toxicity toward both cell spheroids (BxPC-3 cells: up to 54% growth; bEnd-3 cells: up to 44% growth, Figure 3.17, red circles) while the free drug combination (containing 27 μM Captisol-curcumin complex and 20 μM of the doxorubicin) has severe toxicity in both cell lines (shrinkage of spheroids up to 60% in bEnd-3 spheroids, and 56% in BxPC-3 spheroids, Figure 3.17, magenta inverted triangles). We also observed that the peptide-conjugated, drug-encapsulated polymersomes shrunk the AsPC-1 spheroids up to 58% (Figure B7).

3.3. Conclusions

The nuclear localization peptides (NLS) are widely used for delivering drugs inside the cell nucleus[53]. NLS is cell penetrating due to the presence of the positive charges[161]. However, the NLS peptides are non-discriminatory, and the toxicity to the normal cells limits their use in drug delivery. We have prepared triggered release polymersomes, armed with a "masked" NLS peptide. We have demonstrated that the NLS peptides on the surface of the redox-sensitive polymersomes are activated in the presence of high MMP-7 isozyme concentration in the vicinity of tumors. Subsequently, the NLS-decorated vesicles penetrate into the cancer cells, enter the nucleus, and release the encapsulated cytotoxic drugs in response to the local reducing microenvironment. We have demonstrated the efficacy of the polymersomes employing monolayer and three-dimensional cultures of pancreatic cancer cells. We observed that the viability of the cancer cell spheroids is reduced to (9.3 ± 0.1)%, and they shrink to (49 ± 23)% in the presence of a combination of polymersomes encapsulating doxorubicin or curcumin. The results of this study can contribute to the design of polymersome formulations, which are more efficient, compared to the current triggered release vehicles for various malignancies, and especially pancreatic cancer.

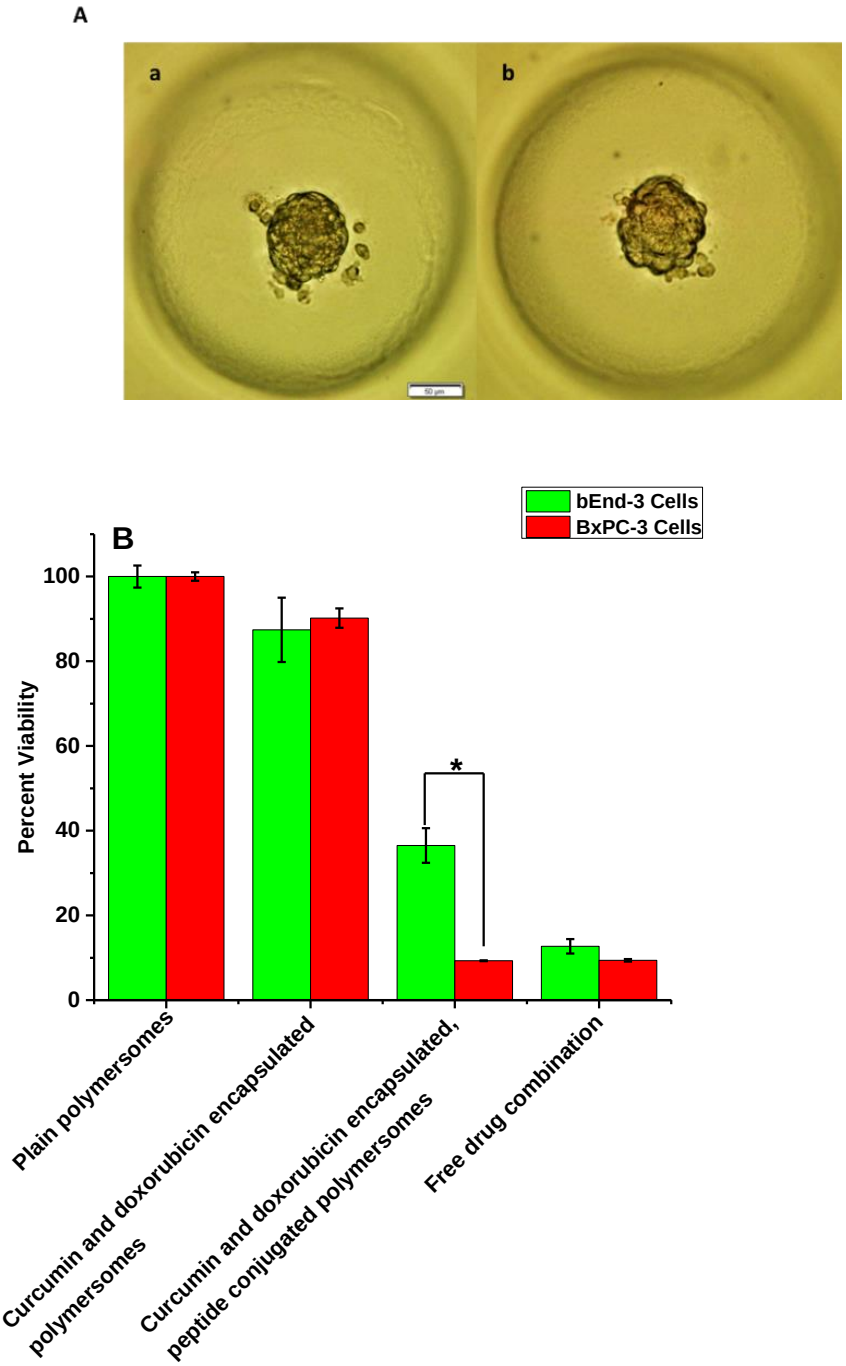

Figure 3.16. Microscopic images of three-dimensional spheroids and their viability after treatment with different polymersome formulations. A: Optical microscopic image of 8-days-old BxPC-3 (a) and bEnd-3 cell (b) spheroids (scale bar: 50 µm). B: The viability of BxPC-3 (red columns) and bEnd-3 cells (green columns) after treatment with different polymersome formulations in 3D spheroids (* $P < 0.05$, $N = 6$).

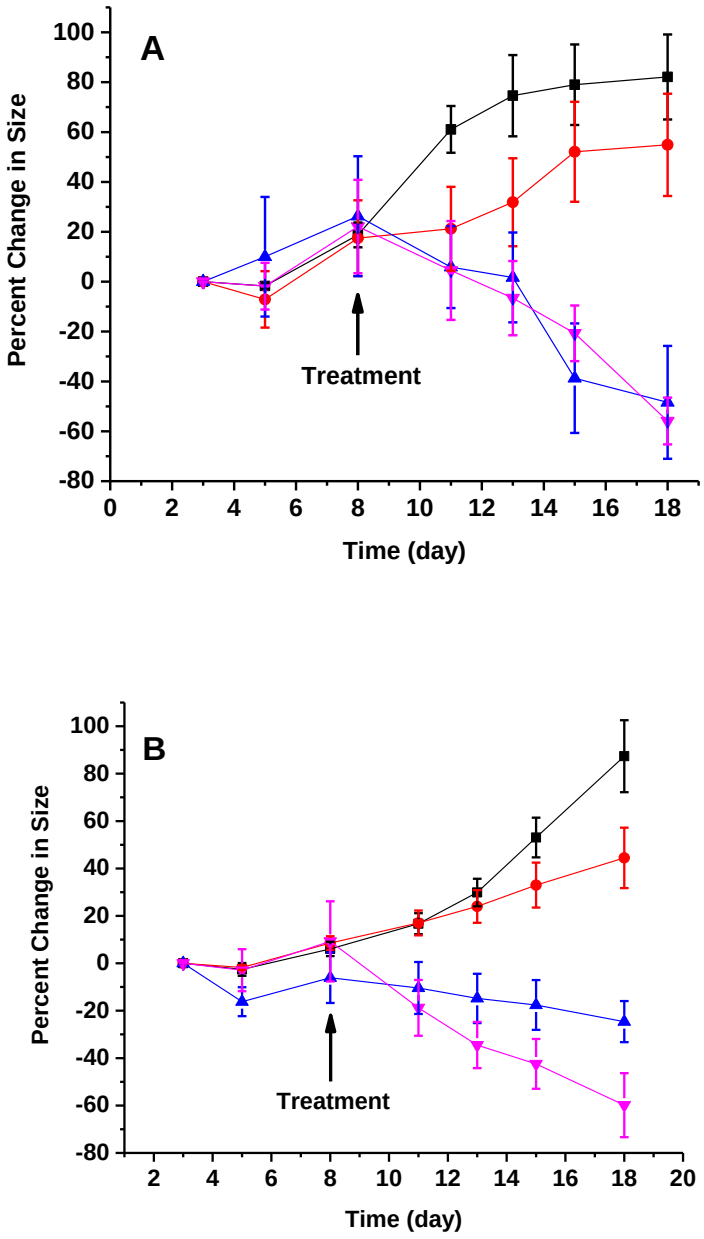

Figure 3.17. Growth curves for the BxPC-3 and bEnd-3 cell spheroids. The 8-day old spheroids of BxPC-3 (A) and bEnd-3 cells (B) were treated with different polymersome formulations, and their growth was monitored for 10 days (N = 12). Black trace with squares: plain polymersomes; red trace with circles: curcumin and doxorubicin encapsulated polymersomes; blue trace with triangles: curcumin and doxorubicin encapsulated, peptide-conjugated polymersomes; magenta trace with inverted triangles: free drug combination.

3.4. Materials and Methods

3.4.1. Polymer Synthesis and Characterization

Two types of block copolymers [PEG (2000)-S-S-PLA (6100), N_3-PEG (2000)-PLA (6000)] (Figure 3.3) have been synthesized applying the ring-opening polymerization and characterized in our laboratory[7, 19].

3.4.2. Synthesis and Purification NLS Peptide with an MMP-7 Cleavable "Mask"

The peptide (hexynoic acid-PKKKRKV-GPMG-IAGQ-EEEE) was synthesized using a microwave-assisted, solid phase peptide synthesizer (Liberty Blue, CEM Corporation, Matthews, SC) using Fmoc-protected amino acids (ChemPep Inc./Chem-Impex International). The synthesized peptide was purified by a reversed phase, high-performance liquid chromatography (RP–HPLC, Shimadzu Scientific Instruments) using a diphenyl preparatory column (PrinstonSPHER, 10 μm particle size, 300 Å pore diameter, 250 mm × 21.2 mm) as the stationary phase. A linear gradient (0-60%) of acetonitrile in water with 0.1% trifluoroacetic acid was used as the mobile phase at a flow rate of 10 mL/min over 60 min. The chromatogram was monitored using a UV detector at 235 nm (Figure B1 A). The purified peptide was characterized using MALDI-TOF mass spectrometry (Applied Biosystems/MDS SCIEX 4800 MALDI TOF/TOF™ Analyzer) (Figure B1).

3.4.3. Enzymatic Peptide Hydrolysis

The synthesized peptide (1mg/mL) was exposed to the recombinant enzymes (MMP-7, MMP-1, and MMP-9, concentration: 2μM) in the presence of 25 mM HEPES buffer (containing 10 mM $CaCl_2$, 10 mM $ZnCl_2$, pH: 7.5) for 1 hour at room temperature. Subsequently, the circular dichroism (CD) spectrometry (Jasco J-815) was used to determine any change in the peptide

structure. For the CD experiments, 0.5 mg/mL peptide in phosphate buffer (8 mM), and 1 mm path-length quartz cuvette was used. For each spectrum, 30 accumulations were recorded at 25 °C.

3.4.4. Cloning, Expression, and Purification of MMP-1 and MMP-7

The catalytic domain of human MMP-1 was cloned in *E. coli*, and the protein was expressed and purified. The coding sequence for the catalytic domain of MMP-1 (amino acid sequence: 98-421) was amplified by PCR using the forward and reverse oligonucleotide primers as 5′-CCAGGGAGCAGCCTCGTTTGTCCTCACTGAGGGGAAC-3′ (Forward Primer), 5′-GCAAAGCACCGGCCTCGTTATTTGGACTCACACCATGTGTTTTCCA-3′ (Reverse Primer). The PCR amplified DNA fragment was cloned into the LIC-His vector and transformed into TOP10® cells (Invitrogen). MMP-1 was expressed and purified from *E. coli* BL21 (DE3) Star® (Invitrogen). Like other MMPs, MMP-1 was found to be confined in the inclusion bodies from where it was purified by solubilizing in buffer (50 mM Tris-HCl, pH 7.5) containing 6 M Urea, 10 mM $CaCl_2$ and 10 µM $ZnCl_2$ followed by subjecting the suspension to serial dialysis against the above buffer with decreasing concentration of urea as described by Tobwala and Srivastava[162]. The folded protein exhibited high catalytic activity and showed a predominant band on SDS-PAGE. The cloning, expression, and purification of human MMP-7 were performed as described by Ganguly et al[163].

3.4.5. Polymersome Preparation

We used the solvent exclusion method[3] to prepare the polymersomes. Briefly, the polymers, PEG-S-S-PLA, and N_3-PEG-PLA were dissolved in tetrahydrofuran (THF) in a 60:40 molar ratios respectively. 5 mg of the polymer solution was added dropwise, while stirring, to 5 mL phosphate buffer (25 mM, pH 7.4) to have a 1mg/ml suspension of polymers. Subsequently, the organic solvent was evaporated by gentle air flow for 45 minutes. The resulted polymersome

solution was then subjected to bath sonication (Aquasonic, 250D, power level 9) for 45 minutes at room temperature. Similar procedure was applied in the preparation of calcein encapsulated polymersomes. In the latter case, the polymer solution was added to a 10 μM calcein solution prepared in the phosphate buffer (25 mM, pH 7.4).

3.4.6. Polymersome-Peptide Conjugation and Characterization

The Copper (II)-catalyzed azide-alkyne cycloaddition ("Click" reaction) was used to form the peptide-polymersomes conjugate. The polymersome solution (1 mg/mL polymer concentration) was mixed with the pure peptide (1:3 molar ratio of azide: alkyne). Copper (II) complex (10 μL of 0.053 M aqueous solution, prepared by mixing an aqueous solution of $CuCl_2$, 0.53 mmol, and *N*,*N*,*N*′,*N*′,*N*″-pentamethyldiethylenetriamine, PMDTA, 2.1 mmol), and sodium ascorbate (10 μL of 27 mg/mL aqueous solution, 1.4 μmol) was added to the mixture and stirred overnight at room temperature[164]. The non-conjugated peptides were separated from the polymersome solution by dialyzing (molecular weight cut off 3500-5000 Da) against phosphate buffer (25mM, pH 7.4) with similar osmolality for 5 days at 4 °C. To verify peptide conjugation, the dialyzed solution (0.4 mg/mL) was subjected to CD spectrometry (8 mM Phosphate buffer, pH: 7.4). A quartz cuvette (1 mm path length) was used in the CD experiments, and 30 accumulations were recorded in each case.

The peptide conjugation was further confirmed by Fourier Transform Infrared spectroscopy (FTIR). A ThermoNicolate, Nexus, 870 spectrometer with a KBr beam splitter in the spectral range of 4000 - 400 cm^{-1} were used at a spectral resolution of 4 cm^{-1} using a mirror velocity of 0.158 cm/s. The experiment was conducted using the transmission accessory. Samples were prepared in the form of pallets using NaCl window. Samples were placed in the universal sample holder for performing the experiment.

3.4.7. Sulfobutyl-β-cyclodextrin (Captisol) - Curcumin Complex Formation

Curcumin (Alfa Aesar, 95% curcuminoid) was solubilized in water in the presence of Captisol (Cydex) according to a reported procedure by the manufacturer (http://www.captisol.com/faq/how-to-solubilize-a-drug-with-captisol/). Briefly, 40% captisol solution was prepared in water, mixed with solid curcumin (92 mg/mL), and stirred in the dark at room temperature for 3 days. Subsequently, the suspension was filtered to remove any non-complexed curcumin.

3.4.8. Preparation of Drug Encapsulated Polymersomes

We prepared two different polymersome formulations encapsulating doxorubicin or curcumin-Captisol complex. For doxorubicin encapsulation, we have used the active pH gradient method[7, 19]. Briefly, we have prepared the polymersomes using the solvent exchange method in citrate buffer (20 mM, pH 4.0). Subsequently, the pH of the external buffer was increased to 7 by adding aqueous sodium bicarbonate solution (2M). Doxorubicin hydrochloride (Bridge Bioservices) was added (0.2 mg/mL of polymersomes) to the polymersome solution and stirred for 1 hour at room temperature. The non-encapsulated doxorubicin was separated from the polymersomes encapsulating the drug using size exclusion chromatography (Sephadex G-100, GE Healthcare). The encapsulation efficacy was estimated by comparing the recorded absorbance spectra of the polymersomes before and after gel filtration.

The curcumin-Captisol complex encapsulated polymersomes were prepared applying the passive encapsulation method, by adding the polymer solution to the curcumin-captisol complex solution. The non-encapsulated complex was removed by passing the polymersomes through a Sephadex G100 gel filtration column. The encapsulation efficiency was calculated by comparing

the absorption spectra of the Captisol-curcumin encapsulated polymersomes with that of the Captisol-curcumin complex.

3.4.9. Size-Distribution and Morphology of the Polymersomes

The hydrodynamic diameter of the polymersomes (1 mg/mL polymer concentration) was determined by dynamic light scattering method using a Zeta Sizer instrument (NanoZS 90, Malvern Instruments). Ten measurements per sample (four repeats) were performed using disposable polystyrene cuvettes, at 90° scattering angle, and the equilibration time was set at 30 seconds for all measurements. Transmission electron microscopy (TEM) was used to verify the structure of the polymersomes. Negatively stained polymersomes were imaged applying a TEM microscope (JEOL JEM 2000).

3.4.10. Determination of the Concentration of Cell Secreted MMP-7

The conditioned media from BxPC-3 and bEnd-3 cells were collected and subsequently concentrated (10 times) using centrifugal devices (PLL, MWCO: 3000 Da). The concentration of MMP-7 was estimated using a commercially-available MMP-7 ELISA kit (RayBiotech) following the manufacturer's protocol.

3.4.11. Release Studies from the Polymersomes

We determined the release of encapsulated calcein (10 μM) in the presence of different concentrations of added reducing agent (GSH, 10 mM, and 50 mM). For the release studies, we prepared the dye-encapsulated polymersomes and subsequently, conjugated the peptide. After conjugation, the fluorescence of the unencapsulated calcein was quenched by 10 mM $CoCl_2$. The release of the encapsulated calcein was determined by monitoring the reduction in fluorescence emission in the presence of added GSH. The experiments were conducted using a 96-well microplate reader (Spectramax M5, Molecular Devices; excitation: 495 nm, emission: 515 nm),

and the release was monitored for 30 minutes after each GSH addition. We also determined the release of encapsulated calcein in the presence of added MMP-7, MMP-9, and MMP-1 (2 μM) without the added GSH (Figure S5).

The release of the drugs (curcumin and doxorubicin) was also tested in the presence of reducing agent. Polymersomes loaded with the drug and were dispensed into a dialysis tube (Spectra/Por Float-A-LyzerG2, MWCO: 3.5-5 kD). The GSH (final concentration 50μM, 10mM, or 50mM) and MMP-7 enzyme (2μM) were added to the polymersome solution, and the release of drug was monitored for 30 minutes after each GSH treatment by UV spectrometry (doxorubicin release was monitored at 483 nm, and curcumin complex at 429 nm). The percent release of the drug from the polymersomes was then calculated.

3.4.12. Atomic Force Microscopic (AFM) Imaging

Polymersomes (1 mg/mL) were treated with 0, 50 μM and 10 mM final concentration of GSH. The samples were prepared by incubating 10 μL of each solution on silicon substrates (University Wafer) for 10 min in a sealed compartment to prevent evaporation at room temperature. The samples were then washed with de-ionized water (Millipore) repeatedly, and dried under purified air flow. The imaging measurements were performed using a commercial atomic force microscope (NT-MDT NTEGRA AFM). The samples were imaged under ambient conditions in semi-contact mode using an AFM tip with a resonant frequency of 190 kHz (Budget sensors).

3.4.13. Cell Culture

The BxPC-3 and AsPC-1 cells (human pancreatic adenocarcinoma, ATTC), were cultured in RPMI-1640 complete growth medium (containing 10% fetal bovine and 1% antibiotic-antimycotic solution, devoid of phenol red) in 75 cm^2 tissue culture flasks incubated at 37 °C in a

humidified atmosphere and 5% CO_2. The bEnd-3 cells (brain endothelial, ATTC) were cultured in DMEM complete medium (devoid of phenol red) under the same conditions.

3.4.14. Nuclear-Targeting Studies

The peptide-conjugated polymersomes encapsulating doxorubicin or curcumin and polymersomes encapsulating doxorubicin or curcumin but devoid of the peptide were used to assess the nuclear targeting in the BxPC-3 and bEnd-3 cells. The concentration of the polymersomes was the same (0.02 mg/mL polymer) for all the experiments. After the cultured cells had been 90% confluent, they were trypsinized and subcultured in 96 well plates (5,000 cells/well). After 12 h, the cells were treated with each formulation (0.02 mg/mL for 1 hour), the nucleus was stained with HOESCHT 33342 dye (Enzo Life Sciences), the cells were washed gently 4 times with sterile HBSS buffer, and subsequently imaged using a fluorescent microscope (Olympus IX81 motorized inverted fluorescent microscope). The 20X objective was used to image the cells and DAPI, FITC, or TRITC filters were used according to the samples.

3.4.15. Three-Dimensional (3D) Spheroid Cell Culture

The three-dimensional (3D) spheroids of all cell lines (BxPC-3, AsPC-1, and bEnd-3) were prepared using an agar mold containing 96 microwells. The mold was cast using a 3D Petri Dish® (Microtissues, natural 3D) in a sterile condition, washed 3 times, and equilibrated with an appropriate cell culture medium overnight. The following day, 10,000 cells were seeded in each microwell according to the manufacturer's guideline. The growth of the spheroids was monitored under a microscope, and the media was changed carefully as needed.

3.4.16. Cell Viability Studies (Two-Dimensional Cell Culture)

The confluent bEnd-3 and BxPC-3 cells were sub-cultured in 96 well cell culture plates. After overnight growth, the cells were divided into 4 treatment groups and treated for 72 hours at

37 ºC. (1) The Control group was treated with phosphate buffer encapsulated polymersomes. (2) Sample 1 was treated with curcumin complex and doxorubicin encapsulated polymersomes (containing 27 and 20 µM of the drugs respectively). (3) Sample 2 was treated with peptide conjugated polymersomes encapsulating curcumin complex and doxorubicin (containing 27 and 20 µM of the drugs respectively). (4) Sample 3 was treated with free drug combination containing both curcumin complex (27 µM) and doxorubicin (20 µM). Each experiment was repeated 6 times. Afterward, the cells were washed, and the viability was determined using the Alamar Blue assay (Life Technologies) following the manufacturer's protocol. The fluorescence intensity of the resorufin was measured using a spectrofluorometer (excitation: 560 nm, emission: 590 nm).

3.4.17. Cell Viability Studies (Three-Dimensional Culture)

A modified Alamar Blue assay was used to assess the viability of the bEnd-, AsPC-1 and BxPC-3 cells in the spheroids. The 8-days old spheroids were treated with the same formulations as the monolayer cultures (described in the previous paragraph). After 72 hours, the spheroids were dislodged from the agar molds by centrifugation, agitated and trypsinized to form single cells, and cultured overnight in a 96 well cell culture plate (6 repeats). The following day, Alamar Blue was added to the wells, and resorufin fluorescence was monitored.

We determined the effect of the drugs and on the growth of the 3D spheroids. The 8-day old spheroids (12 repeats in each group) were treated with the polymersome formulations for 72 hours at 37 °C. The spheroids were washed with phosphate buffer saline, and their growth was monitored for another 10 days. The spheroid images were analyzed using the Image J software, and the percentage growth rate was calculated.

4. TARGETED CYTOPLASMIC CALCIFICATION: A DRUG-FREE, POLYMERSOMAL PROSTATE CANCER THERAPY[4]

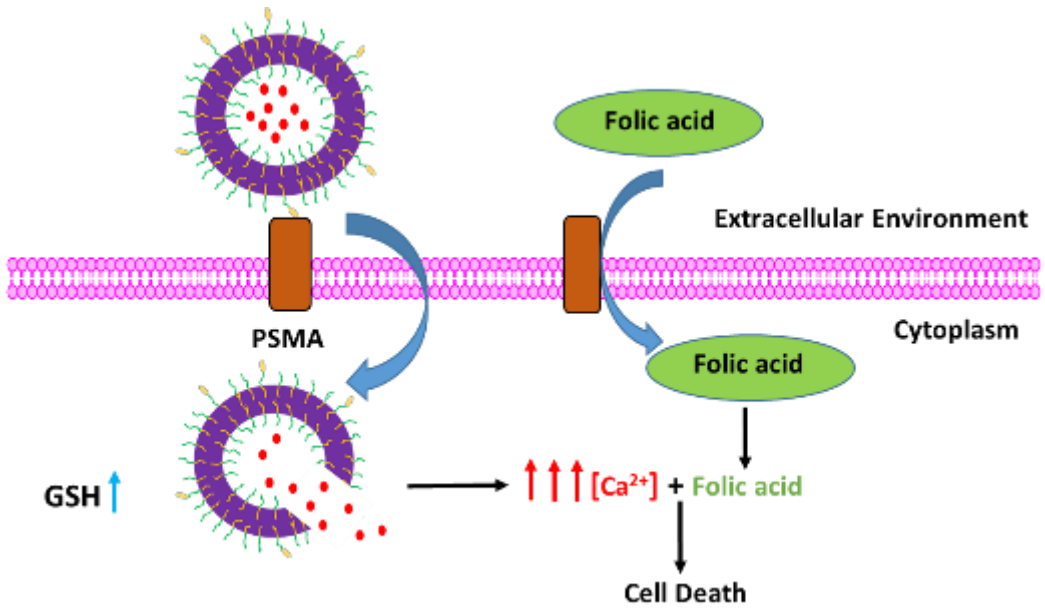

Figure 4.1. Graphical abstract.

4.1. Introduction

Cancer is one of the most lethal diseases around the world. Based on the American Cancer Society estimation, 1,688,780 new cancer cases will be diagnosed, with 600,920 deaths in the US during 2017. Among the various types of malignancies, prostate cancer is the second leading cause of death, especially for men older than 65 years (based on American Cancer Society report).

[4] This section is coauthored by Tayebeh Anajafi, Abbas Sedigh, Seungyong You, Manas K. Haldar, Yongki Choi, D. K. Srivastava, and Sanku Mallik. Tayebeh had primary responsibility to conduct all the experiments, analyze the data in and write the manuscript. Abbas assisted in testing the efficacy of polymersomes. Jamie imaged the polymersomes using AFM. Manas synthetized the polymers. Drs. Choi, Srivastava and Mallik verified the data and advised on experimental designs.

Conventional treatment options for prostate cancer includes surgery, chemotherapy, radiation therapy, and a few others (hormone therapy, vaccine treatment). Most of these treatments have many side effects, which decrease the quality of life of the patients. Development of new technologies with lower side effects is required to treat this devastating disease in the early stages.

Targeted therapy offers the hope of treating cancer with minimum effect on the healthy cells. Both passive and active targeting strategies alter the bio-distribution of therapeutics[165]. The passive targeting utilizes the presence of leaky vasculature in the tumor tissues to deliver nanoparticles loaded with the drug of choice[165]. Furthermore, the drainage of the cancer tissues is also defective, resulting in the retention of the nanoparticles in the tumor sites [the Enhanced Permeation and Retention (EPR) effect[115]]. In active targeting strategy, the presence of a particular protein on the plasma membrane helps to concentrate the nanoparticles in the malignant cells[166].

Prostate Specific Membrane Antigen (PSMA)[167] is an excellent cell surface protein for targeting the prostate cancer. PSMA is overexpressed about one thousand times[85] on the surface of prostate cancer cells and solid tumors neovasculature. This receptor is capable of taking up folate via receptor-mediated endocytosis through clathrin-coated pits[85, 86].

Intracellular calcium ion homeostasis (Figure 4.2) is a complex, finely regulated, and vital mechanism for proper cell function, gene expression, apoptosis regulation, heart muscle contraction, etc. Intracellular calcium ion concentration (~ 100 nM)[168] maintenance is the result of the cooperation of various calcium channels and transporters located on the cellular, mitochondrial, and endoplasmic reticulum membranes[87]. Transient changes in cytoplasmic calcium ion concentration stimulates calcium signaling. However, the elevated calcium ion levels are lowered quickly to maintain the intracellular calcium homeostasis. Dysregulation of calcium ion homeostasis is toxic to the cells and triggers apoptosis via several pathways[169] (Figure 4.3).

Hence, intentionally disturbing the calcium ion homeostasis and stimulating calcium crystal formation could lead to cell death. Zhao et.al have reported that folic acid's carboxylate groups induce the nucleation of calcium crystals on the surface of HeLa cells[88].

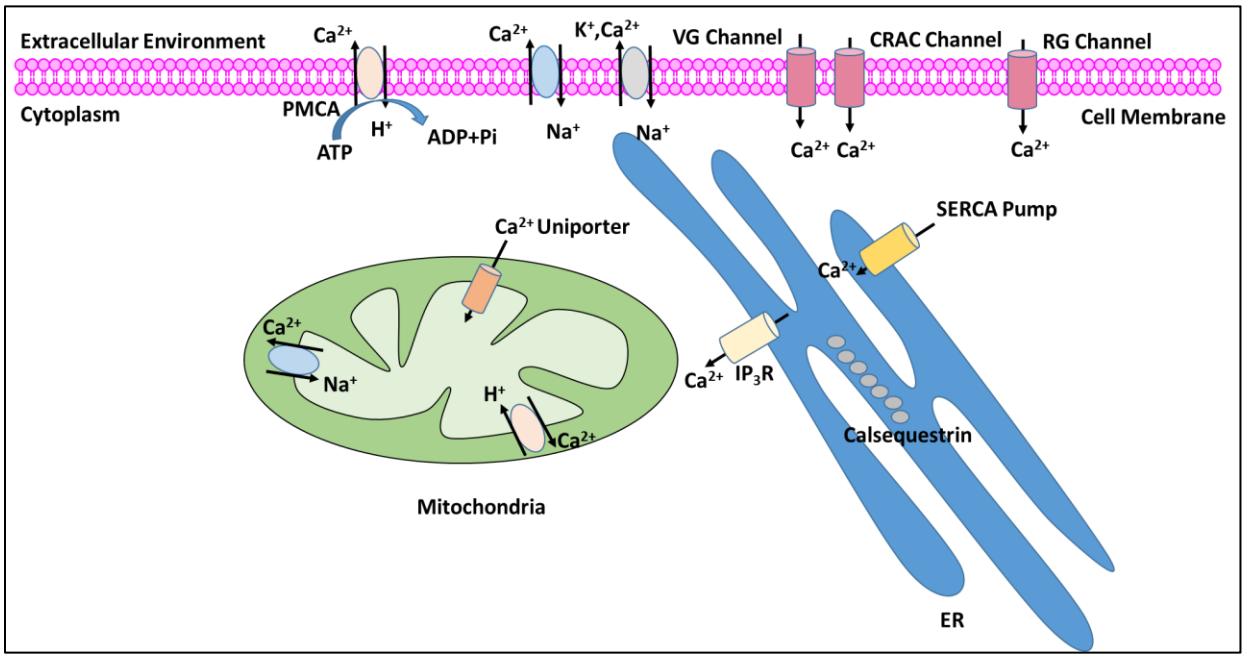

Figure 4.2. Intracellular calcium ion homeostasis. Calcium ion uptake from the extracellular environment occurs through various Ca^{2+} channels [e.g., Voltage-gated (VG) channels, Receptor gated (RG) channels, and Ca^{2+} release activated Ca^{2+} (CRAC) channels]. Intracellular Ca^{2+} can be transported to the endoplasmic reticulum (ER) via sarcoendoplasmic reticulum Ca^{2+} ATPase (SERCA) pump. The Ca^{2+} binding protein calsequestrin stores Ca^{2+} inside the ER. Interaction of the inositol-1,4,5- trisphosphate receptors (IP3R) with its ligand triggers calcium ion release from the ER. Mitochondria is another Ca^{2+} storage organelle in the cells. In this organelle, Ca^{2+} uniporter opens up because of an increase in the cytoplasmic [Ca^{2+}]. In the other hand, Ca^{2+}/Na^{+} and Ca^{2+}/H^{+} exchangers are gates for Ca^{2+} release from the mitochondria. Plasma membrane calcium ATPase (PMCA), and Ca^{2+}ion exchangers are the cytoplasmic calcium export systems embedded on the cell's plasma membrane.

Polymersomes[13] are spherical polymeric bilayers, with an aqueous interior. These nano-vesicles can encapsulate both hydrophobic and hydrophilic compounds and carry them to their site of action with the minimum leakage during their journey[170]. Conjugation of targeting groups on the surface localizes the polymersomes at the intended sites. Selection of appropriate block

copolymers renders the vesicles as biocompatible and biodegradable. Incorporating stimuli-responsive groups in the block copolymers allows spatial and temporal control over the contents release from the vesicles[171]. The intrinsic difference between the cytoplasmic and plasma oxidative states[109] is an excellent stimulus for releasing the polymersomal contents inside the cells. Higher concentration of reducing agent glutathione (GSH) in the cytoplasm (10 mM vs 50 µM in extracellular environment) stimulates the reductive cleavage of the disulfide bonds of the copolymers, resulting in the rapid release of the encapsulated drugs from the vesicles[172]. We have recently used the higher reducing agent concentration to deliver anticancer drugs selectively to cell nuclei.

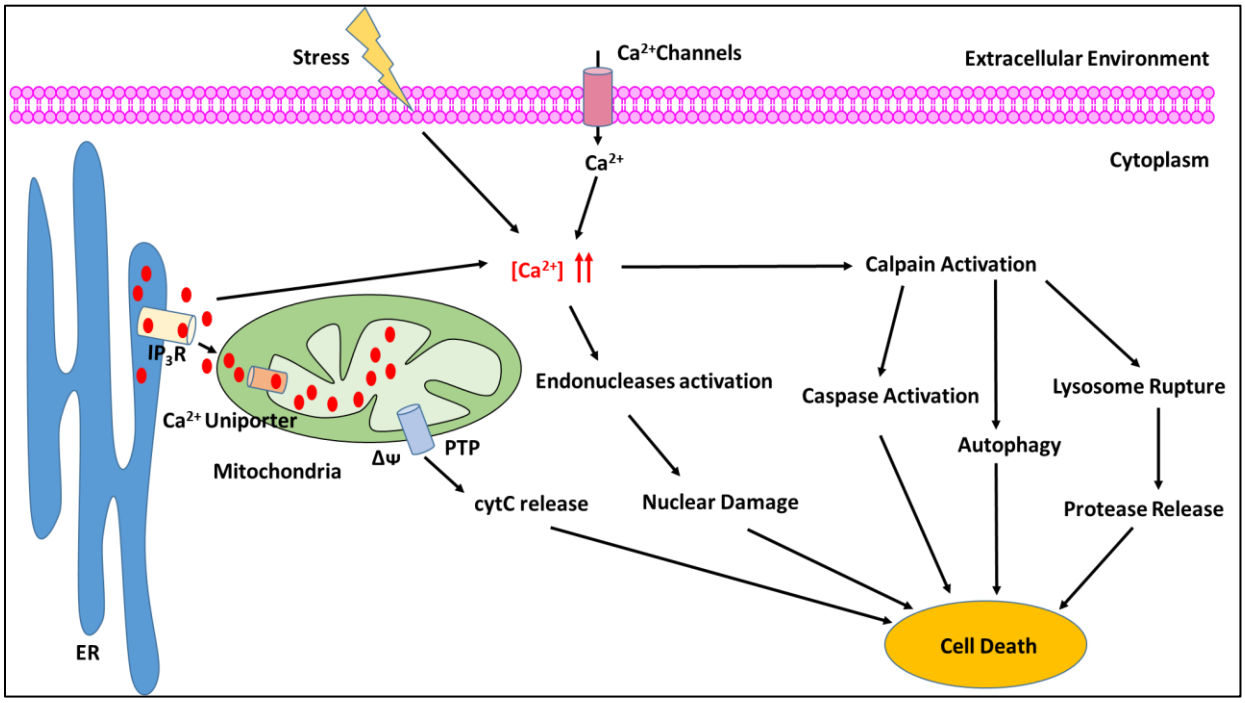

Figure 4.3. The increase in the cytoplasmic Ca^{2+} concentration could be the result of environmental or genetic stress[173, 174]. Calcium ions are imported to the cytoplasm through various Ca^{2+} channels or released from its intracellular storages (ER and mitochondria). Calcium overload in the mitochondria induces the formation of PTP (Permeability Transition Pore)[175] which leads to loss of mitochondrial membrane potential ($\Delta\Psi$) followed by the release of mitochondrial enzymes (e.g., cytochrome C)[173] which promotes cell death. Furthermore, increased cytoplasmic calcium concentration can be sensed by calpain which leads to lysosomal rupture, caspases activation[176], and increase in autophagy[174].

In the present study, we have used folate presenting, redox sensitive polymersomes to target the prostate cancer cells overxpressing the PSMA receptor on the surface. The polymersomes encapsulate a high concentration calcium chloride (50 mM $CaCl_2$). Reduction-triggered release of the encapsulated $CaCl_2$ in the cytoplasm, in presence of folic acid, causes the formation of calcium crystals and dysregulation of calcium homeostasis, leading to apoptosis of the targeted prostate cancer cells.

4.2. Materials and Methods

4.2.1. Polymer Synthesis and Characterization

A disulfide-linked block copolymer [PEG (1900)-S-S-PLA (6100), Figure 4.4A] was synthesized by the ring opening polymerization in our laboratory. The synthesized polymer was purified and characterized by nuclear magnetic resonance spectroscopy[19, 172]. A commercially available (Nanocs Inc.) folate conjugated-phospholipid PEG derivative (DSPE-PEG (2000)-folate) was also used in the preparation of the vesicles (Figure 4.4B).

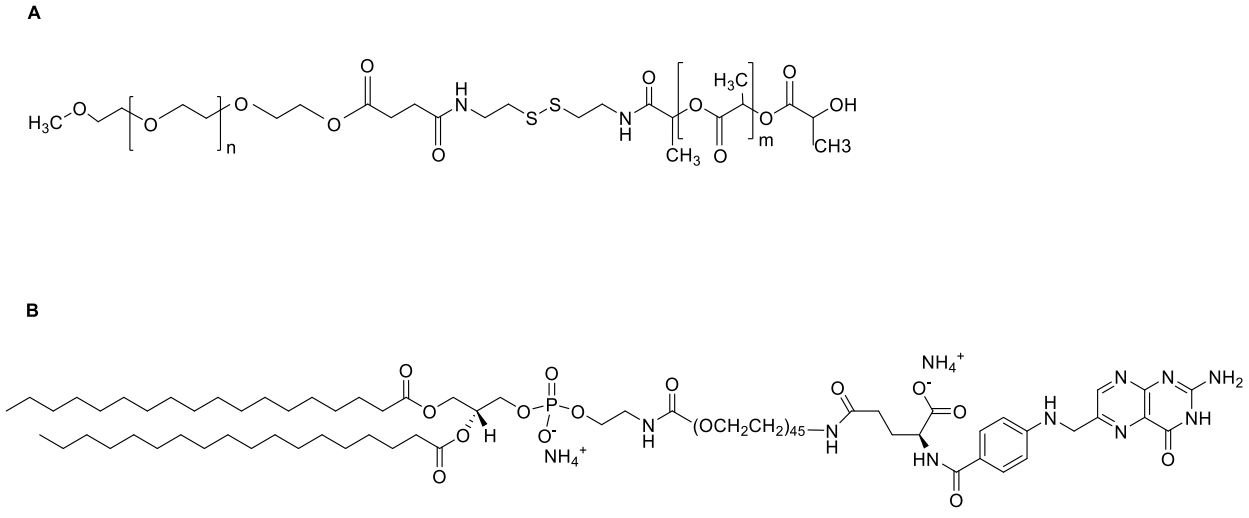

Figure 4.4**.** Structures of (**A**) PEG (2000)-S-S-PLA (6100), and (**B**) DSPE-PEG (2000)-folate.

4.2.2. Polymersome Preparation

The solvent exchange method was used to prepare the polymersomes[3]. The polymer to lipid molar ratio was set at 95:5. Briefly, the folate-conjugated lipid was added to the polymer solution (in tetrahydrofuran, THF). The resultant solution was added dropwise to a phosphate buffer (pH: 7.4) containing 50 mM calcium chloride ($CaCl_2$) to make a 1 mg/mL polymersome solution. The organic solvent then was removed by blowing air through the solution for 45 minutes. Removal of the organic solvent aids the polymersome formation[177]. Subsequently, the solution was sonicated (Aquasonic, 250D, power level 9) for one hour at room temperature. The unencapsulated $CaCl_2$ was removed from the polymersomes using a cation exchange resin (Dowex HCR-W2). We used the same strategy for preparing the calcein encapsulated polymersomes. Calcein (10 μM) was encapsulated into the aqueous core of the polymersomes using the passive encapsulation method[3].

For the polymersomes containing the 1,2-dioleoyl-*sn*-glycero-3-phosphoethanolamine-N-(Lissamine rhodamine B sulfonyl, ammonium salt), we used a molar ratio of polymer: lipid: lissamine rhodamine as 90: 5: 5 respectively. The polymer and the folate lipid were mixed with the lissamine rhodamine lipid in THF, and the solution was added dropwise to the aqueous buffer followed by air blowing and sonication (described in the previous paragraph).

4.2.3. Size-distribution of the Polymersomes

The hydrodynamic diameter of the polymersomes was determined by dynamic light scattering (DLS) employing a zeta sizer instrument (NanoZS 90, Malvern Instruments) at 90° scattering angle. The solutions of the different polymersome solutions (1 mg/mL total polymer) were used, and 10 measurements per sample was monitored (four repeats). Disposable polystyrene cuvettes were used and equilibration time was set to 60 seconds.

4.2.4. Atomic Force Microscopy Imaging

Polymersome morphology was investigated using Atomic Force Microscopy (AFM)[172]. AFM scans were carried out in non-contact mode at a scanning rate of 0.7 Hz and a resonance frequency of 145 kHz using an NT-MDT NTEGRA (NT-MDT America, Tempe, AZ). The scanning areas were 5 μm x 5 μm at the resolution of 512 points per line, respectively. The polymersome solution was dropped on top of a silicon chip. The dropped solution was left at room temperature for 10 minutes. The remaining solution was blown away with an air-blow gun. For the GSH treated polymersome samples, the GSH solution was added into polymersomes to have a final concentration of 10 mM GSH, and the mixture was incubated for 10 minutes.

4.2.5. Calcium Chloride Encapsulation Measurement

To test the amount of encapsulated $CaCl_2$ in the polymersomes, we used Triton-X100 to disrupt the vesicles. Subsequently, we used a calcium colorimetric assay kit (BioVision) to measure the amount of $CaCl_2$ released from the disrupted polymersomes.

4.2.6. Release Studies

We used the calcein-encapsulated polymersomes (40 μl, 1 mg/mL) to demonstrate reduction-triggered release of the contents. The fluorescence from the unencapsulated calcein was quenched using a high concentration of a quencher ($CoCl_2$, 10 mM). The decrease in the calcein fluorescence (excitation: 495 nm, emission: 515 nm) from polymersomes was monitored using a 96-well plate reader (Spectramax M5, Molecular Devices) for 40 minutes in the presence of 50 μM glutathione (GSH). Subsequently, the release was monitored for another 40 minutes in the presence of 10 mM GSH.

4.2.7. Cell Culture

Human Embryonic Kidney 293 cells (HEK-293, ATTC) were cultured in Dulbecco's modified Eagle's (DMEM) medium supplemented with fetal bovine serum (10%), and antibiotic-antimycotic solution (1%). Human prostate adenocarcinoma cells (LNCaP, ATTC) were cultured in RPMI-1640 complete growth medium supplemented with the same components. Both cell lines were incubated at 37°C, 5% CO_2, in a humidified atmosphere.

4.2.8. Crystal Formation

For the crystal formation studies, we used cell culture media (DMEM) containing 500 µg/mL folic acid and 50 mM $CaCl_2$. After 24 hours incubation, brightfield images of crystals was recorded using a microscope (Olympus IX81 motorized inverted fluorescence microscope).

4.2.9. Cellular Uptake Study

To study the role of PSMA in the active targeting, we tested the uptake of the polymersomes with two different cell lines. For the ease of visualization, we incorporated a lipid with the lissamine rhodamine dye (5% molar ratio) in the bilayer of the polymersomes presenting folate on their surface. The LNCaP and HEK-293 cells were sub-cultured in 96 well plates. Once the cells were confluent, the polymersomes were incubated with the cells, and the nuclei were stained with Hoechst 33342 dye (Enzo Life Sciences). Subsequently, the cells were washed with cell culture media (phenol red free), and the uptake of the polymersomes were monitored using 20X objective of a fluorescence microscope.

4.2.10. Spheroid Cell Culture

We cultured the LNCaP and HEK-293 cells in agar molds. The molds were constructed using 3D petridishes (Microtissues, natural 3D). Each petridish has the capacity to grow 96 cell

spheroids. After equilibrating the agar molds with the appropriate cell culture media (DMEM or RPMI), 10,000 cells were cultured in each petridish. The cells then were incubated at 37°C in a humidified atmosphere. After 2 days, the spheroids formed, and we replaced the media with fresh media every other day. The growth of the spheroids was monitored using light microscopy.

4.2.11. Cell Viability Studies (Monolayer Culture)

For the viability studies, we subcultured the HEK-293 and LNCaP cells in 96 well culture plates. After 12 hours, the culture media was replaced with a media containing 500 µg/mL folic acid (HBSS was added to control wells) and incubated for 15 minutes. Following the incubation, the cells were treated with the polymersomes encapsulating $CaCl_2$. The treated cells were then incubated at 37 °C for 24 hours. The cells were subsequently imaged using light microscopy, and the viability was tested using Alamar Blue assay (Life Technologies). The fluorescence intensity of the reduced form of resazurin was measured using spectrofluorometery (excitation: 560 nm, emission: 590 nm).

4.2.12. Cell Viability Studies (Three-Dimensional Culture)

We used the 7-day old spheroids (Figure 4.5) to study the viability after treating with the polymersome formulations. We used four different treatment groups, the control (no treatment), folic acid treatment (media containing 500 µg/mL), polymersomes encapsulating Ca^{2+} ions (0.04 mg/mL), and folic acid + polymersomes encapsulating Ca^{2+} ions. The culture media were removed and replaced with fresh media (control) or media containing the appropriate treatment. The spheroids were incubated at 37°C for 24 hours and then the media was removed. To check the cells viability, we dislodged the cells from the molds and triturated them to make single cell suspensions. Subsequently, the cells were cultured in 96 well plates (6 repeats each treatment

group) and incubated overnight. Then Alamar Blue assay was used to determine the viability of cells in each treatment group.

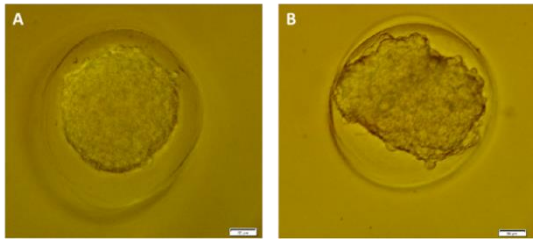

Figure 4.5. Seven-day-old spheroids of (**A**) HEK-293 cells, and (**B**) LNCaP cells. The scale bar is showing 50 µm.

4.2.13. Spheroids Growth Curve

We studied the effect of different treatments on the spheroid's size. We designed the experiments with the same treatment groups as mentioned in the previous section. We monitored the growth of spheroids from the second day. On the seventh day, the spheroids were treated with the polymersomes. After 24 hours, the media was changed and we monitored the growth of the spheroids for 15 days. The percentage change in the spheroid size was calculated and the growth curve was plotted.

4.2.14. Mitochondrial Membrane Permeability (MMP) Assay

Confluent LNCaP cells were incubated with targeted polymersomes encapsulating calcium chloride supplemented with folic acid for 24 hours at 37 °C. Subsequently, the cells were washed with HBSS buffer and stained with 200 nM tetramethylrhodamine methyl ester (TMRM, Molecular Probes) for 30 minutes at 37 °C. Cells were the harvested and analyzed by flow cytometry using a BD Accuri™ C6 flow cytometer. Fluorescence intensity of TMRM-stained cells (20,000 cells per sample) was measured using the FL2 channel.

4.3. Results and Discussion

4.3.1. Polymer Synthesis and Characterization

The ratio of the hydrophilic part to the total mass of the copolymer (*f* value)[13] was considered in preparing the building blocks of the polymersomes. We synthesized the reduction-sensitive block copolymers (Figure 4.4A) with an f value of 0.24. The incorporation of a disulfide bond between the hydrophilic polyethylene glycol (PEG) and the hydrophobic polylactic acid (PLA) blocks endows reduction response to the polymers (Figure 4.4A). Polyethylene glycol (PEG) was used as the hydrophilic block to decrease the uptake of the polymersomes by the reticuloendothelial system and increase the biocompatibility and water solubility[178]. The PEG layer also increases the circulation time of the polymersomes[179]. Polylactic acid (PLA) is a biocompatible polymer[180], and was used as the hydrophobic block in our studies.

4.3.2. Crystal Formation in Cell Culture Media

Incubating the cell culture media for 24 hours containing 500 µg/mL folic acid with $CaCl_2$ (50 mM), resulted in the formation of calcium phosphate crystals, which were visualized using light microscopy with 20X magnification (Figure C1).

4.3.3. Polymersome Preparation and Characterization

The polymersomes were designed to have the ability to target the cancer cells overexpressing the PSMA receptor on the cell membrane. Hence, we incorporated 5 mole% of DSPE–PEG (2000)–folate lipid (Figure 4.4B) in the polymersome bilayer. The inherent reducing environment in the cell cytoplasm[181] was used to trigger content release from the polymersomes in the cytoplasm. Therefore, 95 mole% of the polymersome bilayer was made of the synthesized PEG-S-S-PLA copolymer. The polymersomes were prepared using the solvent exchange method (Materials and Methods). Based on dynamic light scattering, the average hydrodynamic diameter

of the polymersomes was (94 ± 18) nm, and the polydispersity was (0.5 ± 0.01) (Figure 4.6). Atomic force microscopy (AFM) imaging revealed the spherical structure of the polymersomes (Figure 4.8A).

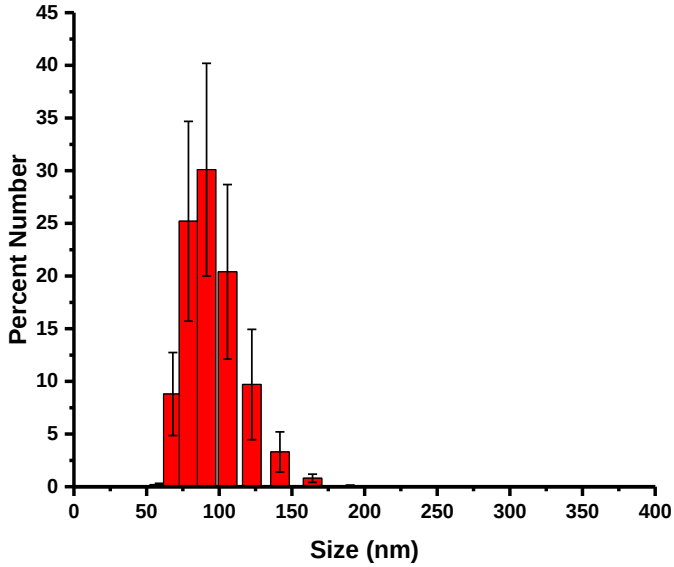

Figure 4.6. Size distribution of the polymersomes measured by dynamic light scattering. The hydrodynamic diameter of the polymersomes was (94 ± 18) nm, and polydispersity of 0.5 ± 0.01 (N=4).

4.3.4. Calcium Chloride Encapsulation in the Polymersomes

Calcium chloride ($CaCl_2$) was successfully encapsulated in the polymersomes aqueous core. To measure the encapsulation efficacy, the polymersomes were treated with Trition-X100 to disrupt the bilayer of the vesicles. The amount of $CaCl_2$ was then quantified by forming a chromogenic complex with *o*-cresolphthalein. Absorption of the complex was measured at 575 nm. The encapsulation efficacy (27 ± 1)% was calculated by comparing the absorption of the complex with a standard curve (Figure C2).

4.3.5. Reduction-Triggered Content Release from the Polymersomes

Human plasma has a more oxidative environment (reducing agent concentration: 10-40 μM)[19, 182] compared to the cell cytoplasm (glutathione concentration 5 – 10 mM)[109,181]. We used this intrinsic difference in reducing agent concentration to trigger the release of polymersome contents. The release of encapsulated dye calcein was monitored using fluorescence spectrometry in the presence of 0, 50 μM, and 10 mM GSH. We observed about 6% release from the polymersomes after 80 minutes in the absence (Figure C3) or in the presence of 50 μM GSH (Figure 4.7). However, the addition of 10 mM GSH, to mimic the cell cytoplasm reductive environment, caused a burst content release of 23% from the polymersomes (Figure 4.7). Furthermore, the structure of the polymersomes was imaged in the presence of 10 mM GSH employing AFM. As shown in the Figure 4.8C, treating with 10 mM GSH quickly deformed the vesicles.

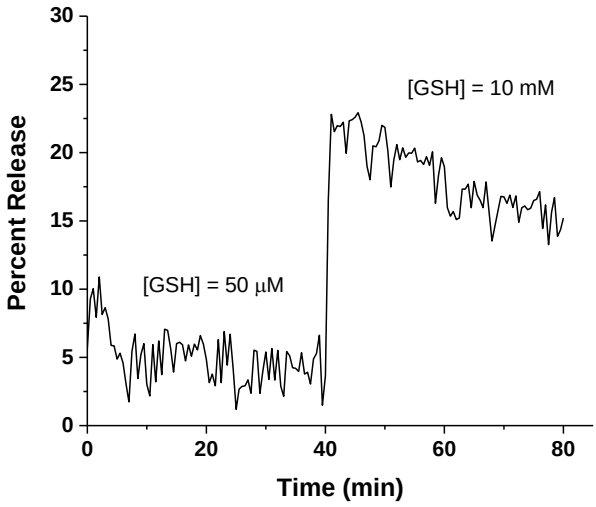

Figure 4.7. Triggered release of encapsulated calcein from the polymersomes. Calcein release was monitored in the presence of 50 μM and 10 mM GSH (N = 6) employing fluorescence spectroscopy (Ex: 495 nm, Em: 515nm).

4.3.6. Monolayer Cell Cultures

To demonstrate the active targeting, we treated the PSMA positive (LNCaP), and PSMA negative (HEK-293) cells with polymersomes incorporating the fluorescent lissamine rhodamine lipid (Ex/Em: 560/583 nm) in their bilayer. This dye is visualized employing the TRITC filter in a fluorescence microscope. The imaging experiments revealed that the polymersomes (after 1 hour incubation) effectively enter the PSMA positive cells (LNCaP cells) and not the HEK-293 cells (Figure 4.9).

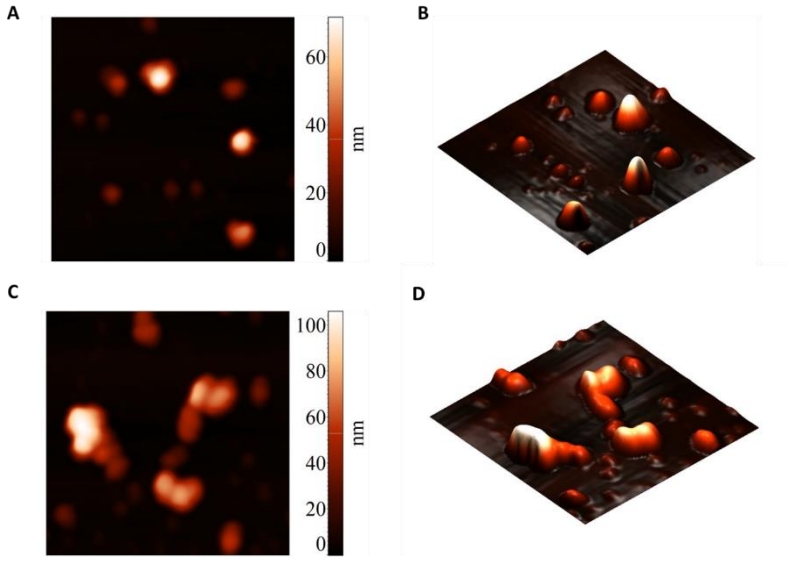

Figure 4.8. Atomic force microscopy (AFM) images of polymersomes before (**A**-**B**) and after treatment with 10 mM GSH (**C**-**D**). Polymersomes' spherical shape is visible in Panels **A** and **B**, and the doformations in Panels **C** and **D**.

To test the toxicity of the formulations in monolayer cell culture, we performed the Alamar Blue assay (Figure 4.10). The results indicated that the calcium ion encapsulated, targeted polymersomes in combination with folic acid is more toxic to the cancer cells (LNCaP) overexpressing the PSMA receptor. However, the same formulation has lower toxicity to the non-cancerous cells (HEK-293) lacking the PSMA receptor on the surface. On the other hand, in the absence of folic acid, the formulation has less toxicity to both cells lines, possibly due to lack of

calcium micro-crystal formation[88]. The viability was more than 80% for both cells (HEK-293 cells: 85 ± 11%, LNCaP cells: 90 ± 17%) in the presence of the targeted polymersomes encapsulating calcium chloride. However, the same polymersomes, in the presence of folic acid, decreased the cell viability to 55 ± 18% and 34 ± 10% for the HEK-293 and LNCaP cells, respectively. Moreover, the non-targeted formulation did not show significant toxicity in both cell lines, indicating the successful targeting strategy (Figure 4.10).

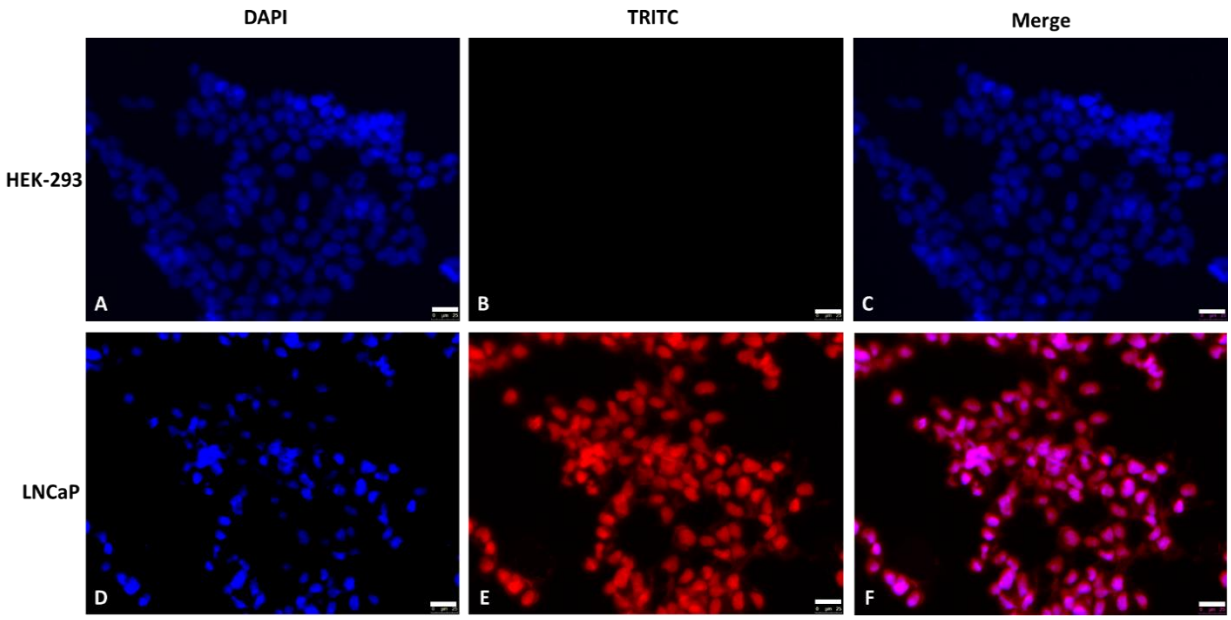

Figure 4.9. Fluorescence microscopic images of the HEK-293 (Panels A-C) and LNCaP cells (Panels D-F) treated with polymersomes presenting folic acid on the surface for 1 h. The cells nuclei are stained with HOESCHT 33342 dye and are imaged using the DAPI filter (A and D). Red fluorescence is originating from the lissamine rhodamine dye incorporated in the bilayer of the polymersomes. TRITC filter is used to image the polymersomes (B and E). The Panels C and F are showing the merged images (scale bars: 25 μm).

4.3.7. Three-dimensional (3D) Spheroids

There are significant differences between the conventional two-dimensional cell culture and the in vivo tumors. For example, the cells in the tumor's core are necrotic and hypoxic, which confers resistance to chemo and radiotherapy[183]. The three-dimensional spheroids resemble the tumors more than the conventional monolayer cells[184]. We cultured the HEK-293 and LNCaP cells

as spheroids using agar molds. Subsequently, the 7- day-old spheroids were treated with different formulations including phosphate buffer, folic acid, polymersomes encapsulating $CaCl_2$, polymersomes encapsulating $CaCl_2$ supplemented with folic acid, and non-targeted polymersomes supplemented with folic acid. After 24 hours, the media was replaced with fresh media. The spheroids were dislodged from the agar molds and disrupted by extensive trituration. The cells were then subcultured in 96 well plates and incubated overnight. The Alamar Blue assay was then performed to measure the toxicity of different formulations in spheroid cultures of the cells (Figure4.11). The viability was 96 ± 9% for HEK-293 cells and 65 ± 4% for LNCaP cells in the presence of targeted polymersomes encapsulating calcium chloride. However, the same polymersomes, in the presence of added folic acid, decreased the cell viability to 59 ± 7% and 38 ± 4% for the HEK-293 and LNCaP cells, respectively. The targeted polymersomes were more toxic to the LNCaP cells compared to the HEK-293, demonstrating the effect of active targeting.

In a separate experiment, we formed HEK-293 and LNCaP cell spheroids and monitored their growth for 15 days. On the seventh day, we treated the spheroids with four different formulations including phosphate buffer, folic acid, polymersomes encapsulating $CaCl_2$, and polymersomes encapsulating $CaCl_2$ supplemented with folic acid. The spheroids were incubated at 37°C for 24 hours. Subsequently, the media was replaced with new media to remove the treatments and the spheroid's growth was monitored for eight more days. Percent change in the size of the spheroids is shown in Figure 4.12. The formulations did not affect the growth of the HEK-293 cell spheroids (Figure 4.12A). We observed that the polymersomes encapsulating $CaCl_2$ supplemented with folic acid have the highest ability to shrink the LNCaP micro-tumors (43% shrinkage) in one week (Figure 4.12B, blue inverted triangles).

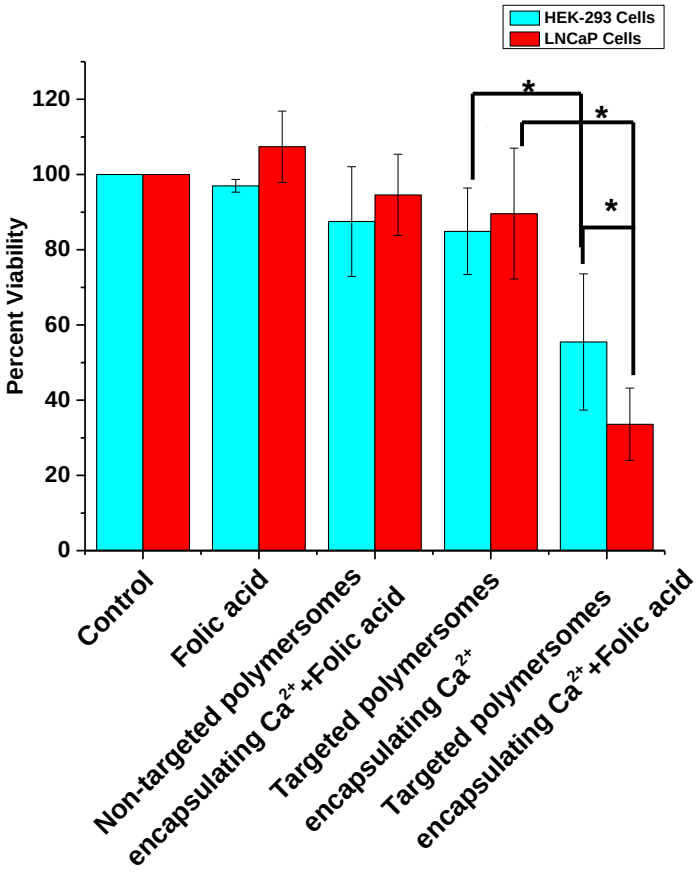

Figure 4.10. Viability of LNCaP (red bars) and HEK-293 (cyan bars) cells in monolayer cultures. The confluent cells were treated with HBSS (control), folic acid, non-targeted polymersomes encapsulating Ca^{2+}, targeted polymersomes encapsulating Ca^{2+}, and targeted polymersomes encapsulating Ca^{2+}+ folic acid for 24 hours. Subsequently, the cell viability was determined employing the Alamar Blue assay (*$P < 0.05$, $N = 6$).

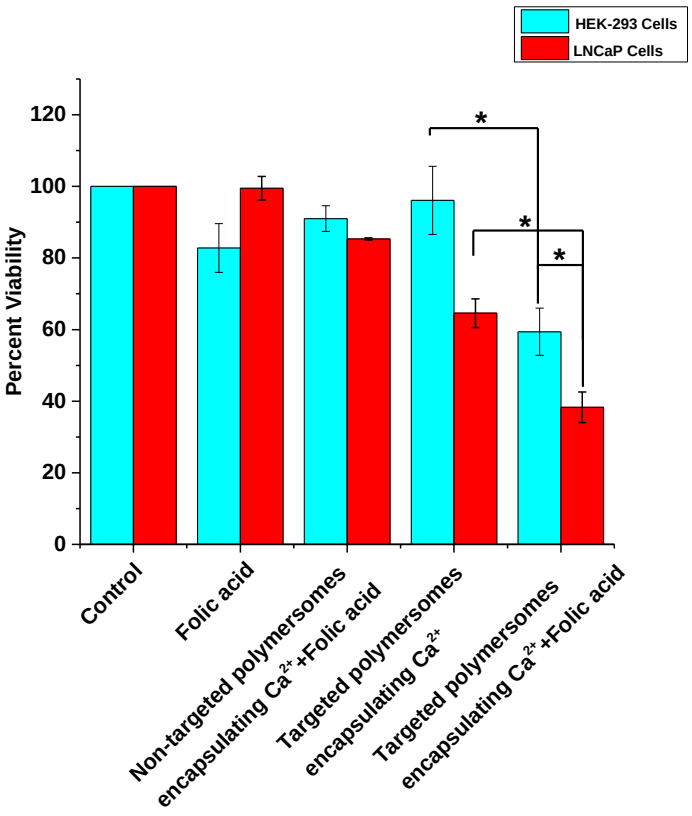

Figure 4.11. Cell viability analysis of LNCaP (red bars) and HEK-293 (cyan bars) spheroids. The 7-day-old spheroids were treated with HBSS (control), folic acid, non-targeted polymersomes encapsulating Ca2+, targeted polymersomes encapsulating Ca2+, and targeted polymersomes encapsulating Ca2++ folic acid for 24 hours. Subsequently, the cell viability was determined employing the Alamar Blue assay (*$P < 0.05$, $N = 6$).

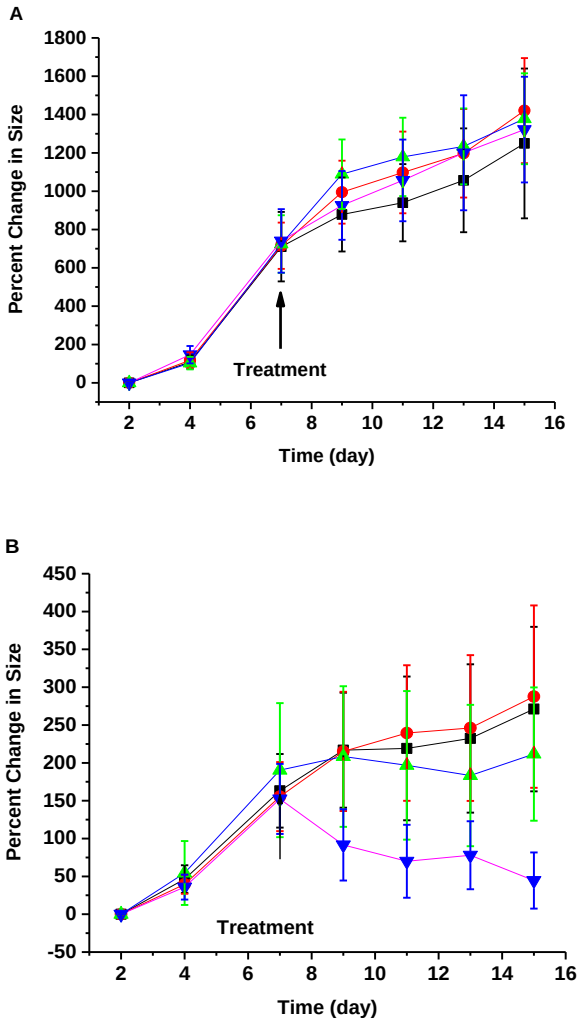

Figure 4.12. The growth curves for the HEK-293 and LNCaP spheroids. The 7-day-old spheroids of HEK293 cells (A), and LNCaP cells (B) were treated with HBSS buffer as a control (black squares), folic acid (red circles), targeted polymersomes encapsulating Ca^{2+} (green triangles), and targeted polymersomes encapsulating Ca^{2+}+ folic acid (blue inverted triangles) for 24 hours. The growth of the spheroids was monitored for a total of 15 days (N = 12).

4.3.8. Loss of Mitochondrial Membrane Potential

To determine the mechanism of cell death, we tested the possible loss of the mitochondrial membrane potential[185]. In this endeavor, we stained the LNCaP cells with TMRM dye, and analyzed the fluorescence intensity (Ex: 548 nm, Em: 574 nm) using flow cytometry. Loss of membrane potential can be recognized by the decreased TMRM fluorescence intensity[186]. We

observed that the cells treated with the targeted polymersomes encapsulating Ca^{2+} in the presence of folic acid showed lower fluorescence intensity compared to the control cells (treated with HBSS) (Figure 4.13). The reduced fluorescence intensity indicates that the loss of mitochondrial membrane potential is a possible mechanism for killing the cancer cells. Table 1 shows the mean fluorescence intensity of the TMRM stained cells measured with the FL2 channel of the flow cytometer.

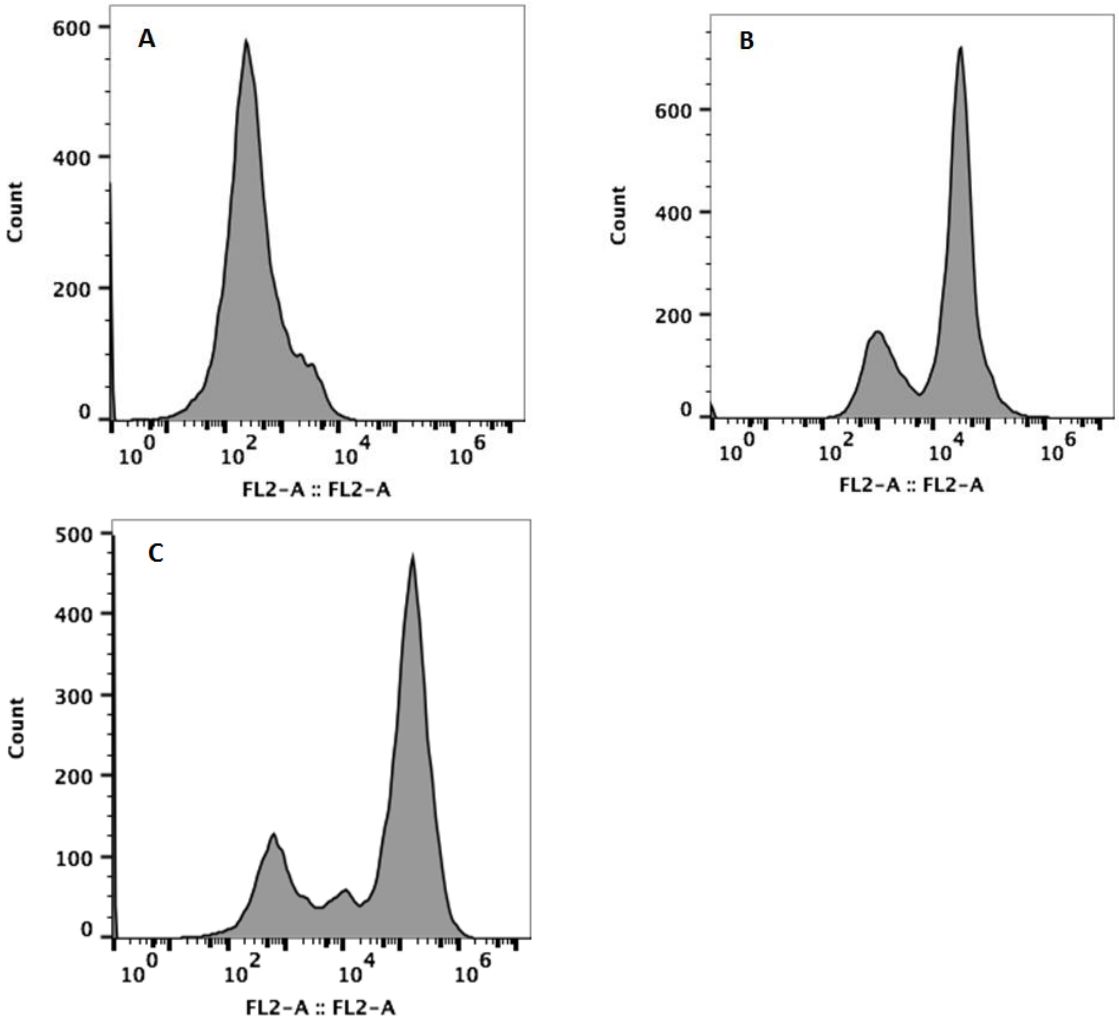

Figure 4.13. Flow cytometry analysis of LNCaP cells treated with the targeted polymersomes encapsulating Ca^{2+}+ folic acid to monitor TMRM-stained cells. Cells treated with formulation (B) are showing lower TMRM mean fluorescence compared to the cells treated with HBSS (C) indicating loss of mitochondrial membrane potential as a result of the treatment. Cells without staining are also shown (A).

4.4. Conclusion

We have used folate presenting, reduction-sensitive polymersomes to actively target the prostate cancer cells overexpressing the PSMA receptor on the surface. The polymersomes encapsulate a high concentration of calcium chloride (50 mM). Releasing the $CaCl_2$ in the cancer cell cytoplasm in presence of folic acid likely formed calcium phosphate crystals, dysregulation of calcium homeostasis, loss of the mitochondrial membrane potential, and cell death. We have not used any toxic anticancer drugs to induce the apoptosis of the cancer cells. This drug free treatment can offer new insights to target and kill the cancer cells by more biologically compatible compounds.

5. OVERALL SUMMARY AND FUTURE DIRECTIONS

Employing the physiochemical differences between the cancer and normal cells can be a promising strategy to target the cancerous tissue. Targeted therapy can help in increasing the therapeutic index of anti-cancer drugs. Both extracellular and intracellular (cytosol and organelles including nucleus, mitochondria) environment can be used to effectively deliver the therapeutic agents to the cancer cells. Nanotechnology, chemistry, and biology are providing the required knowledge and tools to construct smart, stimuli responsive, targeted drug delivery systems. We successfully developed polymersome-based drug delivery vehicles to target the cancer cell nuclei. The vesicles have a PEG layer on the surface to minimize immunogenicity. PEGylation is known to decrease the interaction of the polymersomes with the immune cells and increases the circulation time of the nanoparticles[3]. Due to the presence of reduction sensitive polymers in the building block of polymersomes, they can be engineered to release their content at the intended target site while maintaining stability in the circulation. This delivery strategy can help in effective translocation of the toxic drug to the cell nucleus. To target the cell nuclei, we have used both small molecule (Chapter 2) and nuclear localizing peptide (Chapter 3).

The EPR effect helps in accumulation of the polymersomes in the tumor site and acridine orange drives the polymersomes to the cell nuclei. Acridine orange is a small with an intrinsic affinity toward DNA. Hence, we have conjugated the acridine orange moiety to the surface of the polymersomes to target the cell nuclei. Following the internalization of the polymersomes in the cancer cell nuclei, they release their content (gemcitabine and doxorubicin) in response to the local high reducing agent concentration. Using this strategy, we have simultaneously delivered the chemotherapeutic agents gemcitabine and doxorubicin to the PANC-1 cells. The formulation showed significant toxicity to the cancer cells in both monolayer and 3D spheroid cultures.

Gemcitabine (2′,2′-difluorodeoxycytidine, dFdC) is a nucleoside analog[187] and doxorubicin is an intercalating agent[188]. Therefore, these two drugs induce apoptosis via different mechanisms. We have encapsulated both drugs in the polymersomes to simultaneously use both of these strategies against pancreatic cancer.

The enzyme MMP-7 is overexpressed in the pancreatic cancer tumor microenvironment and aids in the progression of the disease. Hence, we designed an MMP-7 responsive peptide which is cleaved by the enzyme in the tumor microenvironment. This hydrolysis unmasks the nuclear localizing peptide, which mediates the polymersomes' nuclear internalization. The polymersomes are designed to release their content in response to high reducing agent concentration in cell nuclei. We successfully delivered doxorubicin and curcumin to the nuclei of pancreatic cancer cells (BxPC-3 and AsPC-1). The formulation shrunk the pancreatic cancer microtumores without much toxicity to the non-cancerous cells. Curcumin is a natural product, which has shown considerable promises against several types of cancers. Doxorubicin is an FDA-approved chemotherapeutic agent against cancer. We have simultaneously used these two compounds to kill the pancreatic cancer cells.

Prostate specific membrane antigen (PSMA) is overexpressed on the surface of prostate cancer cells. This receptor can be targeted by folic acid. Hence, we used folic acid conjugated polymersomes to actively target the prostate cancer cells. To develop a safer anticancer formulation, we encapsulated the polymersomes with a high concentration of $CaCl_2$. The polymersomes specifically enter the prostate cancer cells through interaction with the PSMA on the cell surface. The formulation is designed to release its content in the cell cytoplasm where the reducing agent concentration is higher than the extracellular matrix. Release of a large amount of calcium ions in the cytoplasm in the presence of folic acid triggers the formation of calcium micro-

crystals, which causes cancer cell death through apoptosis. We have tested this formulation on prostate cancer cells (LN-CaP) in both two and three-dimensional culture. Testing the formulation on animal model would help to demonstrate polymersomes' effectiveness evaluation in vivo. Results of this study suggest the potential use of biocompatible resources to combat cancer.

Considering the progress in developing polymersomes as theranostic nanovesicles, it is envisioned that polymersomes will play an important role as future pharmaceuticals. However, it should be noted that these formulations have some drawbacks. A low drug-loading efficiency, the presence of toxic, residual organic solvents in the final product, a lack of specificity toward the target site, and non-efficient control of the payload release need to be addressed. Therefore, future studies should focus on the preparation methods, which are free of organic solvents, can be scaled up, and possess efficient targeting, and release properties. Although many studies demonstrate the effectiveness of polymersomes in mice or rats, shifting toward species that are evolutionarily closer to humans may accelerate the translational processes. To increase selectivity, polymersomes are usually decorated with ligands for cell-surface receptors of target tissues. However, differences in human's genetic contents and a lack of expression for some receptors in different patients need to be considered [189]. Another important factor that warrants more attention is the polymersomes' pharmacokinetics. For long-term administration, the polymersomes' toxicity on vital organs needs to be studied.

Paper information: Polymersome-based drug-delivery strategies for cancer therapeutics (Ther. Deliv. (2015) 6(4), 521–534). [3]

https://www.ncbi.nlm.nih.gov/pubmed/25996048

REFERENCES

1. De Jong, W. H.; Borm, P. J. A. Drug delivery and nanoparticles: Applications and hazards. *Int J Nanomed* **2008,** *3*, (2), 133-149.

2. Couvreur, P. Nanoparticles in drug delivery: past, present and future. *Adv Drug Deliv Rev* **2013,** *65*, (1), 21-3.

3. Anajafi, T.; Mallik, S. Polymersome-based drug-delivery strategies for cancer therapeutics. *Ther Deliv* **2015,** *6*, (4), 521-34.

4. Wang, J. J.; Zeng, Z. W.; Xiao, R. Z.; Xie, T. A.; Zhou, G. L.; Zhan, X. R.; Wang, S. L. Recent advances of chitosan nanoparticles as drug carriers. *Int J Nanomed* **2011,** *6*, 765-774.

5. Thambi, T.; You, D. G.; Han, H. S.; Deepagan, V. G.; Jeon, S. M.; Suh, Y. D.; Choi, K. Y.; Kim, K.; Kwon, I. C.; Yi, G. R.; Lee, J. Y.; Lee, D. S.; Park, J. H. Bioreducible carboxymethyl dextran nanoparticles for tumor-targeted drug delivery. *Adv Healthc Mater* **2014,** *3*, (11), 1829-38.

6. Li, J.; Wang, X. L.; Zhang, T.; Wang, C. L.; Huang, Z. J.; Luo, X.; Deng, Y. H. A review on phospholipids and their main applications in drug delivery systems. *Asian J Pharm Sci* **2015,** *10*, (2), 81-98.

7. Anajafi, T.; Scott, M. D.; You, S.; Yang, X.; Choi, Y.; Qian, S. Y.; Mallik, S. Acridine Orange Conjugated Polymersomes for Simultaneous Nuclear Delivery of Gemcitabine and Doxorubicin to Pancreatic Cancer Cells. *Bioconjug Chem* **2016,** *27*, (3), 762-71.

8. Gou, M.; Gong, C.; Zhang, J.; Wang, X.; Wang, X.; Gu, Y.; Guo, G.; Chen, L.; Luo, F.; Zhao, X.; Wei, Y.; Qian, Z. Polymeric matrix for drug delivery: honokiol-loaded PCL-PEG-PCL nanoparticles in PEG-PCL-PEG thermosensitive hydrogel. *J Biomed Mater Res A* **2010,** *93*, (1), 219-26.

9. Allen, T. M.; Cullis, P. R. Liposomal drug delivery systems: From concept to clinical applications. *Adv Drug Deliver Rev* **2013,** *65*, (1), 36-48.

10. Kedar, U.; Phutane, P.; Shidhaye, S.; Kadam, V. Advances in polymeric micelles for drug delivery and tumor targeting. *Nanomedicine* **2010,** *6*, (6), 714-29.

11. Slowing, I. I.; Vivero-Escoto, J. L.; Wu, C. W.; Lin, V. S. Y. Mesoporous silica nanoparticles as controlled release drug delivery and gene transfection carriers. *Adv Drug Deliver Rev* **2008,** *60*, (11), 1278-1288.

12. Hammer, D. A.; Robbins, G. P.; Haun, J. B.; Lin, J. J.; Qi, W.; Smith, L. A.; Ghoroghchian, P. P.; Therien, M. J.; Bates, F. S. Leuko-polymersomes. *Faraday Discuss* **2008,** *139*, 129-41; discussion 213-28, 419-20.

13. Discher, B. M.; Won, Y. Y.; Ege, D. S.; Lee, J. C. M.; Bates, F. S.; Discher, D. E.; Hammer, D. A. Polymersomes: Tough vesicles made from diblock copolymers. *Science* **1999,** *284*, (5417), 1143-1146.

14. Meng, F. H.; Zhong, Z. Y. Polymersomes Spanning from Nano- to Microscales: Advanced Vehicles for Controlled Drug Delivery and Robust Vesicles for Virus and Cell Mimicking. *J Phys Chem Lett* **2011,** *2*, (13), 1533-1539.

15. Ahmed, F.; Photos, P. J.; Discher, D. E. Polymersomes as viral capsid mimics. *Drug Develop Res* **2006,** *67*, (1), 4-14.

16. Zhang, J.; Pan, L.; Xu, Y.; Wu, C.; Wang, C.; Cheng, Z.; Zhao, R. Total cholesterol content of erythrocyte membranes in acute coronary syndrome: correlation with apolipoprotein A-I and lipoprotein (a). *Coronary artery disease* **2011,** *22*, (3), 145-52.

17. Discher, D. E.; Ahmed, F. Polymersomes. *Annual review of biomedical engineering* **2006,** *8*, 323-41.

18. Jain, J. P.; Ayen, W. Y.; Kumar, N. Self Assembling Polymers as Polymersomes for Drug Delivery. *Curr Pharm Design* **2011,** *17*, (1), 65-79.

19. Nahire, R.; Haldar, M. K.; Paul, S.; Ambre, A. H.; Meghnani, V.; Layek, B.; Katti, K. S.; Gange, K. N.; Singh, J.; Sarkar, K.; Mallik, S. Multifunctional polymersomes for cytosolic delivery of gemcitabine and doxorubicin to cancer cells. *Biomaterials* **2014,** *35*, (24), 6482-6497.

20. Yin, H.; Kang, H. C.; Huh, K. M.; Bae, Y. H. Effects of cholesterol incorporation on the physicochemical, colloidal, and biological characteristics of pH-sensitive AB(2) miktoarm polymer-based polymersomes. *Colloids and surfaces. B, Biointerfaces* **2014,** *116*, 128-37.

21. Yin, H.; Kang, H. C.; Huh, K. M.; Bae, Y. H. Biocompatible, pH-sensitive AB(2) Miktoarm Polymer-Based Polymersomes: Preparation, Characterization, and Acidic pH-Activated Nanostructural Transformation. *Journal of materials chemistry* **2012,** *22*, (36), 91968-19178.

22. Shum, H. C.; Santanach-Carreras, E.; Kim, J. W.; Ehrlicher, A.; Bibette, J.; Weitz, D. A. Dewetting-Induced Membrane Formation by Adhesion of Amphiphile-Laden Interfaces. *J Am Chem Soc* **2011,** *133*, (12), 4420-4426.

23. Ahmed, F.; Pakunlu, R. I.; Srinivas, G.; Brannan, A.; Bates, F.; Klein, M. L.; Minko, T.; Discher, D. E. Shrinkage of a rapidly growing tumor by drug-loaded polymersomes: pH-triggered release through copolymer degradation. *Molecular pharmaceutics* **2006,** *3*, (3), 340-50.

24. Ahmed, F.; Pakunlu, R. I.; Brannan, A.; Bates, F.; Minko, T.; Discher, D. E. Biodegradable polymersomes loaded with both paclitaxel and doxorubicin permeate and shrink tumors, inducing apoptosis in proportion to accumulated drug. *Journal of controlled release : official journal of the Controlled Release Society* **2006,** *116*, (2), 150-8.

25. Choucair, A.; Soo, P. L.; Eisenberg, A. Active loading and tunable release of doxorubicin from block copolymer vesicles. *Langmuir* **2005,** *21*, (20), 9308-9313.

26. Ahmed, F.; Discher, D. E. Self-porating polymersomes of PEG-PLA and PEG-PCL: hydrolysis-triggered controlled release vesicles. *Journal of controlled release : official journal of the Controlled Release Society* **2004,** *96*, (1), 37-53.

27. Li, S. D.; Huang, L. Stealth nanoparticles: high density but sheddable PEG is a key for tumor targeting. *Journal of controlled release : official journal of the Controlled Release Society* **2010,** *145*, (3), 178-81.

28. Ulbrich, K.; Subr, V. Structural and chemical aspects of HPMA copolymers as drug carriers. *Adv Drug Deliv Rev* **2010,** *62*, (2), 150-166.

29. Chung, Y. I.; Kim, J. C.; Kim, Y. H.; Tae, G.; Lee, S. Y.; Kim, K.; Kwon, I. C. The effect of surface functionalization of PLGA nanoparticles by heparin- or chitosan-conjugated Pluronic on tumor targeting. *Journal of controlled release : official journal of the Controlled Release Society* **2010,** *143*, (3), 374-82.

30. Babu, A.; Templeton, A. K.; Munshi, A.; Ramesh, R. Nanodrug delivery systems: a promising technology for detection, diagnosis, and treatment of cancer. *AAPS PharmSciTech* **2014,** *15*, (3), 709-21.

31. Meng, F. H.; Engbers, G. H. M.; Gessner, A.; Muller, R. H.; Feijen, J. Pegylated polystyrene particles as a model system for artificial cells. *Journal of Biomedical Materials Research Part A* **2004,** *70A*, (1), 97-106.

32. Mishra, V.; Gupta, U.; Jain, N. K. Surface-engineered dendrimers: a solution for toxicity issues. *Journal of biomaterials science. Polymer edition* **2009,** *20*, (2), 141-66.

33. Lee, J. S.; Feijen, J. Polymersomes for drug delivery: design, formation and characterization. *Journal of controlled release : official journal of the Controlled Release Society* **2012,** *161*, (2), 473-83.

34. Tagami, T.; Nakamura, K.; Shimizu, T.; Yamazaki, N.; Ishida, T.; Kiwada, H. CpG motifs in pDNA-sequences increase anti-PEG IgM production induced by PEG-coated pDNA-lipoplexes. *Journal of controlled release : official journal of the Controlled Release Society* **2010,** *142*, (2), 160-6.

35. Zheng, J.; Wan, Y.; Elhissi, A.; Zhang, Z.; Sun, X. Targeted Paclitaxel Delivery to Tumors Using Cleavable PEG-Conjugated Solid Lipid Nanoparticles. *Pharmaceutical research* **2014,** *31*, (8), 2220-33.

36. Pourtau, L.; Oliveira, H.; Thevenot, J.; Wan, Y.; Brisson, A. R.; Sandre, O.; Miraux, S.; Thiaudiere, E.; Lecommandoux, S. Antibody-functionalized magnetic polymersomes: in vivo targeting and imaging of bone metastases using high resolution MRI. *Adv Healthc Mater* **2013,** *2*, (11), 1420-4.

37. Lee, J. S.; Groothuis, T.; Cusan, C.; Mink, D.; Feijen, J. Lysosomally cleavable peptide-containing polymersomes modified with anti-EGFR antibody for systemic cancer chemotherapy. *Biomaterials* **2011,** *32*, (34), 9144-53.

38. Lin, J. J.; Ghoroghchian, P. P.; Zhang, Y.; Hammer, D. A. Adhesion of antibody-functionalized polymersomes. *Langmuir* **2006,** *22*, (9), 3975-9.

39. Meng, F. H.; Engbers, G. H. M.; Feijen, J. Biodegradable polymersomes as a basis for artificial cells: encapsulation, release and targeting. *Journal of Controlled Release* **2005,** *101*, (1-3), 187-198.

40. Egli, S.; Nussbaumer, M. G.; Balasubramanian, V.; Chami, M.; Bruns, N.; Palivan, C.; Meier, W. Biocompatible functionalization of polymersome surfaces: a new approach to surface immobilization and cell targeting using polymersomes. *J Am Chem Soc* **2011,** *133*, (12), 4476-83.

41. Pang, Z.; Lu, W.; Gao, H.; Hu, K.; Chen, J.; Zhang, C.; Gao, X.; Jiang, X.; Zhu, C. Preparation and brain delivery property of biodegradable polymersomes conjugated with OX26. *Journal of controlled release : official journal of the Controlled Release Society* **2008,** *128*, (2), 120-7.

42. Zhang, Y.; Zhang, W.; Johnston, A. H.; Newman, T. A.; Pyykko, I.; Zou, J. Targeted delivery of Tet1 peptide functionalized polymersomes to the rat cochlear nerve. *Int J Nanomedicine* **2012,** *7*, 1015-22.

43. Demirgoz, D.; Pangburn, T. O.; Davis, K. P.; Lee, S.; Bates, F. S.; Kokkoli, E. PR_b-targeted delivery of tumor necrosis factor-alpha by polymersomes for the treatment of prostate cancer. *Soft Matter* **2009,** *5*, (10), 2011-2019.

44. Petersen, M. A.; Yin, L. G.; Kokkoli, E.; Hillmyer, M. A. Synthesis and characterization of reactive PEO-PMCL polymersomes. *Polym Chem-Uk* **2010,** *1*, (8), 1281-1290.

45. Lai, M. H.; Jeong, J. H.; Devolder, R. J.; Brockman, C.; Schroeder, C.; Kong, H. Ellipsoidal Polyaspartamide Polymersomes with Enhanced Cell-Targeting Ability. *Advanced functional materials* **2012,** *22*, (15), 3239-3246.

46. Chen, Y. C.; Chiang, C. F.; Chen, L. F.; Liao, S. C.; Hsieh, W. Y.; Lin, W. L. Polymersomes conjugated with des-octanoyl ghrelin for the delivery of therapeutic and imaging agents into brain tissues. *Biomaterials* **2014,** *35*, (6), 2051-65.

47. Chen, Y. C.; Chiang, C. F.; Chen, L. F.; Liang, P. C.; Hsieh, W. Y.; Lin, W. L. Polymersomes conjugated with des-octanoyl ghrelin and folate as a BBB-penetrating cancer cell-targeting delivery system. *Biomaterials* **2014,** *35*, (13), 4066-81.

48. Robbins, G. P.; Saunders, R. L.; Haun, J. B.; Rawson, J.; Therien, M. J.; Hammer, D. A. Tunable leuko-polymersomes that adhere specifically to inflammatory markers. *Langmuir* **2010,** *26*, (17), 14089-96.

49. Gao, H. L.; Pang, Z. Q.; Fan, L.; Hu, K. L.; Wu, B. X.; Jiang, X. G. Effect of lactoferrin- and transferrin-conjugated polymersomes in brain targeting: in vitro and in vivo evaluations. *Acta Pharmacol Sin* **2010,** *31*, (2), 237-243.

50. Pang, Z.; Feng, L.; Hua, R.; Chen, J.; Gao, H.; Pan, S.; Jiang, X.; Zhang, P. Lactoferrin-conjugated biodegradable polymersome holding doxorubicin and tetrandrine for chemotherapy of glioma rats. *Molecular pharmaceutics* **2010,** *7*, (6), 1995-2005.

51. Hu, K.; Li, J.; Shen, Y.; Lu, W.; Gao, X.; Zhang, Q.; Jiang, X. Lactoferrin-conjugated PEG-PLA nanoparticles with improved brain delivery: in vitro and in vivo evaluations. *Journal of controlled release : official journal of the Controlled Release Society* **2009,** *134*, (1), 55-61.

52. Herbst, R. S.; Shin, D. M. Monoclonal antibodies to target epidermal growth factor receptor-positive tumors: a new paradigm for cancer therapy. *Cancer* **2002,** *94*, (5), 1593-611.

53. Regberg, J.; Srimanee, A.; Langel, U. Applications of cell-penetrating peptides for tumor targeting and future cancer therapies. *Pharmaceuticals (Basel)* **2012,** *5*, (9), 991-1007.

54. Liu, J. N.; Bu, W.; Pan, L. M.; Zhang, S.; Chen, F.; Zhou, L.; Zhao, K. L.; Peng, W.; Shi, J. Simultaneous nuclear imaging and intranuclear drug delivery by nuclear-targeted multifunctional upconversion nanoprobes. *Biomaterials* **2012,** *33*, (29), 7282-90.

55. Egli, S.; Schlaad, H.; Bruns, N.; Meier, W. Functionalization of Block Copolymer Vesicle Surfaces. *Polymers-Basel* **2011,** *3*, (1), 252-280.

56. Yu, M. K.; Park, J.; Jon, S. Targeting strategies for multifunctional nanoparticles in cancer imaging and therapy. *Theranostics* **2012,** *2*, (1), 3-44.

57. Serpe, L.; Gallicchio, M.; Canaparo, R.; Dosio, F. Targeted treatment of folate receptor-positive platinum-resistant ovarian cancer and companion diagnostics, with specific focus on vintafolide and etarfolatide. *Pharmacogenomics and personalized medicine* **2014,** *7*, 31-42.

58. Nukolova, N. V.; Oberoi, H. S.; Cohen, S. M.; Kabanov, A. V.; Bronich, T. K. Folate-decorated nanogels for targeted therapy of ovarian cancer. *Biomaterials* **2011,** *32*, (23), 5417-26.

59. Dhawan, D.; Ramos-Vara, J. A.; Naughton, J. F.; Cheng, L.; Low, P. S.; Rothenbuhler, R.; Leamon, C. P.; Parker, N.; Klein, P. J.; Vlahov, I. R.; Reddy, J. A.; Koch, M.; Murphy, L.; Fourez, L. M.; Stewart, J. C.; Knapp, D. W. Targeting folate receptors to treat invasive urinary bladder cancer. *Cancer research* **2013,** *73*, (2), 875-84.

60. Cagle, P. T.; Zhai, Q. J.; Murphy, L.; Low, P. S. Folate receptor in adenocarcinoma and squamous cell carcinoma of the lung: potential target for folate-linked therapeutic agents. *Archives of pathology & laboratory medicine* **2013,** *137*, (2), 241-4.

61. O'Shannessy, D. J.; Somers, E. B.; Maltzman, J.; Smale, R.; Fu, Y. S. Folate receptor alpha (FRA) expression in breast cancer: identification of a new molecular subtype and association with triple negative disease. *SpringerPlus* **2012,** *1*, 22.

62. D'Angelica, M.; Ammori, J.; Gonen, M.; Klimstra, D. S.; Low, P. S.; Murphy, L.; Weiser, M. R.; Paty, P. B.; Fong, Y.; Dematteo, R. P.; Allen, P.; Jarnagin, W. R.; Shia, J. Folate receptor-alpha expression in resectable hepatic colorectal cancer metastases: patterns and significance. *Modern pathology : an official journal of the United States and Canadian Academy of Pathology, Inc* **2011,** *24*, (9), 1221-8.

63. Chemin, M.; Brun, P. M.; Lecommandoux, S.; Sandre, O.; Le Meins, J. F. Hybrid polymer/lipid vesicles: fine control of the lipid and polymer distribution in the binary membrane. *Soft Matter* **2012,** *8*, (10), 2867-2874.

64. Katz, J. S.; Zhong, S.; Ricart, B. G.; Pochan, D. J.; Hammer, D. A.; Burdick, J. A. Modular synthesis of biodegradable diblock copolymers for designing functional polymersomes. *J Am Chem Soc* **2010,** *132*, (11), 3654-5.

65. Oliveira, H.; Perez-Andres, E.; Thevenot, J.; Sandre, O.; Berra, E.; Lecommandoux, S. Magnetic field triggered drug release from polymersomes for cancer therapeutics. *Journal of controlled release : official journal of the Controlled Release Society* **2013,** *169*, (3), 165-70.

66. Liqing, Y.; Jia, G.; Jiqing, C.; Ran, G.; Fei, C.; Jie, K.; Yanyun, W.; Cheng, Z. Directed differentiation of motor neuron cell-like cells from human adipose-derived stem cells in vitro. *Neuroreport* **2011,** *22*, (8), 370-3.

67. Du, Y.; Chen, W.; Zheng, M.; Meng, F.; Zhong, Z. pH-sensitive degradable chimaeric polymersomes for the intracellular release of doxorubicin hydrochloride. *Biomaterials* **2012,** *33*, (29), 7291-9.

68. Cheng, R.; Meng, F. H.; Ma, S. B.; Xu, H. F.; Liu, H. Y.; Jing, X. B.; Zhong, Z. Y. Reduction and temperature dual-responsive crosslinked polymersomes for targeted intracellular protein delivery. *Journal of materials chemistry* **2011,** *21*, (47), 19013-19020.

69. Gamcsik, M. P.; Kasibhatla, M. S.; Teeter, S. D.; Colvin, O. M. Glutathione levels in human tumors. *Biomarkers : biochemical indicators of exposure, response, and susceptibility to chemicals* **2012,** *17*, (8), 671-91.

70. Broaders, K. E.; Grandhe, S.; Frechet, J. M. A biocompatible oxidation-triggered carrier polymer with potential in therapeutics. *J Am Chem Soc* **2011,** *133*, (4), 756-8.

71. Khorsand, B.; Lapointe, G.; Brett, C.; Oh, J. K. Intracellular drug delivery nanocarriers of glutathione-responsive degradable block copolymers having pendant disulfide linkages. *Biomacromolecules* **2013,** *14*, (6), 2103-11.

72. Cabane, E.; Malinova, V.; Menon, S.; Palivan, C. G.; Meier, W. Photoresponsive polymersomes as smart, triggerable nanocarriers. *Soft Matter* **2011,** *7*, (19), 9167-9176.

73. Cabane, E.; Malinova, V.; Meier, W. Synthesis of Photocleavable Amphiphilic Block Copolymers: Toward the Design of Photosensitive Nanocarriers. *Macromol Chem Phys* **2010,** *211*, (17), 1847-1856.

74. Sun, H.; Guo, B.; Li, X.; Cheng, R.; Meng, F.; Liu, H.; Zhong, Z. Shell-sheddable micelles based on dextran-SS-poly(epsilon-caprolactone) diblock copolymer for efficient intracellular release of doxorubicin. *Biomacromolecules* **2010,** *11*, (4), 848-54.

75. Kulkarni, P. S.; Haldar, M. K.; Nahire, R. R.; Katti, P.; Ambre, A. H.; Muhonen, W. W.; Shabb, J. B.; Padi, S. K.; Singh, R. K.; Borowicz, P. P.; Shrivastava, D. K.; Katti, K. S.; Reindl, K.; Guo, B.; Mallik, S. Mmp-9 responsive PEG cleavable nanovesicles for efficient delivery of chemotherapeutics to pancreatic cancer. *Molecular pharmaceutics* **2014,** *11*, (7), 2390-9.

76. Xu, H. F.; Meng, F. H.; Zhong, Z. Y. Reversibly crosslinked temperature-responsive nano-sized polymersomes: synthesis and triggered drug release. *Journal of materials chemistry* **2009,** *19*, (24), 4183-4190.

77. Ayen, W. Y.; Kumar, N. In vivo evaluation of doxorubicin-loaded (PEG)(3)-PLA nanopolymersomes (PolyDoxSome) using DMBA-induced mammary carcinoma rat model and comparison with marketed LipoDox. *Pharmaceutical research* **2012,** *29*, (9), 2522-33.

78. Jain, J. P.; Jatana, M.; Chakrabarti, A.; Kumar, N. Amphotericin-B-loaded polymersomes formulation (PAMBO) based on (PEG)(3)-PLA copolymers: an in vivo evaluation in a murine model. *Molecular pharmaceutics* **2011,** *8*, (1), 204-12.

79. Pan, L.; He, Q.; Liu, J.; Chen, Y.; Ma, M.; Zhang, L.; Shi, J. Nuclear-targeted drug delivery of TAT peptide-conjugated monodisperse mesoporous silica nanoparticles. *J Am Chem Soc* **2012,** *134*, (13), 5722-5.

80. Jana, A.; Saha, B.; Banerjee, D. R.; Ghosh, S. K.; Nguyen, K. T.; Ma, X.; Qu, Q.; Zhao, Y.; Singh, N. D. Photocontrolled nuclear-targeted drug delivery by single component photoresponsive fluorescent organic nanoparticles of acridin-9-methanol. *Bioconjug Chem* **2013,** *24*, (11), 1828-39.

81. Meldal, M.; Tornoe, C. W. Cu-catalyzed azide-alkyne cycloaddition. *Chem Rev* **2008,** *108*, (8), 2952-3015.

82. Brinkhuis, R. P.; Stojanov, K.; Laverman, P.; Eilander, J.; Zuhorn, I. S.; Rutjes, F. P.; van Hest, J. C. Size dependent biodistribution and SPECT imaging of (111)In-labeled polymersomes. *Bioconjug Chem* **2012,** *23*, (5), 958-65.

83. Yang, J. H.; Dai, G. D.; Hou, Y. H.; Song, Z. H.; Wang, F.; Ji, G. J.; Chen, J. H. Quantification of oxymatrine in rat plasma by UPLC-MS/MS to support the pharmacokinetic analyses of oxymatrine-loaded polymersomes. *Anal Methods-Uk* **2014,** *6*, (6), 1811-1817.

84. Pepper, M. S. Role of the matrix metalloproteinase and plasminogen activator-plasmin systems in angiogenesis. *Arterioscler Thromb Vasc Biol* **2001,** *21*, (7), 1104-17.

85. Ghosh, A.; Heston, W. D. W. Tumor target prostate specific membrane antigen (PSMA) and its regulation in prostate cancer. *J Cell Biochem* **2004,** *91*, (3), 528-539.

86. Yao, V.; Berkman, C. E.; Choi, J. K.; O'Keefe, D. S.; Bacich, D. J. Expression of prostate-specific membrane antigen (PSMA), increases cell folate uptake and proliferation and suggests a novel role for PSMA in the uptake of the non-polyglutamated folate, folic acid. *Prostate* **2010,** *70*, (3), 305-16.

87. Brini, M.; Cali, T.; Ottolini, D.; Carafoli, E. Intracellular calcium homeostasis and signaling. *Met Ions Life Sci* **2013,** *12*, 119-68.

88. Zhao, R.; Wang, B.; Yang, X.; Xiao, Y.; Wang, X.; Shao, C.; Tang, R. A Drug-Free Tumor Therapy Strategy: Cancer-Cell-Targeting Calcification. *Angew Chem Int Ed Engl* **2016,** *55*, (17), 5225-9.

89. Anajafi, T.; Yu, J.; Sedigh, A.; Haldar, M. K.; Muhonen, W. W.; Oberlander, S.; Wasness, H.; Froberg, J.; Molla, M. S.; Katti, K. S.; Choi, Y.; Shabb, J. B.; Srivastava, D. K.; Mallik, S. Nuclear Localizing Peptide-Conjugated, Redox-Sensitive Polymersomes for Delivering Curcumin and Doxorubicin to Pancreatic Cancer Microtumors. *Molecular pharmaceutics* **2017,** *14*, (6), 1916-1928.

90. Moniri, M. R.; Dai, L. J.; Warnock, G. L. The challenge of pancreatic cancer therapy and novel treatment strategy using engineered mesenchymal stem cells. *Cancer gene therapy* **2014,** *21*, (1), 12-23.

91. Rougier, P.; Mitry, E. Chemotherapy in the treatment of neuroendocrine malignant tumors. *Digestion* **2000,** *62 Suppl 1*, 73-8.

92. Rivera, E.; Valero, V.; Arun, B.; Royce, M.; Adinin, R.; Hoelzer, K.; Walters, R.; Wade, J. L., 3rd; Pusztai, L.; Hortobagyi, G. N. Phase II study of pegylated liposomal doxorubicin in combination with gemcitabine in patients with metastatic breast cancer. *Journal of clinical oncology : official journal of the American Society of Clinical Oncology* **2003,** *21*, (17), 3249-54.

93. Fabi, A.; Ferretti, G.; Papaldo, P.; Salesi, N.; Ciccarese, M.; Lorusso, V.; Carlini, P.; Carpino, A.; Mottolese, M.; Cianciulli, A. M.; Giannarelli, D.; Sperduti, I.; Felici, A.; Cognetti, F. Pegylated liposomal doxorubicin in combination with gemcitabine: a phase II study in anthracycline-naive and anthracycline pretreated metastatic breast cancer patients. *Cancer chemotherapy and pharmacology* **2006,** *57*, (5), 615-23.

94. Liu, D.; Chen, Y.; Feng, X.; Deng, M.; Xie, G.; Wang, J.; Zhang, L.; Liu, Q.; Yuan, P. Micellar nanoparticles loaded with gemcitabine and doxorubicin showed synergistic effect. *Colloids and surfaces. B, Biointerfaces* **2014,** *113*, 158-68.

95. Weinberg, S. E.; Chandel, N. S. Targeting mitochondria metabolism for cancer therapy. *Nature chemical biology* **2015,** *11*, (1), 9-15.

96. Yamada, Y.; Harashima, H. [Targeting mitochondria: innovation from mitochondrial drug delivery system (DDS) to mitochondrial medicine]. *Yakugaku zasshi : Journal of the Pharmaceutical Society of Japan* **2012,** *132*, (10), 1111-8.

97. Cohen, O.; Granek, R. Nucleus-targeted drug delivery: theoretical optimization of nanoparticles decoration for enhanced intracellular active transport. *Nano Lett* **2014,** *14*, (5), 2515-21.

98. Deepthi A, R. S., Kalyani A, Udaya Kiran M, Vanaja A Targeted Drug Delivery to the Nucleus and its Potential Role in Cancer Chemotherapy. *Jurnal of Pharmaceutical Science and Research* **2013,** *5*, (2), 48 - 56.

99. Strambio-De-Castillia, C.; Niepel, M.; Rout, M. P. The nuclear pore complex: bridging nuclear transport and gene regulation. *Nat Rev Mol Cell Bio* **2010,** *11*, (7), 490-501.

100. Ribbeck, K.; Gorlich, D. Kinetic analysis of translocation through nuclear pore complexes. *Embo J* **2001,** *20*, (6), 1320-1330.

101. Smith, A. E.; Slepchenko, B. M.; Schaff, J. C.; Loew, L. M.; Macara, I. G. Systems analysis of Ran transport. *Science* **2002,** *295*, (5554), 488-491.

102. Oeffinger, M.; Zenklusen, D. To the pore and through the pore: A story of mRNA export kinetics. *Bba-Gene Regul Mech* **2012,** *1819*, (6), 494-506.

103. Kastrup, L.; Oberleithner, H.; Ludwig, Y.; Schafer, C.; Shahin, V. Nuclear envelope barrier leak induced by dexamethasone. *Journal of cellular physiology* **2006,** *206*, (2), 428-34.

104. Elbayoumi, T. A.; Torchilin, V. P. Enhanced cytotoxicity of monoclonal anticancer antibody 2C5-modified doxorubicin-loaded PEGylated liposomes against various tumor cell lines. *European journal of pharmaceutical sciences : official journal of the European Federation for Pharmaceutical Sciences* **2007,** *32*, (3), 159-68.

105. Goren, D.; Horowitz, A. T.; Tzemach, D.; Tarshish, M.; Zalipsky, S.; Gabizon, A. Nuclear delivery of doxorubicin via folate-targeted liposomes with bypass of multidrug-resistance efflux pump. *Clinical cancer research : an official journal of the American Association for Cancer Research* **2000,** *6*, (5), 1949-57.

106. Liu, C. H.; Sahoo, S. L.; Tsao, M. H. Acridine orange coated magnetic nanoparticles for nucleus labeling and DNA adsorption. *Colloids and surfaces. B, Biointerfaces* **2014,** *115*, 150-6.

107. Iyer, A. K.; Khaled, G.; Fang, J.; Maeda, H. Exploiting the enhanced permeability and retention effect for tumor targeting. *Drug Discov Today* **2006,** *11*, (17-18), 812-818.

108. Cheng, R.; Meng, F. H.; Ma, S. B.; Xu, H. F.; Liu, H. Y.; Jing, X. B.; Zhong, Z. Y. Reduction and temperature dual-responsive crosslinked polymersomes for targeted intracellular protein delivery. *J Mater Chem* **2011,** *21*, (47), 19013-19020.

109. Go, Y. M.; Jones, D. P. Redox compartmentalization in eukaryotic cells. *Biochimica et biophysica acta* **2008,** *1780*, (11), 1273-90.

110. Go, Y. M.; Jones, D. P. Redox control systems in the nucleus: mechanisms and functions. *Antioxidants & redox signaling* **2010,** *13*, (4), 489-509.

111. Agorastos, N.; Borsig, L.; Renard, A.; Antoni, P.; Viola, G.; Spingler, B.; Kurz, P.; Alberto, R. Cell-specific and nuclear targeting with [M(CO)(3)](+) (M=(99m)Tc, Re)-based complexes conjugated to acridine orange and bombesin. *Chemistry* **2007,** *13*, (14), 3842-52.

112. Zelenka, K.; Borsig, L.; Alberto, R. Metal complex mediated conjugation of peptides to nucleus targeting acridine orange: a modular concept for dual-modality imaging agents. *Bioconjug Chem* **2011,** *22*, (5), 958-67.

113. Udovich, J. A.; Besselsen, D. G.; Gmitro, A. F. Assessment of acridine orange and SYTO 16 for in vivo imaging of the peritoneal tissues in mice. *Journal of microscopy* **2009,** *234*, (2), 124-9.

114. Matsubara, T.; Kusuzaki, K.; Matsumine, A.; Murata, H.; Nakamura, T.; Uchida, A.; Sudo, A. Clinical Outcomes of Minimally Invasive Surgery Using Acridine Orange for Musculoskeletal Sarcomas Around the Forearm, Compared With Conventional Limb Salvage Surgery After Wide Resection. *J Surg Oncol* **2010,** *102*, (3), 271-275.

115. Stylianopoulos, T.; Jain, R. K. Design considerations for nanotherapeutics in oncology. *Nanomedicine* **2015,** *11*, (8), 1893-907.

116. Cerqueira, B. B.; Lasham, A.; Shelling, A. N.; Al-Kassas, R. Nanoparticle therapeutics: Technologies and methods for overcoming cancer. *European journal of pharmaceutics and biopharmaceutics : official journal of Arbeitsgemeinschaft fur Pharmazeutische Verfahrenstechnik e.V* **2015,** *97*, (Pt A), 140-51.

117. Ahmed, F.; Pakunlu, R. I.; Brannan, A.; Bates, F.; Minko, T.; Discher, D. E. Biodegradable polymersomes loaded with both paclitaxel and doxorubicin permeate and shrink tumors, inducing apoptosis in proportion to accumulated drug. *J Control Release* **2006,** *116*, (2), 150-8.

118. Markovic, J.; Garcia-Gimenez, J. L.; Gimeno, A.; Vina, J.; Pallardo, F. V. Role of glutathione in cell nucleus. *Free Radical Res* **2010,** *44*, (7), 721-733.

119. Lee, S.; Oh, S. Y.; Kim, B. G.; Kwon, H. C.; Kim, S. H.; Rho, M. H.; Kim, Y. H.; Rho, M. S.; Jeong, J. S.; Kim, H. J. Second-Line Treatment With a Combination of Continuous 5-Fluorouracil, Doxorubicin, and Mitomycin-C (Conti-Fam) in Gemcitabine-Pretreated Pancreatic and Biliary Tract Cancer. *Am J Clin Oncol-Canc* **2009,** *32*, (4), 348-352.

120. Raghavan, S.; Ward, M. R.; Rowley, K. R.; Wold, R. M.; Takayama, S.; Buckanovich, R. J.; Mehta, G. Formation of stable small cell number three-dimensional ovarian cancer spheroids using hanging drop arrays for preclinical drug sensitivity assays. *Gynecol Oncol* **2015,** *138*, (1), 181-189.

121. Ruppen, J.; Wildhaber, F. D.; Strub, C.; Hall, S. R. R.; Schmid, R. A.; Geiser, T.; Guenat, O. T. Towards personalized medicine: chemosensitivity assays of patient lung cancer cell spheroids in a perfused microfluidic platform. *Lab Chip* **2015,** *15*, (14), 3076-3085.

122. Perche, F.; Patel, N. R.; Torchilin, V. P. Accumulation and toxicity of antibody-targeted doxorubicin-loaded PEG-PE micelles in ovarian cancer cell spheroid model. *Journal of Controlled Release* **2012,** *164*, (1), 95-102.

123. Napolitano, A. P.; Chai, P.; Dean, D. M.; Morgan, J. R. Dynamics of the self-assembly of complex cellular aggregates on micromolded nonadhesive hydrogels. *Tissue Eng* **2007,** *13*, (8), 2087-2094.

124. Zhang, S.; Zhao, Y. Controlled release from cleavable polymerized liposomes upon redox and pH stimulation. *Bioconjug Chem* **2011,** *22*, (4), 523-8.

125. Nahire, R.; Haldar, M. K.; Paul, S.; Mergoum, A.; Ambre, A. H.; Katti, K. S.; Gange, K. N.; Srivastava, D. K.; Sarkar, K.; Mallik, S. Polymer-coated echogenic lipid nanoparticles with dual release triggers. *Biomacromolecules* **2013,** *14*, (3), 841-53.

126. Gottesman, M. M.; Fojo, T.; Bates, S. E. Multidrug resistance in cancer: role of ATP-dependent transporters. *Nat Rev Cancer* **2002,** *2*, (1), 48-58.

127. Xu, X.; Ho, W.; Zhang, X.; Bertrand, N.; Farokhzad, O. Cancer nanomedicine: from targeted delivery to combination therapy. *Trends Mol Med* **2015,** *21*, (4), 223-32.

128. Trabulo, S.; Cardoso, A. L.; Mano, M.; De Lima, M. C. Cell-Penetrating Peptides-Mechanisms of Cellular Uptake and Generation of Delivery Systems. *Pharmaceuticals (Basel)* **2010,** *3*, (4), 961-993.

129. Hyndman, L.; Lemoine, J. L.; Huang, L.; Porteous, D. J.; Boyd, A. C.; Nan, X. HIV-1 Tat protein transduction domain peptide facilitates gene transfer in combination with cationic liposomes. *Journal of controlled release : official journal of the Controlled Release Society* **2004,** *99*, (3), 435-44.

130. Trabulo, S.; Mano, M.; Faneca, H.; Cardoso, A. L.; Duarte, S.; Henriques, A.; Paiva, A.; Gomes, P.; Simoes, S.; de Lima, M. C. S4(13)-PV cell penetrating peptide and cationic liposomes act synergistically to mediate intracellular delivery of plasmid DNA. *J Gene Med* **2008,** *10*, (11), 1210-22.

131. Mano, M.; Teodosio, C.; Paiva, A.; Simoes, S.; Pedroso de Lima, M. C. On the mechanisms of the internalization of S4(13)-PV cell-penetrating peptide. *Biochem J* **2005,** *390*, (Pt 2), 603-12.

132. Gupta, S. P. Matrix metalloproteinase inhibitors: specificity of binding and structure-activity relationships. *EXS* **2012,** *103*, v-vi.

133. Brauer, P. R. MMPs--role in cardiovascular development and disease. *Front Biosci* **2006,** *11*, 447-78.

134. Gialeli, C.; Theocharis, A. D.; Karamanos, N. K. Roles of matrix metalloproteinases in cancer progression and their pharmacological targeting. *FEBS J* **2011,** *278*, (1), 16-27.

135. Spinale, F. G. Myocardial matrix remodeling and the matrix metalloproteinases: influence on cardiac form and function. *Physiol Rev* **2007,** *87*, (4), 1285-342.

136. Rome, C.; Arsaut, J.; Taris, C.; Couillaud, F.; Loiseau, H. MMP-7 (matrilysin) expression in human brain tumors. *Molecular carcinogenesis* **2007,** *46*, (6), 446-52.

137. Bruun, J.; Larsen, T. B.; Jolck, R. I.; Eliasen, R.; Holm, R.; Gjetting, T.; Andresen, T. L. Investigation of enzyme-sensitive lipid nanoparticles for delivery of siRNA to blood-brain barrier and glioma cells. *Int J Nanomedicine* **2015,** *10*, 5995-6008.

138. Johnson, J. A.; Finn, M. G.; Koberstein, J. T.; Turro, N. J. Construction of linear polymers, dendrimers, networks, and other polymeric architectures by copper-catalyzed azide-alkyne cycloaddition "Click" chemistry (vol 29, pg 1052, 2008). *Macromol Rapid Comm* **2008,** *29*, (16), 1421-1421.

139. Discher, D. E.; Ortiz, V.; Srinivas, G.; Klein, M. L.; Kim, Y.; David, C. A.; Cai, S. S.; Photos, P.; Ahmed, F. Emerging applications of polymersomes in delivery: From molecular dynamics to shrinkage of tumors. *Prog Polym Sci* **2007,** *32*, (8-9), 838-857.

140. Discher, D. E.; Ahmed, F. Polymersomes. *Annu Rev Biomed Eng* **2006,** *8*, 323-341.

141. Marfori, M.; Mynott, A.; Ellis, J. J.; Mehdi, A. M.; Saunders, N. F. W.; Curmi, P. M.; Forwood, J. K.; Boden, M.; Kobe, B. Molecular basis for specificity of nuclear import and prediction of nuclear localization. *Bba-Mol Cell Res* **2011,** *1813*, (9), 1562-1577.

142. Patel, L. N.; Zaro, J. L.; Shen, W. C. Cell penetrating peptides: Intracellular pathways and pharmaceutical perspectives. *Pharmaceutical research* **2007,** *24*, (11), 1977-1992.

143. Li, J.; Liu, F.; Shao, Q.; Min, Y.; Costa, M.; Yeow, E. K.; Xing, B. Enzyme-responsive cell-penetrating peptide conjugated mesoporous silica quantum dot nanocarriers for controlled release of nucleus-targeted drug molecules and real-time intracellular fluorescence imaging of tumor cells. *Adv Healthc Mater* **2014,** *3*, (8), 1230-9.

144. Nagase, H., Substrate specificity of MMPs. In *Matrix Metalloproteinase Inhibitors in Cancer Therapy*, Clendeninn, N. J.; Appelt, K., Eds. Humana press Inc.: Totowa, NJ, 2001; pp 39-66.

145. Kuhlmann, K. F. D.; van Till, J. W. O.; Boermeester, M. A.; de Reuver, P. R.; Tzvetanova, I. D.; Offerhaus, G. J. A.; ten Kate, F. J. W.; Busch, O. R. C.; van Gulik, T. M.; Gouma, D. J.; Crawford, H. C. Evaluation of matrix metalloproteinase 7 in plasma and pancreatic juice as a biomarker for pancreatic cancer. *Cancer Epidem Biomar* **2007,** *16*, (5), 886-891.

146. Kamal, H. M. K.; Zimam, E. H. Synthesis and characterization of some new Benzotriazole derivatives via 1,3-dipolar cycloaddition reactions. *International Journal of Pharma Sciences* **2014,** *4*, (4), 677-688.

147. Schofield, K.; Grimmett, M. R.; Keene, B. R. T., *Heteroaromatic Nitrogen Compounds: The Azoles*. CUP Archive: 1976.

148. Lieber, E.; Rao, C. N. R.; Chao, T. S.; Hoffman, C. W. W. Infrared Spectra of Organic Azides. *Anal Chem* **1957,** *29*, (6), 916-918.

149. Elshahawy, A. Vibrational-Spectra of Deuterated Phenyl Azide and 2,6-Dimethylphenyl Azide. *Spectrochim Acta A* **1983,** *39*, (2), 115-117.

150. Siviero, A.; Gallo, E.; Maggini, V.; Gori, L.; Mugelli, A.; Firenzuoli, F.; Vannacci, A. Curcumin, a golden spice with a low bioavailability. *J Herb Med* **2015,** *5*, (2), 57-70.

151. Punfa, W.; Yodkeeree, S.; Pitchakarn, P.; Ampasavate, C.; Limtrakul, P. Enhancement of cellular uptake and cytotoxicity of curcumin-loaded PLGA nanoparticles by conjugation with anti-P-glycoprotein in drug resistance cancer cells. *Acta Pharmacol Sin* **2012,** *33*, (6), 823-31.

152. Priyadarsini, K. I. The Chemistry of Curcumin: From Extraction to Therapeutic Agent. *Molecules* **2014,** *19*, (12), 20091-20112.

153. Wang, S. W.; Konorev, E. A.; Kotamraju, S.; Joseph, J.; Kalivendi, S.; Kalyanaraman, B. Doxorubicin induces apoptosis in normal and tumor cells via distinctly different mechanisms - Intermediacy of H2O2- and p53-dependent pathways. *J Biol Chem* **2004,** *279*, (24), 25535-25543.

154. Lupertz, R.; Watjen, W.; Kahl, R.; Chovolou, Y. Dose- and time-dependent effects of doxorubicin on cytotoxicity, cell cycle and apoptotic cell death in human colon cancer cells. *Toxicology* **2010,** *271*, (3), 115-121.

155. Lee, T. K. W.; Lau, T. C. M.; Ng, I. O. L. Doxorubicin-induced apoptosis and chemosensitivity in hepatoma cell lines. *Cancer chemotherapy and pharmacology* **2002,** *49*, (1), 78-86.

156. Yagublu, V.; Caliskan, N.; Lewis, A. L.; Jesenofsky, R.; Gasimova, L.; Lohr, J. M.; Keese, M. Treatment of experimental pancreatic cancer by doxorubicin-, mitoxantrone-, and irinotecan-drug eluting beads. *Pancreatology* **2013,** *13*, (1), 79-87.

157. Wang, S.; Konorev, E. A.; Kotamraju, S.; Joseph, J.; Kalivendi, S.; Kalyanaraman, B. Doxorubicin induces apoptosis in normal and tumor cells via distinctly different mechanisms. intermediacy of H(2)O(2)- and p53-dependent pathways. *J Biol Chem* **2004,** *279*, (24), 25535-43.

158. Crawford, H. C.; Scoggins, C. R.; Washington, M. K.; Matrisian, L. M.; Leach, S. D. Matrix metalloproteinase-7 is expressed by pancreatic cancer precursors and regulates acinar-to-ductal metaplasia in exocrine pancreas. *J Clin Invest* **2002,** *109*, (11), 1437-44.

159. He, X. J.; Jiang, X. T.; Ma, Y. Y.; Xia, Y. J.; Wang, H. J.; Guan, T. P.; Shao, Q. S.; Tao, H. Q. REG4 contributes to the invasiveness of pancreatic cancer by upregulating MMP-7 and MMP-9. *Cancer Sci* **2012,** *103*, (12), 2082-91.

160. Edmondson, R.; Broglie, J. J.; Adcock, A. F.; Yang, L. J. Three-Dimensional Cell Culture Systems and Their Applications in Drug Discovery and Cell-Based Biosensors. *Assay Drug Dev Techn* **2014,** *12*, (4), 207-218.

161. Lee, B. J.; Cansizoglu, A. E.; Suel, K. E.; Louis, T. H.; Zhang, Z.; Chook, Y. M. Rules for nuclear localization sequence recognition by karyopherin beta 2. *Cell* **2006,** *126*, (3), 543-58.

162. Tobwala, S.; Srivastava, D. K. Cooperative binding of calcium ions modulates the tertiary structure and catalytic activity of matrix metalloproteinase-9. *Adv. Enzyme Res.* **2013,** *1*, 17-29.

163. Ganguly, B.; Banerjee, J.; Elegbede, A. I.; Klocke, D. J.; Mallik, S.; Srivastava, D. K. Intrinsic selectivity in binding of matrix metalloproteinase-7 to differently charged lipid membranes. *Febs Lett* **2007,** *581*, (29), 5723-5726.

164. Zhang, S. Y.; Zhao, Y. Controlled Release from Cleavable Polymerized Liposomes upon Redox and pH Stimulation. *Bioconjugate Chem* **2011,** *22*, (4), 523-528.

165. Torchilin, V. P. Passive and active drug targeting: drug delivery to tumors as an example. *Handb Exp Pharmacol* **2010**, (197), 3-53.

166. Zwicke, G. L.; Mansoori, G. A.; Jeffery, C. J. Utilizing the folate receptor for active targeting of cancer nanotherapeutics. *Nano Rev* **2012,** *3*.

167. Chang, S. S. Overview of prostate-specific membrane antigen. *Rev Urol* **2004,** *6 Suppl 10*, S13-8.

168. Syntichaki, P.; Tavernarakis, N. The biochemistry of neuronal necrosis: rogue biology? *Nat Rev Neurosci* **2003,** *4*, (8), 672-84.

169. Orrenius, S.; Zhivotovsky, B.; Nicotera, P. Regulation of cell death: the calcium-apoptosis link. *Nat Rev Mol Cell Biol* **2003,** *4*, (7), 552-65.

170. Scarpa, E.; Bailey, J. L.; Janeczek, A. A.; Stumpf, P. S.; Johnston, A. H.; Oreffo, R. O.; Woo, Y. L.; Cheong, Y. C.; Evans, N. D.; Newman, T. A. Quantification of intracellular payload release from polymersome nanoparticles. *Sci Rep* **2016,** *6*, 29460.

171. Meng, F.; Zhong, Z.; Feijen, J. Stimuli-responsive polymersomes for programmed drug delivery. *Biomacromolecules* **2009,** *10*, (2), 197-209.

172. Anajafi, T.; Scott, M. D.; You, S.; Yang, X. Y.; Choi, Y.; Qian, S. Y.; Mallik, S. Acridine Orange Conjugated Polymersomes for Simultaneous Nuclear Delivery of Gemcitabine and Doxorubicin to Pancreatic Cancer Cells. *Bioconjugate Chem* **2016,** *27*, (3), 762-771.

173. Haupt, S.; Raghu, D.; Haupt, Y. p53 calls upon CIA (Calcium Induced Apoptosis) to counter stress. *Front Oncol* **2015,** *5*, (57).

174. Vlachos, M.; Tavernarakis, N. Non-apoptotic cell death in Caenorhabditis elegans. *Dev Dyn* **2010,** *239*, (5), 1337-51.

175. Herzig, S.; Maundrell, K.; Martinou, J. C. Life without the mitochondrial calcium uniporter. *Nat Cell Biol* **2013,** *15*, (12), 1398-1400.

176. Samara, C.; Tavernarakis, N. Calcium-dependent and aspartyl proteases in neurodegeneration and ageing in C. elegans. *Ageing Res Rev* **2003,** *2*, (4), 451-71.

177. Oltra, N. S.; Nair, P.; Discher, D. E. From stealthy polymersomes and filomicelles to "self" Peptide-nanoparticles for cancer therapy. *Annu Rev Chem Biomol Eng* **2014,** *5*, 281-99.

178. Prencipe, G.; Tabakman, S. M.; Welsher, K.; Liu, Z.; Goodwin, A. P.; Zhang, L.; Henry, J.; Dai, H. PEG branched polymer for functionalization of nanomaterials with ultralong blood circulation. *J Am Chem Soc* **2009,** *131*, (13), 4783-7.

179. Kataoka, K.; Harada, A.; Nagasaki, Y. Block copolymer micelles for drug delivery: design, characterization and biological significance. *Adv Drug Deliv Rev* **2001,** *47*, (1), 113-31.

180. Shive, M. S.; Anderson, J. M. Biodegradation and biocompatibility of PLA and PLGA microspheres. *Adv Drug Deliv Rev* **1997,** *28*, (1), 5-24.

181. West, K. R.; Otto, S. Reversible covalent chemistry in drug delivery. *Curr Drug Discov Technol* **2005,** *2*, (3), 123-60.

182. Saito, G.; Swanson, J. A.; Lee, K. D. Drug delivery strategy utilizing conjugation via reversible disulfide linkages: role and site of cellular reducing activities. *Adv Drug Deliv Rev* **2003,** *55*, (2), 199-215.

183. Brown, J. M. Tumor hypoxia in cancer therapy. *Method Enzymol* **2007,** *435*, 297-+.

184. Edmondson, R.; Broglie, J. J.; Adcock, A. F.; Yang, L. Three-dimensional cell culture systems and their applications in drug discovery and cell-based biosensors. *Assay Drug Dev Technol* **2014,** *12*, (4), 207-18.

185. Gottlieb, E.; Armour, S. M.; Harris, M. H.; Thompson, C. B. Mitochondrial membrane potential regulates matrix configuration and cytochrome c release during apoptosis. *Cell Death Differ* **2003,** *10*, (6), 709-17.

186. Li, R.; Jen, N.; Yu, F.; Hsiai, T. K. Assessing mitochondrial redox status by flow cytometric methods: vascular response to fluid shear stress. *Curr Protoc Cytom* **2011,** *Chapter 9*, Unit9 37.

187. Ewald, B.; Sampath, D.; Plunkett, W. Nucleoside analogs: molecular mechanisms signaling cell death. *Oncogene* **2008,** *27*, (50), 6522-6537.

188. Agudelo, D.; Bourassa, P.; Berube, G.; Tajmir-Riahi, H. A. Intercalation of antitumor drug doxorubicin and its analogue by DNA duplex: Structural features and biological implications. *Int J Biol Macromol* **2014,** *66*, 144-150.

189. Pawar, P. V.; Gohil, S. V.; Jain, J. P.; Kumar, N. Functionalized polymersomes for biomedical applications. *Polym Chem-Uk* **2013,** *4*, (11), 3160-3176.

APPENDIX A. SUPPORTING INFORMATION FOR CHAPTER 2

A1. Confocal Fluorescence Microscopic Images of PANC-1 Cells

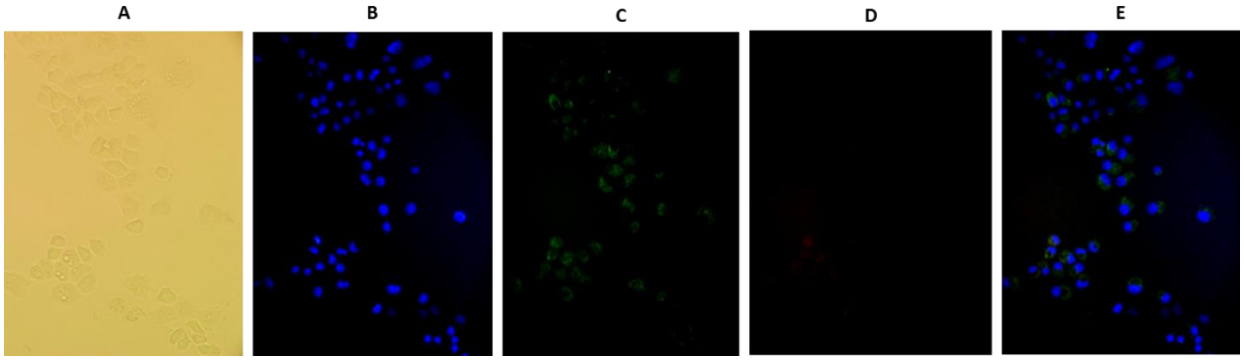

Figure A1. Confocal fluorescence microscopic images of nuclear localization of AO-polymersomes in PANC-1 cells without dexamethasone pre-treatment. (A) Bright field microscopy image; (B) Hoechst stained nuclei of the cells (DAPI filter); (C) image recorded with FITC filter (the green color is showing the AO location); (D) image recorded using TRITC filter (the red color is showing the presence of lissamine rhodamine); and (E) overlayed images (scale bars: 200 μm).

A2. ESI Mass Spectrum of the Alkyne Conjugated Acridine Orange

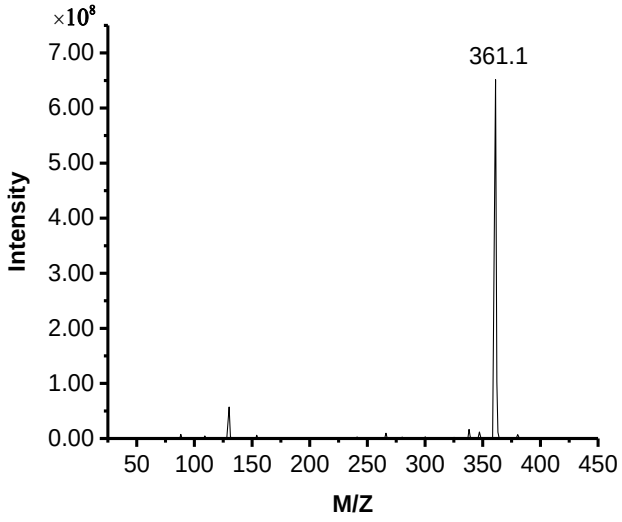

Figure A2. ESI mass spectrum of the alkyne conjugated acridine orange. The calculated molecular mass is: 361.2

A3. Absorbance Spectra of Polymersomes Before and After Size Exclusion Chromatography

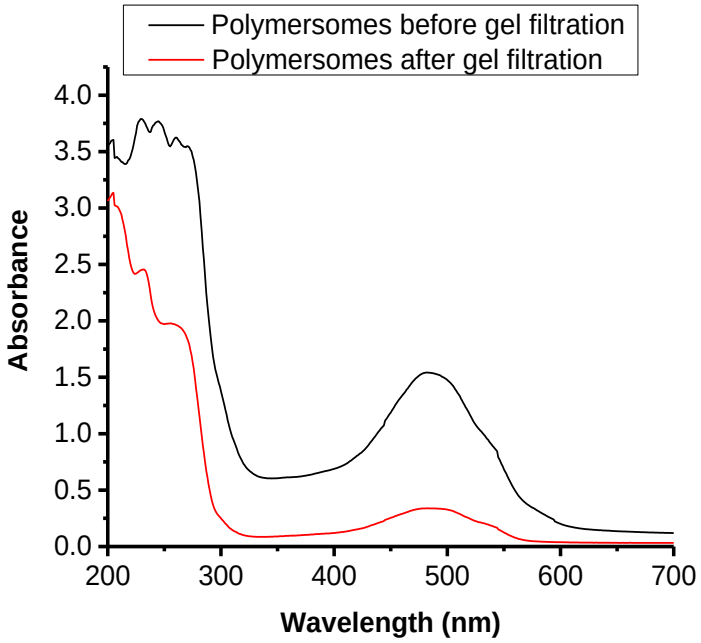

Figure A3. Absorbance spectra of the drug-encapsulated polymersomes before (black trace), and after (red trace) size exclusion chromatography.

A4. Images of Spheroid Cell Cultures at Multiple Focal Planes

Legend for Movie:

The link for the short video that we have obtained by confocal microscopy from multiple focal planes of an 8-day old spheroid: https://youtu.be/qxj6hkeghgs

APPENDIX B. SUPPORTING INFORMATION FOR CHAPTER 3

B1. Peptide Purification and Characterization

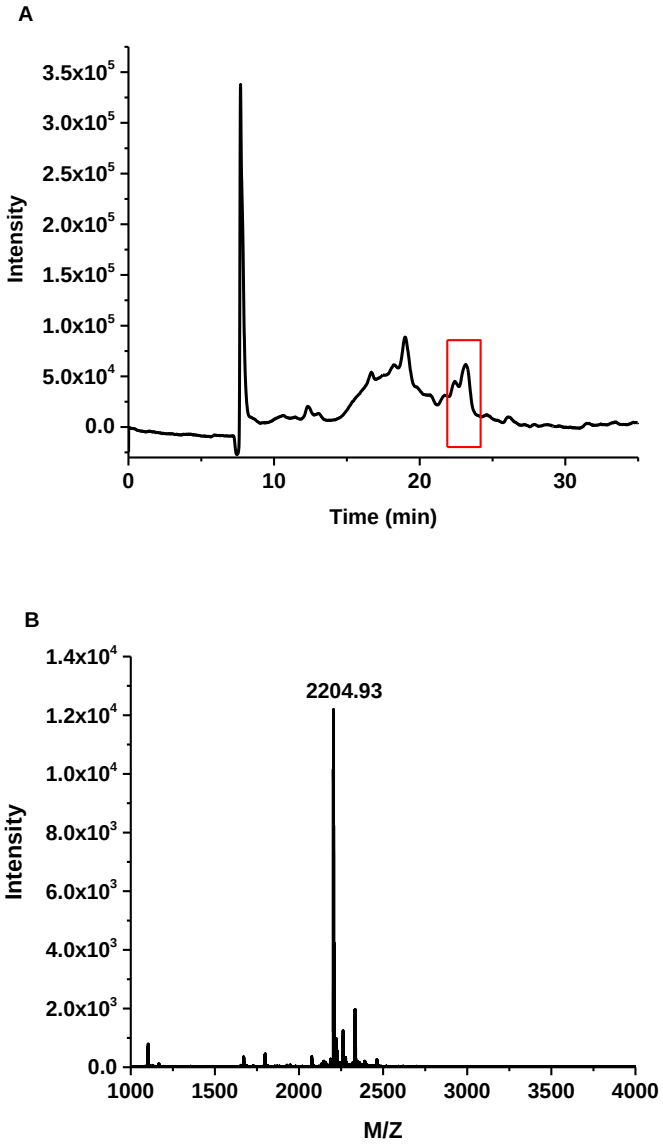

Figure B1. Peptide purification and characterization using RP-HPLC and MS spectrometry. (A) RP-HPLC chromatogram of the crude peptide (the marked peak is showing the pure peptide fraction). (B) MS analysis of purified peptide (calculated exact mass: 2204.16).

B2. Captisol-Curcumin Complexation

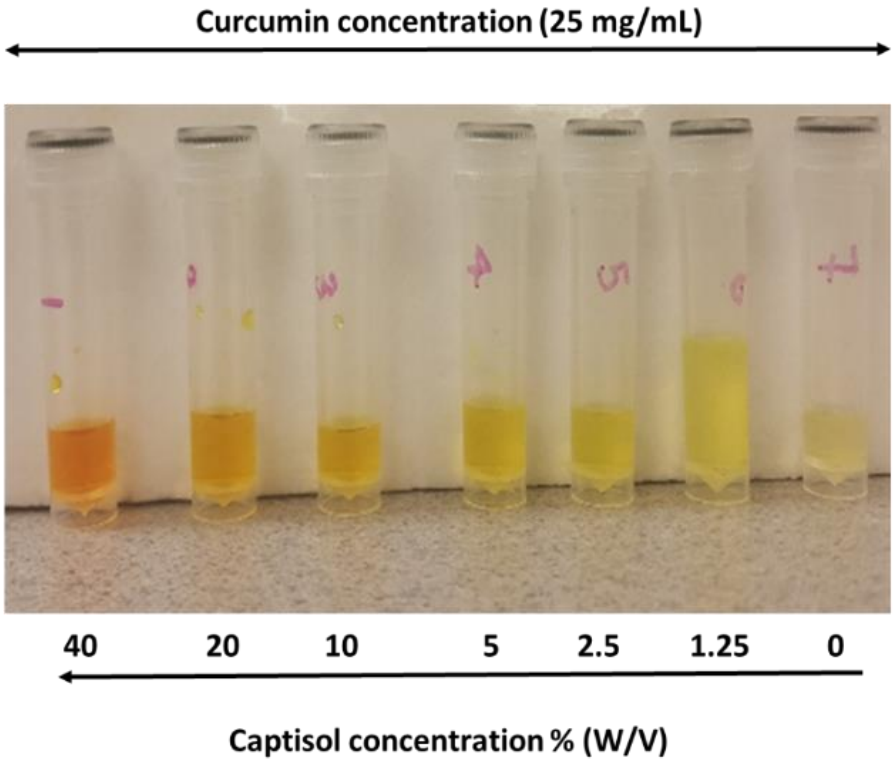

Figure B2. Curcumin-Captisol complexation. Curcumin amount was kept constant (25 mg). Increasing the concentration of captisol in water from 0 to 40% (W/V) increased the solubility of curcumin. The complexation was carried out at room temperature for 3 days.

B3. Calibration Curve for Measuring Curcumin Concentration

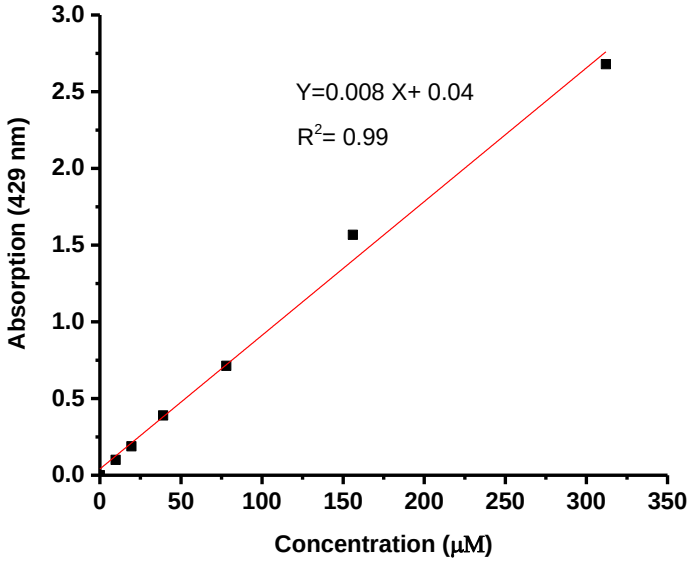

Figure B3. Calibration curve for measuring the curcumin concentration. Absorbance was recorded at 429 nm.

B4. Drug Encapsulation in Polymersomes

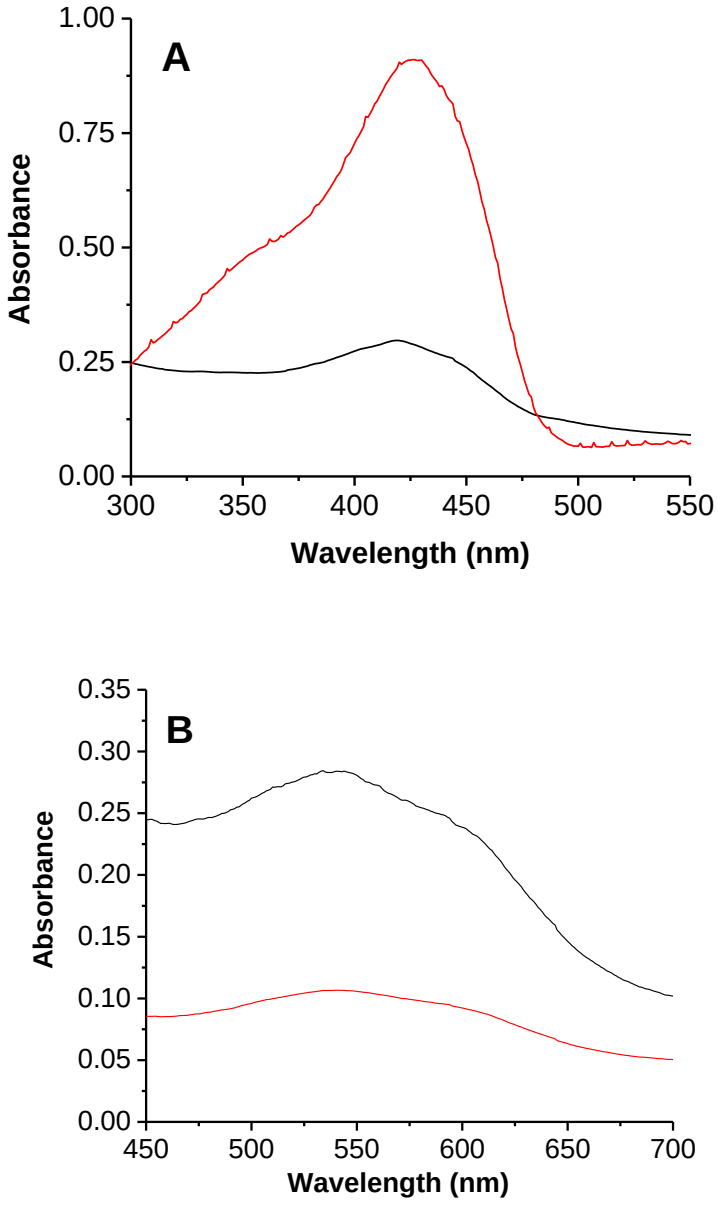

Figure B4. Drug encapsulation in polymersomes. (A) The presence of a peak at 420 nm is indicating the presence of the Captisol-curcumin complex in the polymersomes' aqueous core. The red trace is indicating the Captisol-curcumin complex absorption spectra, and the black trace is showing absorption spectra of polymersomes encapsulating curcumin complex. (B) The absorption spectra of the polymersomes encapsulating doxorubicin before (black trace), and after (red trace) size exclusion chromatography shows the presence of doxorubicin in the vesicles.

B5. Calcein Release from the Polymersomes in the Presence of MMPs

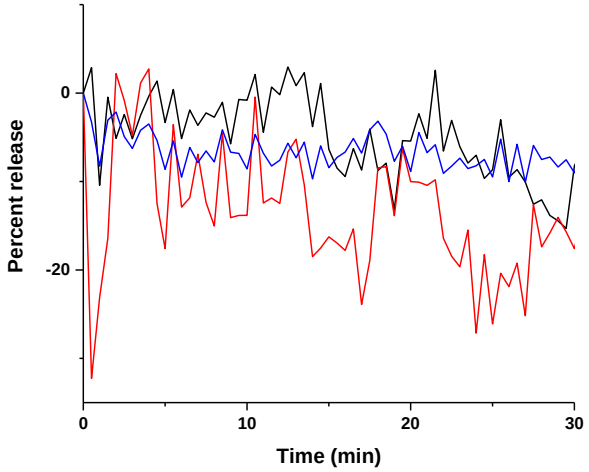

Figure B5. The release of calcein from the polymersomes in the presence of added MMP-7, MMP-9, and MMP-1 enzyme (2 μM each). Calcein release was monitored for 30 minutes in the presence of added MMP-9 (black trace), MMP-7 (blue trace), and MMP-1 (red trace).

B6. Growth Curves for the AsPC-1 Cell Spheroids

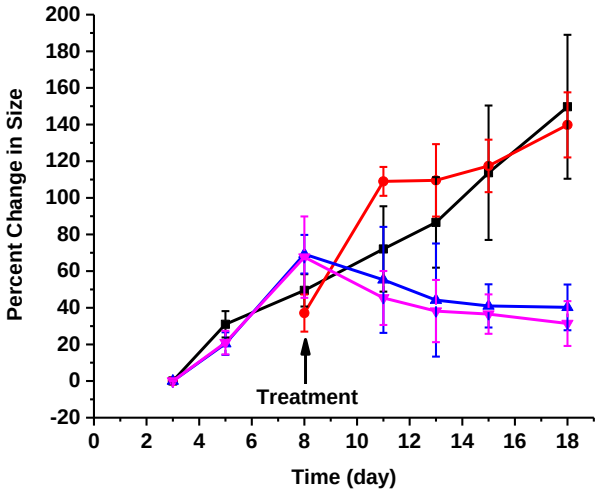

Figure B6. Growth curves for the AsPC-1 cell spheroids. The 8-day old spheroids were treated with different polymersome formulations, and their growth was monitored for 10 days (N = 8). Black trace with squares: plain polymersomes; red trace with circles: curcumin and doxorubicin encapsulated polymersomes; blue trace with triangles: curcumin and doxorubicin encapsulated, peptide conjugated polymersomes; magenta trace with inverted triangles: free drug combination.

B7. Cell Viability of Three-dimensional Spheroids (AsPC-1 cells)

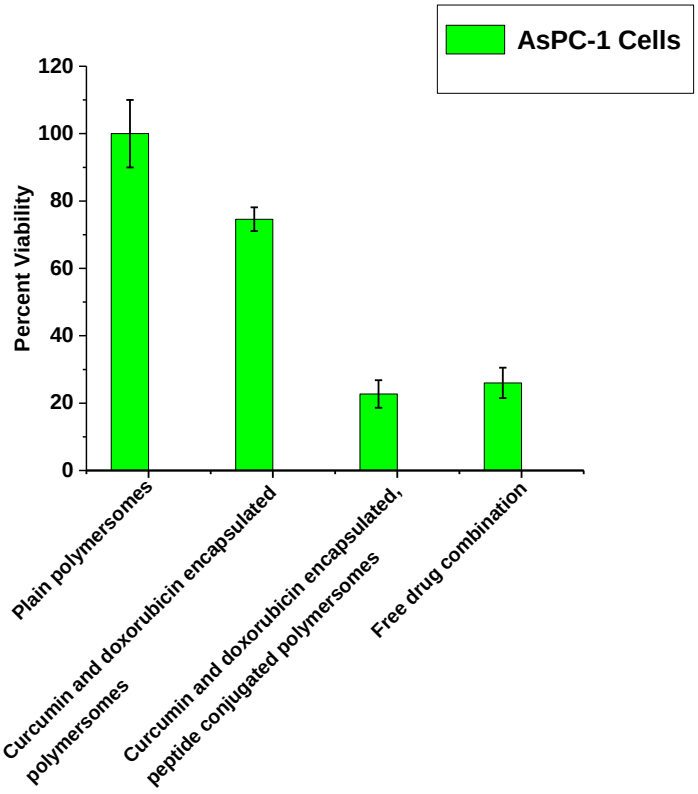

Figure B7. Cell viability of three-dimensional spheroids (AsPC-1 cells) after treatment with different polymersome formulations (N = 6).

APPENDIX C. SUPPORTING INFORMATION FOR CHAPTER 4

C1. Formation of Calcium Phosphate Crystals in the Cell Culture Media

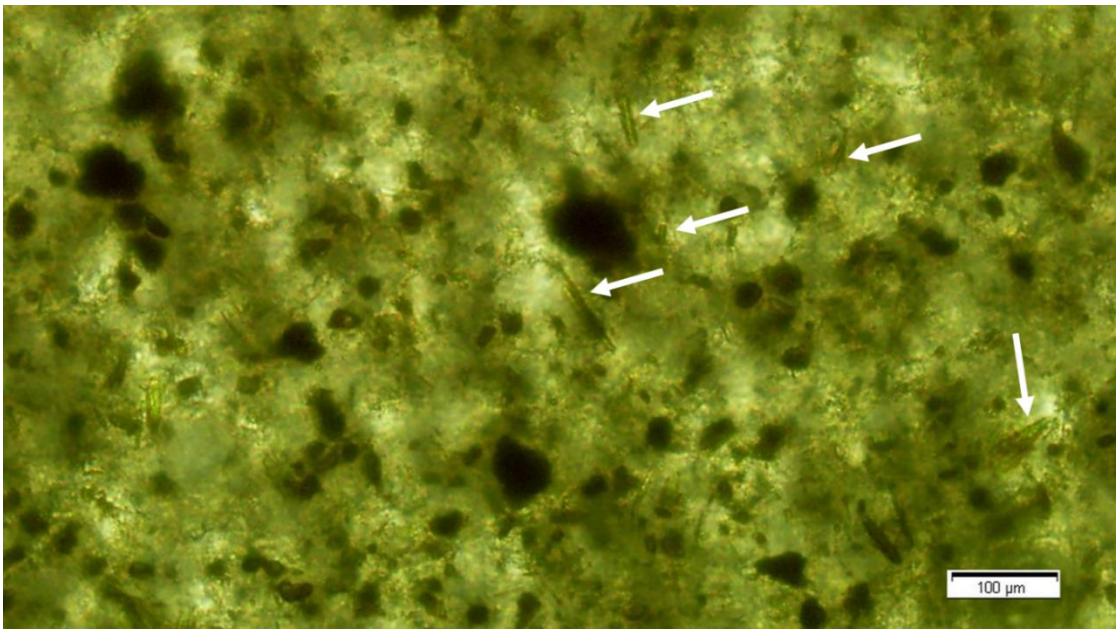

Figure C1. Formation of calcium phosphate crystals in the cell culture media (marked with the white arrows) in the presence of folic acid (500 µg/mL) and $CaCl_2$ (50 mM). RPMI-1640 complete growth medium supplemented with fetal bovine serum (10%), and antibiotic-antimycotic solution (1%) was used. Magnification: 20X.

C2. Calibration Curve for Measuring the Concentration of Polymersome-Encapsulated Ca^{2+}

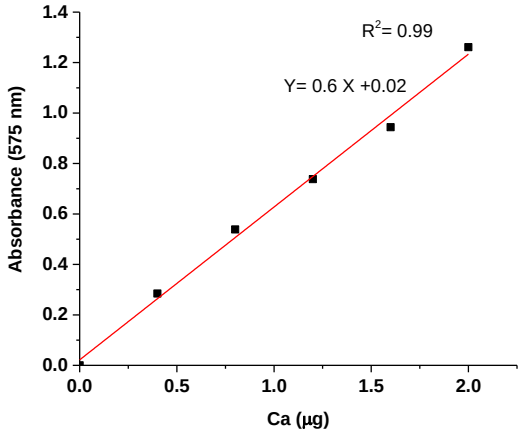

Figure C2. Calibration curve for measuring the concentration of polymersome-encapsulated Ca^{2+}. The squares are showing the observed data points, while the Red line is showing the fitted straight line.

C3. Calcein Release from the Polymersomes in the Absence of GSH

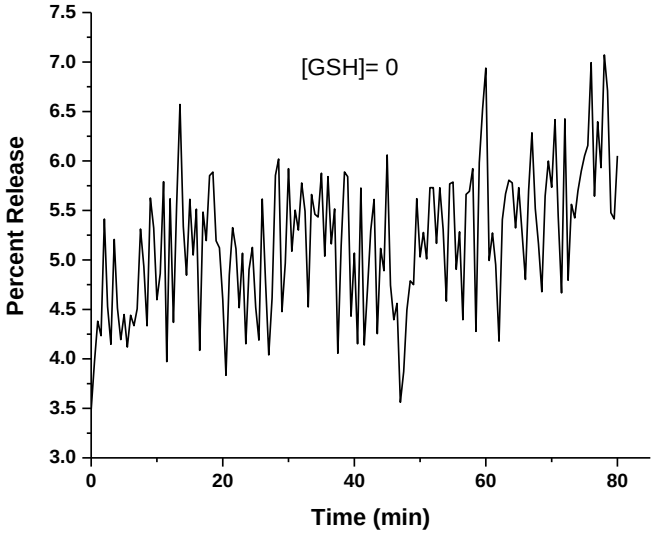

Figure C3. Calcein release from the polymersomes in the absence of GSH. The release was monitored for 80 minutes.